

UCSF

UC San Francisco Electronic Theses and Dissertations

Title

Harnessing CRISPR-Cas13a Towards the Direct Detection of RNA Viruses

Permalink

<https://escholarship.org/uc/item/0vc0v23d>

Author

Fozouni, Parinaz

Publication Date

2020

Peer reviewed|Thesis/dissertation

Harnessing CRISPR-Cas13a Towards the Direct Detection of RNA Viruses

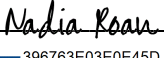
by
Parinaz Fozouni

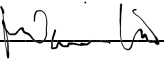
DISSERTATION
Submitted in partial satisfaction of the requirements for degree of
DOCTOR OF PHILOSOPHY

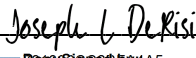
in
Biomedical Sciences

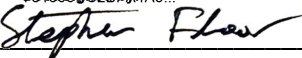
in the
GRADUATE DIVISION
of the
UNIVERSITY OF CALIFORNIA, SAN FRANCISCO

Approved:

DocuSigned by:

396763E03E0E45D... Nadia Roan
Chair

DocuSigned by:

DocuSigned by:
40C... Melanie Ott

DocuSigned by:

DocuSigned by:
4A5... Joseph L DeRisi

DocuSigned by:

3709C3C6AF93461... Stephen Floor

Committee Members

Copyright 2020

by

Parinaz Fozouni

Dedication

This dissertation is dedicated to my grandmothers: Pari Fozouni, my namesake, and Forough Yazdani, who raised me.

Acknowledgments

I am grateful to many people who provided support, comfort, and encouragement throughout my graduate work. Below is a small sampling of the people who raised me up.

First and foremost, I am indebted to my research advisor, Dr. Melanie Ott, for her mentorship over the last four and a half years. She supported me in pursuing a seemingly random idea I had after a talk which then grew into my dissertation work, and ensured I had the tools and collaborators to succeed in my endeavors. I admire her drive, tenacity, and impressive, almost super-human, ability to work without coffee. I will always be grateful for the opportunities she provided for me to grow and succeed as a scientist, and for the example she provided of a woman who can do it all.

I am grateful to Daniel Richter and Dr. Nicole King for taking in a freshman student in 2015 at UC Berkeley with no prior lab experience and initially no intention to pursue a PhD. It was through my experiences in the King Lab and under their mentorship and guidance that I had the desire to pursue a PhD, as well as the tools to succeed. Dan and Nicole have long served as my role models for how to conduct curiosity-driven research, and I am grateful for the formative experience with them.

I would like to thank Dr. Joe DeRisi for mentoring me during my first rotation at UCSF and continuing to provide critical advice, mentorship and support as a dissertation committee member and MSTP advisor. I am always inspired by his relentless energy and willingness to tackle difficult problems and push the boundaries of science. I am grateful to Dr. Michael Rosenblum for also serving as a rotation mentor and his continued support and advice on my clinical and research pursuits. I would like to thank Dr. Stephen Floor, who served as both a qualifying committee and dissertation committee member, for his valuable feedback. I will always deeply appreciate his support, kindness, and advice during the more challenging parts of my graduate work. I would also like to thank Dr. Nadia Roan, my dissertation committee chair, for her excellent suggestions, feedback, and encouragement during my PhD. Finally, I would like to thank my qualifying

committee members, Dr. Bruce Conklin, Dr. Joe Bondy-Denomy, and Dr. Satish Pillai, for their valuable questions, suggestions, and feedback early on and throughout my graduate work.

I am very grateful to Ryan Conrad, who served as my rotation mentor in the Ott Lab and my role model throughout my time in the lab. His guidance and advice as both a friend and mentor have been invaluable, and he provided me a road map for how a PhD should be done.

In and outside of the lab, I have appreciated the close friendship, listening ears, and advice of Krystal Fontaine and Ansumana Hull. Kristoffer Leon, Jennifer Hayashi, Albert Vallejo-Gracia, Mir Khalid, Irene Chen, Daniela Boehm, and Chia-Lin Tsou have been fantastic lab mates and confidants throughout the years. I have had the distinct privilege of working with multiple talented technicians in the lab – namely Carley Gray, Jeffrey Shu, and Stephanie Stephens – and I am excited to continue to follow their careers and accomplishments for years to come. Many Ott lab members through the years have served as great sources of advice, humor, and camaraderie for which I am thankful: Ibraheem Ali, Nathan Meyers, Camille Simoneau, Olivia Sims, Sakshi Tomar, Ursula Schulze-Gahmen, Veronica Fonseca, Gili Aviv, Danielle Lyons, Jesse Chen, Kathrin Roesch, Takako Tabata, Taha Taha, Bharath Sreekumar, and Lauren Weiser. On the fifth floor, I have also appreciated the help and friendship of Andrea Gramatica, Mauricio Montano, and of many Verdin lab members.

I am indebted to Dr. Jennifer Doudna, Alexandra East-Seletsky, and Gavin Knott for their critical support and collaboration over the many years which enabled us to apply CRISPR-Cas13a to viral detection. I am grateful to Dr. Dan Fletcher, María Díaz de León Derby, and Sungmin Son for bringing our science to life in the form of a portable device. The collaboration with both groups has been nothing short of enjoyable, and I am grateful to have worked with such a remarkable group of scientists. I would also like to express my deep appreciation and gratitude of Dr. Anita Sil, Bastian Joehnk, and Keith Walcott, who spent the early days of the COVID-19 pandemic helping us set up the aerosol BSL-3 and begin our SARS-CoV-2 work. We could not have done

this work without their generosity. I would like to thank the Weissman lab for generously allowing us to use their plate reader for many years, which enabled most of these experiments.

To Geri Ehle, Demian Sainz, Amanda Andonian, Ned Molyneaux, and Andres Zepeda, I am grateful for their many years spent tolerating my emails, questions, and requests. Thank you for all that you do to make our programs better. I would like to thank Dr. Mark Anderson, Dr. Cathy Lomen-Hoerth, and Dr. Mark Ansel for their continued support, advice and guidance. I am grateful for the community I have found in the MSTP Women's Group, and for all of the women who have provided reassurance and encouragement, and shared their journeys. I thank the NIH, specifically the NIAID, and the UCSF Discovery Fellowship for supporting my research and providing me with funding.

I would like to thank my dear friends for their unending support and encouragement: Michael Diaz, Michael Wang, Hedieh Attai, Sahra Mirbabaei, Betty Zong, Ada Li, Eva Li, Tommy Queally, Hana Dahi, Hilary Mazzone, Gabrielle Sanders, Amy Hahn, Kayla Berringer, Wendi Gu, Hilary Chan, Sharon Hong, Tishiana Mann, Vicky Hwang, Katya Popova, Austin Hsu, Alexis Krup, Jen Wang, and Johnny Yu. Adventures with you all have made my time away from the lab valuable and restoring. I would also like to thank the motley crew of MSTPs who I have been privileged to embark on this journey with: Theo Roth, Joe Hiatt, David Wu, Lay Kodama, Nick Woods, Adam Rao, Jon Schor, Simon Pan, and Kevin Lou. I had no expectation to become such close friends with my classmates, and I admire you all. Thank you to Jonathan Ostrem for being my MSTP role model and inspiration, and my big sibs Sophie Levan and Shelly Mintz for being my first mentors at UCSF and your continued friendship and guidance.

Finally, and most importantly, I would like to thank my family for their continued support – they pushed me over the finish line. To Parpar, who passed during my third year, I am grateful for the flexibility of the PhD years which allowed me to continue visiting and seeing you through the end. To Mom, thank you for the years of phone calls asking me, “But when will you finish?” To Dad, thank you for your philosophical and practical wisdom in navigating academia, and for

encouraging my social science skills which served me well even in the “hard” sciences. Thank you to Maman Forough, Farnaz, Laila, and Sudeep for the support and humor through the years. To the munchkins – Ava and Nilu – playing peek-a-boo with you both has always been a welcome respite from lab.

Contributions

This dissertation encompasses four and half years of graduate education and research. Included in this dissertation are bodies of work I contributed substantially to in inception and execution. **Chapter II** represents unpublished, in-progress work, for which I am grateful to Carley Gray, Jeffrey Shu, Daniela Boehm, Ursula Schulze-Gahmen, Sungmin Son, María Díaz de León Derby, Michael D'Ambrosio, Alexandra East-Seletsky, Gavin Knott, Bette Korber, James Theiler, Steve Deeks, Jennifer Doudna, Daniel Fletcher, and Melanie Ott for their contributions.

Chapter III represents the formal narrative of my scientific progress as a doctoral student. For this chapter, I am grateful to all my co-authors: Sungmin Son, María Díaz de León Derby, Gavin Knott, Carley Gray, Michael D'Ambrosio, Chunyu Zhao, Neil Switz, Renuka Kumar, Stephanie Stephens, Daniela Boehm, Chia-Lin Tsou, Jeffrey Shu, Abdul Bhuiya, Maxim Armstrong, Andrew Harris, Pei-Yi Chen, Jeannette Osterloh, Anke Meyer-Franke, Bastian Joehnk, Keith Walcott, Anita Sil, Charles Langelier, Katherine Pollard, Emily Crawford, Andreas Puschnik, Maira Phelps, Amy Kistler, Joseph DeRisi, Jennifer Doudna, Daniel Fletcher, and Melanie Ott. This work has been accepted and peer-reviewed, and the citation is as follows:

Fozouni P, Son S, Díaz de León Derby M, Knott GJ, Gray CN, D'Ambrosio MV, Zhao C, Switz NA, Kumar GR, Stephens SI, Boehm D, Tsou CL, Shu J, Bhuiya A, Armstrong M, Harris AR, Chen PY, Osterloh JM, Meyer-Franke A, Joehnk B, Walcott K, Sil A, Langelier C, Pollard KS, Crawford ED, Puschnik AS, Phelps M, Kistler A, DeRisi JL, Doudna JA, Fletcher DA, Ott M. Amplification-free detection of SARS-CoV-2 with CRISPR-Cas13a and mobile phone microscopy. *Cell*. 2020 Dec 4:S0092-8674(20)31623-8. doi: 10.1016/j.cell.2020.12.001. Epub ahead of print. PMID: 33306959.

Harnessing CRISPR-Cas13a Towards the Direct Detection of RNA Viruses

Parinaz Fozouni

Abstract

Viral diagnostics largely rely on reverse transcription before PCR-based amplification of the viral genome, which cannot be easily performed outside a specialized laboratory. There is an urgent need for rapid and portable diagnostics that can quantitatively detect viruses. The December 2019 outbreak of a novel respiratory virus, SARS-CoV-2, has become an ongoing global pandemic due in part to the challenge of quickly identifying and isolating asymptomatic and pre-symptomatic carriers of the virus. CRISPR diagnostics can augment gold-standard PCR-based testing if they can be made rapid, portable and accurate. Here, we report the development of an amplification-free CRISPR-Cas13a assay for the direct detection and quantification of viral RNA using a mobile phone microscope. When applied to the detection of SARS-CoV-2 RNA, the assay achieved ~100 copies/ μ L sensitivity in under 30 minutes of measurement time and accurately detected pre-extracted RNA from a set of positive clinical samples in under 5 minutes. To improve sensitivity and specificity, we combined crRNAs targeting SARS-CoV-2 RNA, and directly quantified viral load using enzyme kinetics. Integrated with a reader device based on a mobile phone, this assay has the potential to enable rapid, low-cost, point-of-care screening for SARS-CoV-2. We further applied this approach towards the direct detection of HIV-1 RNA, which could serve as a tool for both identifying HIV at the earliest stage of initial infection and detecting HIV rebound in treated individuals following treatment interruption. Together, this work lays the framework for the development of amplification-free CRISPR diagnostics towards RNA viruses.

Table of Contents

Chapter 1: Introduction.....	1
References.....	17
Chapter 2: Harnessing CRISPR-Cas13 towards direct detection of HIV-1 RNA.....	24
References.....	39
Chapter 3: Amplification-free detection of SARS-CoV-2 with CRISPR-Cas13a and mobile phone microscopy.....	43
References.....	88
Chapter 4: Outlook and Conclusions.....	96
References.....	97

List of Figures

Figure 2.1: CRISPR-Cas13a can be paired with an RNA-based quenched-fluorescent reporter to provide specific detection of HIV RNA.....	32
Figure 2.2: Schematic of crRNA 3 and crRNA 5 recognition sites overlaid on the HIV-1 RNA genome.....	33
Figure 2.3: Cas13a RNPs detect HIV transcripts from diverse cell lines and combining crRNAs improves sensitivity	34
Figure 2.4: Optimization of the Cas13a assay leads to improved detection of target RNA.....	35
Figure 2.5: Screening of 100 candidate crRNAs reveals potential crRNAs for sensitive HIV-1 detection.....	37
Figure 3.1: Quantitative Direct Detection of Viral SARS-CoV-2 RNA with Cas13a.....	63
Figure 3.2: Combining crRNAs Improves Sensitivity of Cas13a.....	65
Figure 3.3: Cas13a Directly Detects SARS-CoV-2 RNA in Patient Samples.....	66
Figure 3.4: Harnessing the Mobile Phone Camera as a Portable Plate Reader.....	68
Figure S3.1: Individual crRNAs Quantitatively Detect SARS-CoV-2 RNA.....	70
Figure S3.2: Combining crRNAs Improves SARS-CoV-2 Detection.....	71
Figure S3.3: Comparison of the Cas13a Reaction Measured in the Plate Reader and the Mobile Phone Device.....	73
Figure S3.4: Limit of Detection of the Mobile Phone Device.....	74

List of Tables

Table S3.1: Related to Figures 3.1-3.4 and S3.1-S3.4. List of custom oligonucleotides used in this study.....	85
--	-----------

Chapter 1: Introduction

Rapid, point-of-care diagnostics: an urgent need

Humans have contended with the burden of infectious diseases since the dawn of humanity, locked in an infinite arms race with pathogens. As the world has become increasingly interconnected, spillover events at wildlife-human interfaces (zoonotic viruses) have experienced greater spread and impact on the human species, and pose one of the greatest public health challenges of the twenty-first century (Grubaugh et al., 2018). In the last 120 years, eight notable pandemics have occurred: 1918 Spanish flu, 1957 Asian flu, 1968 Hong Kong flu, 1981 HIV, 2003 SARS, 2009 Swine flu, 2015 Zika virus, and 2019 COVID-19 (Madhav et al., 2017). The likelihood of pandemics has increased over time as a result of globalization, including global travel, urbanization, and increased exploitation of the natural environment. In particular, these trends predispose to the crossover and emergence of zoonotic diseases to which humans may have limited or no pre-existing immunity. The ability to rapidly respond to these existing and emerging threats will determine whether these spillover events lead to a contained local outbreak or a pandemic. To this end, rapid and portable diagnostics become a major player in identifying and isolating infectious carriers.

Over the past two decades, many advances in molecular techniques, especially next-generation sequencing, have been made that have allowed for the rapid identification of novel pathogens in outbreaks. The causative agent of COVID-19, severe acute respiratory syndrome (SARS)-coronavirus (CoV)-2, was quickly identified as a result of next-generation sequencing (Wu et al., 2020; Zhou et al., 2020). The rapid acquisition of the genetic sequence of the novel coronavirus was astonishing: on December 30, 2019, the initial report of cluster of the pneumonias of unknown origin was made to the China National Health Commission; on January 7, 2020, the novel virus was isolated; and on January 12, 2020, the whole genome sequence was shared with the World Health Organization (Wang et al., 2020). This enabled the rapid development of diagnostic quantitative real-time polymerase chain reaction (qPCR) tests as well

as allowed researchers to get an early start on developing vaccines. Moderna's mRNA-1273 vaccine, for example, was designed by January 13, 2020. Despite this, the virus has spread across the globe, with over 71.5 million reported infections worldwide and 16 million in the United States alone as of December 2020 (Dong et al., 2020).

To efficiently manage this pandemic and prepare us for future pandemics, novel, rapid, point-of-care diagnostics are essential. "Without diagnostics, medicine is blind" (Schroeder et al., 2016). Point-of-care diagnostics have increasingly been recognized as an essential component of our response to infectious diseases. Compared with other diseases, infectious diseases pose a unique threat, as they can be transmitted exponentially among people in very short periods of time (Chen et al., 2019). Although clinical laboratories can offer highly sensitive and specific assays, these tests are usually time and labor intensive and require specialized equipment and highly trained operators. In the United States in particular, a major driver in the massive number of COVID-19 cases has been the failure to effectively identify and isolate pre-symptomatic and asymptomatic carriers of SARS-CoV-2. Most testing thus far has relied on qPCR, which often has a minimum sample-to-result time of 24-48 hours, and with an average wait time of 4.1 days (Lazer et al., 2020). The national backlog in processing these laboratory-based tests, as well as the difficulty of acquiring one to begin with, has allowed for the exponential spread of COVID-19 in the United States. However, recent modeling suggests that repeated screening using less sensitive, point-of-care tests has the ability to break the transmission cycle. Testing frequency was found to be the primary driver of population-epidemic control, with only a small improvement from using a more sensitive test (Larremore et al., 2020). For the broad screening of a population, the key is not sensitivity alone, but how quickly and effectively infections can be recognized by the repeated use of a given test (Mina et al., 2020). Without rapid, point-of-care tests to identify and isolate infectious carriers, controlling the pandemic before widespread vaccination will be difficult.

Point-of-care viral diagnostics can also serve additional purposes than just the acute response to a widespread pandemic. In the case of HIV-1, another virus with a pre-symptomatic phase, point-of-care tests or self-tests can serve multiple purposes. HIV self-testing can counter barriers that patients face when testing is exclusively performed in health care settings, including the ability to reach at-risk individuals who otherwise rarely test and overcoming the social stigma of HIV (Steehler et al., 2019). Given that HIV testing is the main point of entry into HIV care and prevention services, and nearly 14% of infected Americans are unaware of their infection status, increasing access to testing is a major goal (Steehler et al., 2019). Previous studies suggest a high acceptability and often a preference for HIV self-testing among youth, men who have sex with men, racial/ethnic minorities, pregnant women, and transgender women (Steehler et al., 2019). The only over-the-counter option, the OraQuick in-home HIV test, is an antibody-based test. Given that there is a three-month window before antibodies against HIV could appear and be detected, this test can give false negatives during that time frame and allow continued spreading of HIV. Nucleic-acid based tests are thought to be the gold standard during this period, and as such, there is an urgent need for nucleic-acid based self-tests. These tests can provide more accurate results with less regard to the timing of the exposure, allowing those who are most at-risk to test regularly without the inconvenience of going to a clinic or test site.

Moreover, HIV self-testing may serve as a valuable tool in HIV cure trials and analytical treatment interruptions. Despite a dramatic reduction in morbidity and mortality in people infected with HIV as a result of antiretroviral therapy (ART), life-long treatment is still required. ART can make viral RNA levels undetectable, but cessation of treatment usually results in rapid viral rebound (Castagna et al., 2019; Stohr et al., 2013) and eventually progression to Acquired Immunodeficiency Syndrome (AIDS) and death (Holkmann Olsen et al., 2007). Over the last decade, there has been a concerted effort to develop an HIV cure or interventions to control HIV viral replication without ART (Deeks et al., 2016). To determine the efficacy of these interventions, cessation of ART and subsequent monitoring of viral loads is necessary. Typically, this entails

close follow-up, with repeated collection of whole blood at least every week for assessment of viral loads by qPCR (Julg et al., 2019; Pannus et al., 2020). This requires participants to regularly visit a clinical site for blood draws. Although more frequent testing is desired from a clinical and scientific perspective, this poses a major burden on participants and can lead to reduced participant retention for longer studies (Julg et al., 2019). Creating nucleic acid-based HIV self-tests that allow participants to quickly and easily monitor their viral load from home could appease this burden and improve data collection and monitoring in these trials.

In summary, the investment of significant resources toward developing highly programmable, rapid, and portable diagnostics for viruses has an urgent need, and will continue to be critical in combatting future viral outbreaks.

A brief history of emerging viruses in the twenty-first century

Emerging viruses, in particular zoonotic viruses that originate from a reservoir species and jump to humans, can pose major challenges depending on its ability to transmit among humans. In the best case, it could result in a localized outbreak that can be controlled by public health interventions; in the worst case, it could develop into a large epidemic or global pandemic. In the twenty-first century, novel viruses have emerged, including the SARS and MERS coronaviruses, as well as outbreaks of known viruses including Ebola, Zika, and influenza of swine or avian origin (Grubaugh et al., 2018). Complicating basic, virus-intrinsic factors such as infectivity or transmission is the new, human factor of globalization, where millions of people are transported by air from one part of the planet to another, providing rapid “trafficking” of these novel microbes to all parts of the globe (Zappa et al., 2009).

The first pandemic of the new millennium was severe acute respiratory syndrome (SARS), which began in Guangdong, China in 2002. The Guangdong region is characterized by a high concentration of stock farms and markets of live and domestic animals, which facilitates zoonotic transmission (Zappa et al., 2009). Two cross-species passages were sufficient for SARS-

Coronavirus to reach and spread in humans. The first cross-species jump was from bats, the natural reservoir, to susceptible animals such as the civet and racoons, “spillover hosts.” The second cross-species jump was to humans (Shi and Hu, 2008). How SARS spread across the globe was traced back to the overnight stay of a physician from Guangdong at the Metropole hotel in Hong Kong. During his stay, he unwittingly infected 13 foreign guests, who upon returning to their home countries, allowed the spread of SARS far from the origin of the pandemic. In all, SARS caused approximately 8,000 cases and 900 deaths in 30 different countries – but was controlled within eight months and eventually eradicated from the human population in 200 (Zappa et al., 2009). Compared with SARS-CoV-2, SARS was more lethal but less transmissible, and intense public health mitigation measures were sufficient to eradicate the virus in the absence of a vaccine (Petersen et al., 2020).

The next pandemic that emerged in the twenty-first century was the 2009 influenza A H1N1 pandemic, colloquially referred to as the “Swine Flu.” H1N1 first emerged in spring 2009 in Mexico and the US (Girard et al., 2010). As a result of gene segmentation and reassortment, in part enabling cross-species transmission, influenza viruses pose a unique threat to the human population. The initial R_0 , or basic reproductive rate, of the 2009 H1N1 virus was 1.7, and later estimated between 0.17 and 1.3 after mitigation was initiated. For comparison, the R_0 for SARS-CoV-2 is estimated at 2.5, and the R_0 for the 1918 Spanish influenza is estimated at 2.0 (Petersen et al., 2020). The actual number of cases worldwide is unknown, as most cases were diagnosed clinically and not confirmed by laboratory tests; however, estimates of the disease in the USA are that ~1 of 6 Americans had been infected, accounting for 50 million cases (Girard et al., 2010). A defining feature of the 2009 pandemic is that it disproportionately affected children and young adults, compared to older age groups. It was mostly a mild and self-limiting upper respiratory tract illness, with nearly 50% of patients presenting with gastrointestinal symptoms. About 2-5% of confirmed cases in the US required hospitalization, with a fifth of them requiring clinical management in the intensive care unit. Most of these patients had underlying conditions, with

asthma being a significant risk factor for severe disease in children (Girard et al., 2010). Overall, the 2009 H1N1 virus was clearly less virulent than the 1918 virus, but gave the world a sobering lesson on our inability to predict the specific influenza subtypes that could emerge and cause pandemics (Nistal-Villán and García-Sastre, 2020).

Although it did not cause a widespread, sustained pandemic, the 2013-2016 Ebola outbreak in West Africa posed a major global threat. Ebola virus disease (EVD) is a fatal viral hemorrhagic illness of zoonotic origin that was first identified in Zaire, Africa (presently the Democratic Republic of Congo) in 1976 (Hasan et al., 2019). Most outbreaks can be traced to a single spillover event into humans from an unknown reservoir. Human-to-human Ebola virus transmission primarily takes place through close bodily contact with the infected patient, their fluids, or contaminated tissues and surfaces. Traditional burial practices also play a major role in human-to-human disease transmission (Hasan et al., 2019). The 2013-2016 outbreak was the largest to date, leading to 28,652 infections and 11,325 deaths (Jacob et al., 2020). Although there was a concentration of cases in the three contiguous countries of Guinea, Sierra Leone, and Liberia, additional cases spread across seven other nations on three continents. This was the first EVD outbreak that had spread this widely, primarily through air travel, and the first outbreak that had documented transmission outside of the African continent (Parra et al., 2014; Shultz et al., 2016). As a result of the unmitigated transmission during this outbreak, EVD candidate vaccines were developed and evaluated at an accelerated pace, with the rVSVΔG-ZEBOV-GP live attenuated recombinant vesiculovirus candidate vaccine approved by the US Food and Drug Administration and the European Commission (Jacob et al., 2020).

Finally, the Zika virus (ZIKV) pandemic in 2015 gained special attention due to its ability to cause congenital defects in fetuses and infants, and due to the fact that primary transmission is from an arboviral vector, rather than horizontal human-to-human transmission. Although ZIKV was first discovered in Africa in 1947 and detected in Asia as early as 1966, it did not gain attention until the outbreaks in the Pacific from 2007 to 2015, and especially the widespread transmission

in the Americas in 2015. This pandemic highlighted the virus's ability to efficiently transmit in aedes mosquito-infested settings, and to spread across wide regions through human travel. Although most infections of adults were mild or asymptomatic, severe complications became more prominent, including Guillain-Barré syndrome in French Polynesia and a dramatic increase in microcephaly cases in newborns in Brazil. As of January 2018, more than 3700 cases of congenital birth defects associated with ZIKV infection had been documented in the Americas. The outbreak was also characterized by a high infection rate in affected populations, with some communities at the epicenter in northeast Brazil reporting that more than 60% of the exposed population was infected (Musso et al., 2019).

Viruses will continue to emerge and spread rapidly in the human population. Human activity has contributed greatly enabling viruses to gain hold in the global population. Without significant investment in surveillance, diagnostics, and public health infrastructure to identify and contain novel or reemerging viruses, the question of the next pandemic is not *if* but *when*.

HIV: the silent pandemic

Human immunodeficiency viruses (HIV), the causative agents of AIDS, was first identified in 1983, two years after AIDS was recognized as a new disease (Barre-Sinoussi et al., 1983; Gallo et al., 1984). HIV-1 and HIV-2 are both the result of multiple cross-species transmissions of simian immunodeficiency viruses (SIVs), which naturally infect African primates, which likely occurred sporadically throughout the 1900s. Although most of these transfers resulted in viruses that spread in humans to a limited extent, one transmission event, SIVcpz from chimpanzees in southeastern Cameroon, gave rise to the primary driver of the AIDS pandemic: HIV-1 group M (Sharp and Hahn, 2011). Unlike most viruses with pandemic potential, HIV-1 primarily spreads as a sexually transmitted disease and is not transmitted by casual contact. Since its identification, HIV-1 has infected over 75 million people and caused over 33 million deaths, and there are 38 million people living with HIV globally at the end of 2019 (UNAIDS). HIV is unique from prior

pandemics in that it causes a persistent, life-long infection, as HIV is a retrovirus that stably integrates into the host genome. Currently, there is no widespread cure for HIV, and patients must take antiretroviral therapy for life to control the virus.

In the 2010s, the United Nations set targets to diagnose 90% of all people living with HIV-1 by 2020, although this effort was hampered significantly by the COVID-19 pandemic. The World Health Organization (WHO) estimates that only 81% of people infected with HIV-1 currently know their HIV-1 status, and the Center for Disease Control and Prevention (CDC) approximates that persons unaware of their HIV status account for ~40% of ongoing transmissions in the United States (Dailey et al., 2017). The CDC additionally estimates that the median diagnosis delay is currently 3 years (Dailey et al., 2017). People who know their infection status early can be referred to immediate antiretroviral therapy (ART). Early ART is now recognized to maximize benefits for the individual's health and can prevent transmission to sexual and drug injecting partners and prevent mother-to-child transmission of HIV-1 (Branson et al., 2006).

Upon infection, HIV-1 primarily infects CD4⁺ T cells, taking hold in the mucosal tissues, and within days spreads to the lymphoid organs – this is termed the “eclipse” phase. At approximately the tenth day after exposure, the virus becomes detectable in the blood. The virus then continues to spread through the body in an exponential manner in the “acute” phase over the next few weeks and typically peaks at about day 30, when HIV antibody levels become detectable and begin to control the virus to a certain degree. A “set point” in viral load is established, in which the level of HIV replication remains fairly stable for years. Over time, HIV causes progressive loss of these CD4⁺ T cells, which eventually results in immunodeficiency. At this stage – AIDS – is when patients first presented early in the pandemic, usually with an opportunistic infection or oncological complication. Thus, HIV infection is often “silent” for many years until this stage and the infected person can unknowingly pass on the virus, unless they are tested through pro-active screening. When untreated, the typical person progresses to death over a period of approximately ten years. However, ART can suppress viral replication to undetectable

levels, improving immune function and greatly reducing the risk of developing AIDS (Deeks et al., 2015).

HIV persists as a lifelong infection as a result of stably integrating into the host genome. After gaining entry into a cell, HIV's genome, a single-stranded RNA, is reverse transcribed into DNA and integrated into the host chromatin. By hijacking host enzymes, HIV is transcribed from the host genome, proteins are produced, and mature virions are assembled and released for infection of additional cells. ART functions by blocking various stages of the viral lifecycle, including viral attachment to the cell, fusion to the cell, reverse transcription, integration, maturation, and blocking the viral proteases. However, once integrated as a provirus, the virus is nearly impossible to excise from all infected cells, although this is an area of active research. In fact, HIV establishes a quiescent (or latent) infection within memory CD4⁺ T cells, which form the long-lived viral reservoir that can be established in as few as 3 days after infection. These cells are maintained indefinitely, primarily through homeostatic proliferation. Importantly, to date, there is no clear single biomarker to identify the latent reservoir – latently infected CD4⁺ T cells are undistinguishable from uninfected cells to both researchers and the immune system. Although ART can prevent the infection of new cells, it cannot eliminate the already infected cells that make up the reservoir. Thus, once ART is stopped or interrupted, viral rebound occurs rapidly as a result of this persistent, latent reservoir. (Deeks et al., 2015). As a result, the development of an HIV cure or sustained ART-free viral suppression has become a major priority of the HIV field. To validate potential HIV cure drugs, patients must undergo analytical treatment interruptions (ATIs), which require rigorous monitoring of HIV RNA levels for potential viral rebound.

As an RNA virus, HIV-1 evolves rapidly within individual hosts and accumulates mutations that allow the viral population to evade immune recognition and makes vaccine, drug, and diagnostic development more challenging. Mutations can arise during reverse transcription, during forward transcription by the human RNA polymerase II, or through host factor-mediated mutagenesis. In particular, host cytidine deaminases of the A3 family result in hypermutated viral

sequences. The HIV-1 reverse transcriptase also plays a major role in the high mutation rate, as it lacks proofreading activity and has an estimated error rate on the order of about 3×10^{-5} per base per round of copying (Cuevas et al., 2015; Zanini et al., 2017). Many of these mutations result in defective proviruses, rather than intact ones that are competent to replicate and produce infective virus. These defective proviruses often contain fatal defects such as large deletions or hypermutations. Many standard PCR assays use short subgenomic amplicons in conserved regions that are unable to distinguish intact and defective proviruses (Bruner et al., 2016; Bruner et al., 2019). This has complicated attempts to quantify the viral reservoir, and the high variability of HIV sequences requires that diagnostics are able to identify conserved regions.

Despite nearly 40 years since its emergence, the HIV pandemic remains an urgent public health priority. The Joint United Nations Programme on HIV/AIDS (UNAIDS) launched the 90-90-90 project to achieve the following goals by the year 2020: 1) identify 90% of people living with HIV, 2) initiate 90% of all people who know their status on ART, and 3) maintain viral suppression among 90% of people receiving ART. Point-of-care HIV viral load testing will serve as an essential tool for ensuring a sustainable response to enable an end to the HIV/AIDS pandemic (Drain et al., 2019). The development of rapid and portable HIV RNA self-tests will enable not only the identification of new infections, but also serve as a critical tool for expanding ATI studies. Self-tests will allow at-risk individuals to access testing without the barriers that health care settings traditionally pose, and empower HIV cure trial participants to monitor their viral load status without repeated clinic visits.

SARS-CoV-2: the pandemic that defined 2020

SARS-CoV-2 was the third highly pathogenic coronavirus to emerge in the human population in the twenty-first century, after SARS-CoV in 2002 and Middle East respiratory syndrome coronavirus (MERS-CoV) in 2012. Emerging coronaviruses are a new, major public health concern in the twenty first century. SARS-CoV-2 has surpassed SARS and MERS in both

the number of people infected and the wide geographic spread of epidemic areas. The first recorded case was reported in December 2019 as a pneumonia of unknown cause. By the end of the month, there were 27 cases of pneumonia of unknown cause in Wuhan. These patients showed symptoms of viral pneumonia, including fever, cough, and in severe cases dyspnea and bilateral lung infiltration apparent on CT. Most of these cases were linked to the Huanan Seafood Wholesale Market, a wet market in Wuhan that sells live animals, including poultry and wildlife (Hu et al., 2020).

The virus was quickly identified as a novel coronavirus by January 9, 2020 using metagenomic RNA sequencing, and the first genome was published on January 10, 2020. Meanwhile, cases continued to grow in patients with no history of exposure to the wet market, suggesting human-to-human transmission of the new virus. Within 1 month, the novel coronavirus had spread to all 34 provinces in China. By the end of January, the WHO declared the outbreak a public health emergency of international concern (Hu et al., 2020). By late February, the daily number of new cases in China started to decrease, but the international spread was only just accelerating. As a result of the high transmission efficiency of SARS-CoV-2 and international travel, the virus spread worldwide rapidly. On March 11, 2020, the WHO officially recognized the global COVID-19 outbreak as a pandemic. By August, 216 countries and regions from all six continents had reported more than 20 million cases of COVID-19. High mortality occurred when the health-care resources were overwhelmed, even in countries like the United States (Hu et al., 2020). Importantly, up to ~40% of patients were found to be asymptomatic and capable of spread, complicating efforts to identify and isolate infected individuals (Bai et al., 2020; Chamie et al., 2020; Lavezzo et al., 2020).

SARS-CoV-2 is a betacoronavirus, sharing 79% sequence identity with SARS-CoV. It is a nearly 30 kilobase, positive-sense, single-stranded RNA virus and has a similar genome organization with other betacoronaviruses. It has six functional open reading frame (ORFs) – from 5' to 3' they are the replicase (ORF1ab), spike (S), envelope (E), membrane (M), and

nucleocapsid (N). There are also seven putative ORFS that encode accessory proteins. The replicase gene encompasses the majority of the viral genome (nearly two-thirds) and is proteolytically cleaved into 16 non-structural proteins involved in transcription and virus replication (Hu et al., 2020). Similar to other positive-strand RNA viruses, replication of the genome involved continuous negative strand RNA synthesis to create a full-length complementary template. To create progeny genomes, this template is copied into multiple positive strand genomes. This replication is accomplished by the viral RNA-dependent RNA polymerase (RdRp), with other replicative enzymes that form the replication-transcription complex. RNA virus replication is typically a highly error-prone process that leads to the virus existing as diverse populations of genome mutants or “quasispecies.” Importantly, coronaviruses have a unique 3’ to 5’ exonuclease proofreading function encoded by nsp14 that ensures the maintenance and replication fidelity of the large SARS-CoV-2 genome (Robson et al., 2020). This reduced error rate and therefore mutation rate is promising for diagnostic and vaccine development.

Many countries, such as Australia, South Korea, Singapore, and Taiwan, managed to contain the COVID-19 pandemic early. The United States, on the other hand, has the most cases and deaths in the world, characterized by a highly disorganized and ineffectual response. One key factor to the failures of the US response to COVID-19 has been testing, which has played a major role in COVID-19 control elsewhere. Testing to identify people infected was extremely slow to start, and is still not ramped up to this day. In January and February, testing was delayed as the Centers for Disease Control and Prevention (CDC) distributed faulty test kits and then failed to efficiently approve working tests developed by the WHO or by local public health laboratories. The US has largely fallen back on an inconsistent series of nonpharmacologic interventions (NPIs), including mask mandates and stay-at-home orders, that vary wildly by state, county, and city. The continued shortage of test materials has forced a very narrow testing strategy, and long test-to-result turnaround times. This leads to delayed identification and isolation of symptomatic, pre-symptomatic, and asymptomatic people, and allows for continued and unmitigated spread of

disease. The lack of testing not only hampers diagnosis of patients, but also makes epidemic forecasting models more uncertain and unreliable. Given the long period of time some states have had business closures and other restrictions, the public is increasingly frustrated with these models and many are calling for ending the restrictions, despite rising cases and dropping ICU bed availability. Expanding testing and using rapid tests could not only break transmission chains, but improve government planning and public trust (Schneider, 2020). The over-reliance on the gold standard diagnostic tool, RT-qPCR, has further hampered testing efforts, as backlogs have led to varying sample-to-result turnaround times that range from 24 hours to 10 days. Faster assays with lower limits of detection have the potential to break the pandemic transmission cycle if used to screen populations repeatedly (Larremore et al., 2020).

Until the population has been broadly vaccinated to ensure herd immunity, the ongoing COVID-19 pandemic will continue to pose a major burden on society without intervention. Rapid, portable diagnostics are urgently needed to allow the US to gain control of the pandemic, identify and isolate asymptomatic individuals, and allow society to reopen.

CRISPR ushers in a new age of rapid and portable diagnostics

CRISPR-Cas13a is a type VI CRISPR enzyme first characterized in 2016 that assembles with CRISPR RNAs (crRNAs) to recognize and cleave RNA substrates matching the virally derived segment of the crRNA, or spacer (Abudayyeh et al., 2016; East-Seletsky et al., 2016). Cas13a is a component of the bacterial adaptive immune system thought to interfere with invading viruses. Cas13a has two conserved HEPN (Higher Eukaryotes and Prokaryotes Nucleotide-binding) domains, which are frequently suggestive of RNase activity (Shmakov et al., 2015). Although most prokaryotic adaptive immune systems generally target DNA substrates, Cas13a specifically cleaves single-stranded (ss) RNA substrates. CRISPR-Cas13a binds and cleaves target ssRNAs in a sequence-specific manner (*cis*-cleavage) and subsequently exerts general RNase activity (*trans*-cleavage) (Abudayyeh et al., 2016; East-Seletsky et al., 2016). Upon

binding of the Cas13a-crRNA complex to its target RNA, Cas13a undergoes significant conformational changes. The target RNA serves as an activator, bringing the catalytic residues of HEPN1 and HEPN2 into close proximity. The two conserved HEPN domains of Cas13a fold closely together to form the active catalytic site for RNA-guided RNA cleavage (Liu et al., 2017a). While the catalytic pockets face the inside of the protein in Cas9, Cas12a, and Cas12b, the Cas13a RNA-guided RNA cleavage site is located on the outer surface of Cas13a. The exposed location of this catalytic pocket is hypothesized to contribute to the promiscuous RNA cleavage activity of Cas13a (Liu et al., 2017b). It has been posited that because target cleavage occurs at the outer surface of Cas13a and away from the guide-target RNA duplex region, the external positioning of the catalytic site allows for cooperative cleaving of target RNA by multiple Cas13a molecules (Liu et al., 2017b). The proposed model is that the exposed HEPN catalytic site of activated Cas13a indiscriminately captures any exposed RNAs and cleaves them in a non-specific manner (Liu et al., 2017a). Cas13a can be programmed with crRNAs for specific RNA sensing.

Over the last several years, CRISPR-Cas13a has emerged as a viable alternative to conventional methods of detecting and quantifying RNA with RT-PCR and can be leveraged for CRISPR-based diagnostics. Attomolar (10^{-18} molar) or zeptomolar (10^{-21} molar) sensitivity is often required for diagnostic applications and can be obtained using qPCR or digital droplet (dd) PCR in HIV detection (Gootenberg et al., 2017). An ideal Cas13a-based diagnostic would achieve similar sensitivity and specificity, and directly detect replication-competent HIV RNA without RT or PCR-based amplification steps. Most reports thus far have indicated sensitivities in the femtomolar (10^{-15} molar) range (East-Seletsky et al., 2017; Gootenberg et al., 2017). In 2017, the laboratory of Dr. Feng Zhang reported a Cas13a-based detection system that reached attomolar sensitivity in detecting Zika virus by using an additional reverse transcription (RT) step for isothermal amplification of Zika virus cDNA, which was ultimately back-transcribed into RNA for RNA-based Cas13a detection, a method referred to as “SHERLOCK” (Specific High Sensitivity

Enzymatic Reporter UnLOCKing) (Gootenberg et al., 2017). A subsequent study found that detection could be pushed to the zeptomolar scale, bringing it to single molecule/milliliter sensitivity (Gootenberg et al., 2018). Additional work has been done on other CRISPR enzymes, especially Cas12a, which recognizes DNA. In 2018, CRISPR-Cas12a, a type V CRISPR, was shown to bind DNA and unleashed indiscriminate single-stranded DNA cleavage activity. This activity was harnessed for sensitive detection of DNA virus human papillomavirus (HPV) in an assay termed “DETECTR” (DNA endonuclease-targeted CRISPR trans reporter) (Chen et al., 2018).

With the COVID-19 pandemic, CRISPR diagnostics (CRISPR dx) have gained increasing attention for their speed and portability. Many CRISPR-based SARS-CoV-2 diagnostics have since been developed and published that can provide sensitive results in under an hour (Broughton et al., 2020; Hou et al., 2020; Joung et al., 2020). CRISPR dx have also been developed to test for many pathogens simultaneously to provide for broader pathogen surveillance and discovery in CARMEN-Cas13 (Combinatorial Arrayed Reactions for Multiplexed Evaluation of Nucleic acids and Cas13 detection) (Ackerman et al., 2020). There have been increasing efforts to develop these technologies into a one-pot, extraction free, and field deployable format (Arizti-Sanz et al., 2020; Myhrvold et al., 2018). With further development and refinement, CRISPR dx stands to serve as an important tool for rapid and portable nucleic acid-based diagnostics.

Dissertation objective and hypothesis

The objective of this dissertation was to develop amplification-free strategies for CRISPR-Cas13-based detection of HIV and SARS-CoV-2 RNA. Although previous methods improved the sensitivity of Cas13a, they introduce two unwanted steps in the RT and *in vitro* transcription steps, and provide only qualitative, not quantitative, data. I hypothesize that these steps are not necessary for sensitive HIV RNA detection if the Cas13a system is rigorously optimized. By

systematically improving all components of the system, I demonstrate a rationally designed assay amenable for sensitive and specific SARS-CoV-2 and HIV RNA detection and quantification.

REFERENCES

- Abudayyeh, O.O., Gootenberg, J.S., Konermann, S., Joung, J., Slaymaker, I.M., Cox, D.B., Shmakov, S., Makarova, K.S., Semenova, E., Minakhin, L., *et al.* (2016). C2c2 is a single-component programmable RNA-guided RNA-targeting CRISPR effector. *Science* 353, aaf5573.
- Ackerman, C.M., Myhrvold, C., Thakku, S.G., Freije, C.A., Metsky, H.C., Yang, D.K., Ye, S.H., Boehm, C.K., Kosoko-Thoroddsen, T.F., Kehe, J., *et al.* (2020). Massively multiplexed nucleic acid detection with Cas13. *Nature* 582, 277-282.
- Arizti-Sanz, J., Freije, C.A., Stanton, A.C., Boehm, C.K., Petros, B.A., Siddiqui, S., Shaw, B.M., Adams, G., Kosoko-Thoroddsen, T.F., Kemball, M.E., *et al.* (2020). Integrated sample inactivation, amplification, and Cas13-based detection of SARS-CoV-2. *bioRxiv*.
- Bai, Y., Yao, L., Wei, T., Tian, F., Jin, D.Y., Chen, L., and Wang, M. (2020). Presumed Asymptomatic Carrier Transmission of COVID-19. *JAMA*.
- Barre-Sinoussi, F., Chermann, J.C., Rey, F., Nugeyre, M.T., Chamaret, S., Gruest, J., Dauguet, C., Axler-Blin, C., Vezinet-Brun, F., Rouzioux, C., *et al.* (1983). Isolation of a T-lymphotropic retrovirus from a patient at risk for acquired immune deficiency syndrome (AIDS). *Science* 220, 868-871.
- Branson, B.M., Handsfield, H.H., Lampe, M.A., Janssen, R.S., Taylor, A.W., Lyss, S.B., Clark, J.E., Centers for Disease, C., and Prevention (2006). Revised recommendations for HIV testing of adults, adolescents, and pregnant women in health-care settings. *MMWR Recomm Rep* 55, 1-17; quiz CE11-14.
- Broughton, J.P., Deng, X., Yu, G., Fasching, C.L., Servellita, V., Singh, J., Miao, X., Streithorst, J.A., Granados, A., Sotomayor-Gonzalez, A., *et al.* (2020). CRISPR–Cas12-based detection of SARS-CoV-2. *Nature Biotechnology* 38, 870-874.

- Bruner, K.M., Murray, A.J., Pollack, R.A., Soliman, M.G., Laskey, S.B., Capoferri, A.A., Lai, J., Strain, M.C., Lada, S.M., Hoh, R., *et al.* (2016). Defective proviruses rapidly accumulate during acute HIV-1 infection. *Nat Med* 22, 1043-1049.
- Bruner, K.M., Wang, Z., Simonetti, F.R., Bender, A.M., Kwon, K.J., Sengupta, S., Fray, E.J., Beg, S.A., Antar, A.A.R., Jenike, K.M., *et al.* (2019). A quantitative approach for measuring the reservoir of latent HIV-1 proviruses. *Nature* 566, 120-125.
- Castagna, A., Muccini, C., Galli, L., Bigoloni, A., Poli, A., Spagnuolo, V., Nozza, S., Racca, S., Galli, A., Cinque, P., *et al.* (2019). Analytical treatment interruption in chronic HIV-1 infection: time and magnitude of viral rebound in adults with 10 years of undetectable viral load and low HIV-DNA (APACHE study). *J Antimicrob Chemother* 74, 2039-2046.
- Chamie, G., Marquez, C., Crawford, E., Peng, J., Petersen, M., Schwab, D., Schwab, J., Martinez, J., Es, D.J., Black, D., *et al.* (2020). SARS-CoV-2 Community Transmission disproportionately affects Latinx population during Shelter-in-Place in San Francisco. *Clin Infect Dis*.
- Chen, H., Liu, K., Li, Z., and Wang, P. (2019). Point of care testing for infectious diseases. *Clin Chim Acta* 493, 138-147.
- Chen, J.S., Ma, E., Harrington, L.B., Da Costa, M., Tian, X., Palefsky, J.M., and Doudna, J.A. (2018). CRISPR-Cas12a target binding unleashes indiscriminate single-stranded DNase activity. *Science* 360, 436-439.
- Cuevas, J.M., Geller, R., Garijo, R., Lopez-Aldeguer, J., and Sanjuan, R. (2015). Extremely High Mutation Rate of HIV-1 In Vivo. *PLoS Biol* 13, e1002251.
- Dailey, A.F., Hoots, B.E., Hall, H.I., Song, R., Hayes, D., Fulton, P., Jr., Prejean, J., Hernandez, A.L., Koenig, L.J., and Valleroy, L.A. (2017). Vital Signs: Human Immunodeficiency Virus Testing and Diagnosis Delays - United States. *MMWR Morb Mortal Wkly Rep* 66, 1300-1306.

- Deeks, S.G., Lewin, S.R., Ross, A.L., Ananworanich, J., Benkirane, M., Cannon, P., Chomont, N., Douek, D., Lifson, J.D., Lo, Y.-R., *et al.* (2016). International AIDS Society global scientific strategy: towards an HIV cure 2016. *Nature Medicine* 22, 839-850.
- Deeks, S.G., Overbaugh, J., Phillips, A., and Buchbinder, S. (2015). HIV infection. *Nat Rev Dis Primers* 1, 15035.
- Dong, E., Du, H., and Gardner, L. (2020). An interactive web-based dashboard to track COVID-19 in real time. *Lancet Infect Dis* 20, 533-534.
- Drain, P.K., Dorward, J., Bender, A., Lillis, L., Marinucci, F., Sacks, J., Bershteyn, A., Boyle, D.S., Posner, J.D., and Garrett, N. (2019). Point-of-Care HIV Viral Load Testing: an Essential Tool for a Sustainable Global HIV/AIDS Response. *Clin Microbiol Rev* 32.
- East-Seletsky, A., O'Connell, M.R., Burstein, D., Knott, G.J., and Doudna, J.A. (2017). RNA Targeting by Functionally Orthogonal Type VI-A CRISPR-Cas Enzymes. *Mol Cell* 66, 373-383 e373.
- East-Seletsky, A., O'Connell, M.R., Knight, S.C., Burstein, D., Cate, J.H., Tjian, R., and Doudna, J.A. (2016). Two distinct RNase activities of CRISPR-C2c2 enable guide-RNA processing and RNA detection. *Nature* 538, 270-273.
- Gallo, R.C., Salahuddin, S.Z., Popovic, M., Shearer, G.M., Kaplan, M., Haynes, B.F., Palker, T.J., Redfield, R., Oleske, J., Safai, B., *et al.* (1984). Frequent detection and isolation of cytopathic retroviruses (HTLV-III) from patients with AIDS and at risk for AIDS. *Science* 224, 500-503.
- Girard, M.P., Tam, J.S., Assossou, O.M., and Kieny, M.P. (2010). The 2009 A (H1N1) influenza virus pandemic: A review. *Vaccine* 28, 4895-4902.
- Gootenberg, J.S., Abudayyeh, O.O., Kellner, M.J., Joung, J., Collins, J.J., and Zhang, F. (2018). Multiplexed and portable nucleic acid detection platform with Cas13, Cas12a, and Csm6. *Science* 360, 439-444.

- Gootenberg, J.S., Abudayyeh, O.O., Lee, J.W., Essletzbichler, P., Dy, A.J., Joung, J., Verdine, V., Donghia, N., Daringer, N.M., Freije, C.A., *et al.* (2017). Nucleic acid detection with CRISPR-Cas13a/C2c2. *Science* 356, 438-442.
- Grubaugh, N.D., Ladner, J.T., Lemey, P., Pybus, O.G., Rambaut, A., Holmes, E.C., and Andersen, K.G. (2018). Tracking virus outbreaks in the twenty-first century. *Nature Microbiology* 4, 10-19.
- Hasan, S., Ahmad, S.A., Masood, R., and Saeed, S. (2019). Ebola virus: A global public health menace: A narrative review. *J Family Med Prim Care* 8, 2189-2201.
- Holkmann Olsen, C., Mocroft, A., Kirk, O., Vella, S., Blaxhult, A., Clumeck, N., Fisher, M., Katlama, C., Phillips, A., and Lundgren, J. (2007). Interruption of combination antiretroviral therapy and risk of clinical disease progression to AIDS or death. *HIV medicine* 8.
- Hou, T., Zeng, W., Yang, M., Chen, W., Ren, L., Ai, J., Wu, J., Liao, Y., Gou, X., Li, Y., *et al.* (2020). Development and evaluation of a rapid CRISPR-based diagnostic for COVID-19. *PLoS Pathog* 16, e1008705.
- Hu, B., Guo, H., Zhou, P., and Shi, Z.-L. (2020). Characteristics of SARS-CoV-2 and COVID-19. *Nature Reviews Microbiology*, 1-14.
- Jacob, S.T., Crozier, I., Fischer, W.A., Hewlett, A., Kraft, C.S., Vega, M.-A.d.L., Soka, M.J., Wahl, V., Griffiths, A., Bollinger, L., *et al.* (2020). Ebola virus disease. *Nature Reviews Disease Primers* 6, 1-31.
- Joung, J., Ladha, A., Saito, M., Kim, N.G., Woolley, A.E., Segel, M., Barretto, R.P.J., Ranu, A., Macrae, R.K., Faure, G., *et al.* (2020). Detection of SARS-CoV-2 with SHERLOCK One-Pot Testing. *N Engl J Med* 383, 1492-1494.
- Julg, B., Dee, L., Ananworanich, J., Barouch, D.H., Bar, K., Caskey, M., Colby, D.J., Dawson, L., Dong, K.L., Dube, K., *et al.* (2019). Recommendations for analytical antiretroviral treatment interruptions in HIV research trials-report of a consensus meeting. *Lancet HIV* 6, e259-e268.

- Larremore, D.B., Wilder, B., Lester, E., Shehata, S., Burke, J.M., Hay, J.A., Tambe, M., Mina, M.J., and Parker, R. (2020). Test sensitivity is secondary to frequency and turnaround time for COVID-19 screening. *Science Advances*.
- Lavezzo, E., Franchin, E., Ciavarella, C., Cuomo-Dannenburg, G., Barzon, L., Vecchio, C.D., Rossi, L., Manganelli, R., Loregian, A., Navarin, N., *et al.* (2020). Suppression of a SARS-CoV-2 outbreak in the Italian municipality of Vo'. *Nature*, 1-5.
- Lazer, D., Santillana, M., Perlis, R.H., Ognyanova, K., Baum, M.A., Quintana, A., Druckman, J., Della Volpe, J., Chwe, H., and Simonson, M. (2020). THE STATE OF THE NATION: A 50-STATE COVID-19 SURVEY REPORT #8: FAILING THE TEST. OSF Preprints.
- Liu, L., Li, X., Ma, J., Li, Z., You, L., Wang, J., Wang, M., Zhang, X., and Wang, Y. (2017a). The Molecular Architecture for RNA-Guided RNA Cleavage by Cas13a. *Cell* 170, 714-726 e710.
- Liu, L., Li, X., Wang, J., Wang, M., Chen, P., Yin, M., Li, J., Sheng, G., and Wang, Y. (2017b). Two Distant Catalytic Sites Are Responsible for C2c2 RNase Activities. *Cell* 168, 121-134 e112.
- Madhav, N., Oppenheim, B., Gallivan, M., Mulembakani, P., Rubin, E., and Wolfe, N. (2017). Pandemics: Risks, Impacts, and Mitigation. In *Disease Control Priorities: Improving Health and Reducing Poverty*, rd, D.T. Jamison, H. Gelband, S. Horton, P. Jha, R. Laxminarayan, C.N. Mock, and R. Nugent, eds. (Washington (DC)).
- Mina, M.J., Parker, R., and Larremore, D.B. (2020). Rethinking Covid-19 Test Sensitivity — A Strategy for Containment. *New England Journal of Medicine*.
- Musso, D., Ko, A.I., and Baud, D. (2019). Zika Virus Infection - After the Pandemic. *N Engl J Med* 381, 1444-1457.
- Myhrvold, C., Freije, C.A., Gootenberg, J.S., Abudayyeh, O.O., Metsky, H.C., Durbin, A.F., Kellner, M.J., Tan, A.L., Paul, L.M., Parham, L.A., *et al.* (2018). Field-deployable viral diagnostics using CRISPR-Cas13. *Science* 360, 444-448.

- Nistal-Villán, E., and García-Sastre, A. (2020). Attacking the flu: New prospects for the rational design of antivirals. *Nature Medicine* 15, 1253-1254.
- Pannus, P., Rutsaert, S., De Wit, S., Allard, S.D., Vanham, G., Cole, B., Nescoi, C., Aerts, J., De Spiegelaere, W., Tsoumanis, A., *et al.* (2020). Rapid viral rebound after analytical treatment interruption in patients with very small HIV reservoir and minimal on-going viral transcription. *J Int AIDS Soc* 23, e25453.
- Parra, J.M., Salmeron, O.J., and Velasco, M. (2014). The first case of Ebola virus disease acquired outside Africa. *N Engl J Med* 371, 2439-2440.
- Petersen, E., Koopmans, M., Go, U., Hamer, D.H., Petrosillo, N., Castelli, F., Storgaard, M., Al Khalili, S., and Simonsen, L. (2020). Comparing SARS-CoV-2 with SARS-CoV and influenza pandemics. *Lancet Infect Dis* 20, e238-e244.
- Robson, F., Khan, K.S., Le, T.K., Paris, C., Demirbag, S., Barfuss, P., Rocchi, P., and Ng, W.L. (2020). Coronavirus RNA Proofreading: Molecular Basis and Therapeutic Targeting. *Mol Cell* 79, 710-727.
- Schneider, E.C. (2020). Failing the Test - The Tragic Data Gap Undermining the U.S. Pandemic Response. *N Engl J Med* 383, 299-302.
- Schroeder, L., Amukele, T., and Piai, M. (2016). Why The World Needs An Essential Diagnostics List. In *Forbes*.
- Sharp, P.M., and Hahn, B.H. (2011). Origins of HIV and the AIDS pandemic. *Cold Spring Harb Perspect Med* 1, a006841.
- Shi, Z., and Hu, Z. (2008). A review of studies on animal reservoirs of the SARS coronavirus. *Virus Res* 133, 74-87.
- Shmakov, S., Abudayyeh, O.O., Makarova, K.S., Wolf, Y.I., Gootenberg, J.S., Semenova, E., Minakhin, L., Joung, J., Konermann, S., Severinov, K., *et al.* (2015). Discovery and Functional Characterization of Diverse Class 2 CRISPR-Cas Systems. *Mol Cell* 60, 385-397.

- Shultz, J.M., Espinel, Z., Espinola, M., and Rechkemmer, A. (2016). Distinguishing epidemiological features of the 2013-2016 West Africa Ebola virus disease outbreak. *Disaster Health* 3, 78-88.
- Steehler, K., Siegler, A.J., and Kraft, C.S. (2019). Bringing HIV Self-Testing to Scale in the United States: a Review of Challenges, Potential Solutions, and Future Opportunities. *Journal of Clinical Microbiology*.
- Stohr, W., Fidler, S., McClure, M., Weber, J., Cooper, D., Ramjee, G., Kaleebu, P., Tambussi, G., Schechter, M., Babiker, A., *et al.* (2013). Duration of HIV-1 viral suppression on cessation of antiretroviral therapy in primary infection correlates with time on therapy. *PLoS One* 8, e78287.
- Wang, C., Horby, P.W., Hayden, F.G., and Gao, G.F. (2020). A novel coronavirus outbreak of global health concern. *Lancet* 395, 470-473.
- Wu, F., Zhao, S., Yu, B., Chen, Y.M., Wang, W., Song, Z.G., Hu, Y., Tao, Z.W., Tian, J.H., Pei, Y.Y., *et al.* (2020). A new coronavirus associated with human respiratory disease in China. *Nature* 579, 265-269.
- Zanini, F., Puller, V., Brodin, J., Albert, J., and Neher, R.A. (2017). In vivo mutation rates and the landscape of fitness costs of HIV-1. *Virus Evol* 3, vex003.
- Zappa, A., Amendola, A., Romano, L., and Zanetti, A. (2009). Emerging and re-emerging viruses in the era of globalisation. *Blood Transfus* 7, 167-171.
- Zhou, P., Yang, X.L., Wang, X.G., Hu, B., Zhang, L., Zhang, W., Si, H.R., Zhu, Y., Li, B., Huang, C.L., *et al.* (2020). A pneumonia outbreak associated with a new coronavirus of probable bat origin. *Nature* 579, 270-273.

Chapter 2: Harnessing CRISPR-Cas13a Towards Direct Detection of HIV-1 RNA

Detection of viral RNA is the gold standard of HIV-1 diagnostics, but current *state-of-the-art* testing requires laboratory access and cannot be performed at home. In addition, a reverse transcription (RT) step is commonly used before PCR-based quantitative detection, which diminishes sensitivity and reproducibility of the current laboratory-based assay (Bustin et al., 2015). Moreover, detection and quantification of HIV in other contexts, such as in laboratory estimations of the latent reservoir, has been problematic. To date, no PCR-based assay provides a precise and internally consistent indication of the amount of replication-competent HIV in resting cells, as such assays frequently detect defective proviruses that cannot produce infectious virus (Crooks et al., 2015). There is a critical need to develop new technologies for sensitive, easy-to-handle detection of HIV-1 RNA that allows frequent at-home testing and preferentially involves no RT step. Failure to address this need will delay progress towards an effective functional cure, prolong the HIV-1 epidemic, and continue to shorten life- and health-spans of infected individuals, especially the most vulnerable and economically deprived.

Offering accurate and sensitive testing in the privacy of somebody's home combined with assisted partner notification is considered a cornerstone of a consolidated community- and facility-based screening campaign to reduce the burden of HIV-1 worldwide. However, accurate detection of HIV-1 in acute and chronic infections is challenging. Acute HIV-1 infection is the phase of HIV-1 disease immediately after infection and is characterized by detectable HIV-1 viremia or p24 antigen, but a yet undetectable antibody response (Branson et al., 2006; Pilcher et al., 2010). However, to date, all HIV self-testing products are serology-based, detecting antibodies to HIV-1 on average four weeks to three months after exposure. Some fourth-generation assays combine antibody detection with p24 antigen measurements, which allows HIV-1 detection sometimes as early as ~18 days after exposure but has a large 18–90 days detection window. This window is currently a major argument against HIV-1 self-testing, as self-tests with a large window period can provide false-negative results during acute infection, false reassurance, and can promote sex

between discordant partners at the time of highest infectivity (Wood et al., 2014). As a result, the majority of early testing is currently laboratory-based and directed against nucleic acids of the viral genome (NAT), reliably detecting HIV-1 RNA about one week after exposure. However, self-testing is overwhelmingly preferred with the majority of study participants indicating that they would test more often if a rapid self-test were available (Wood et al., 2014). In addition, current guidelines recommend ART treatment for all individuals infected with HIV-1, including during very early infections where the latent reservoir is seeded within days (Whitney et al., 2014). Similarly, frequent NAT-based testing is required after treatment interruptions of chronically infected individuals who all present antibodies and are thus limited to NAT-based, and not antibody-based, strategies and subject to frequent laboratory visits. Development of a sensitive NAT-based self-test addresses both the issue of early detection in acute infection and detection of viral re-emergence in the presence of positive antibody titers.

We hypothesize that the RNA-binding properties of newly discovered CRISPR/Cas13a proteins (previously called C2c2) are suitable for sensitive at-home detection of HIV-1 RNA in biological samples without employing RT or amplification steps. The Cas13a system in combination with HIV-specific guide or CRISPR RNAs (crRNAs) can be adapted to sensitive detection of HIV-1 RNAs without amplification steps. Comprehensive exploration of the biological properties of the Cas13a system in combination with optimized detection methods will enable direct HIV-1 RNA measurements with unique advantages for self-testing: a single-step procedure, mobile-based detection technology, no RT and amplification steps. By coupling the Cas13a reaction to an RNA-based fluorescent reporter, we can harness Cas13a's collateral or non-specific RNase activity for HIV detection (**Figure 2.1**). The RNA-stimulated cleavage of substrates by Cas13a in *trans* can be utilized to detect specific RNA as it is proportional to the concentration of “activator” RNA. By adding a fluorophore quencher-labelled reporter RNA that is cleaved upon “activator” RNA-triggered RNase activation of Cas13a (in our case HIV-1 RNA), HIV-specific transcripts can be measured in a dose-responsive manner using fluorescence as read-out.

In order to truly replace qPCR as the gold-standard laboratory test for NAT and HIV diagnosis, a Cas13a-based diagnostic must achieve similar sensitivity and specificity. Frequently, attomolar sensitivity is required for diagnostic applications and can be obtained using qPCR and digital droplet (dd) PCR in HIV diagnosis (Gootenberg et al., 2017). Although studies on Cas13a are limited as it was first described in 2016 (Abudayyeh et al., 2016; East-Seletsky et al., 2016; Shmakov et al., 2015), most reports thus far have indicated sensitivities in the femtomolar range (East-Seletsky et al., 2017; Gootenberg et al., 2017). In 2017, the lab of Dr. Feng Zhang reported a Cas13a-based detection system that reached attomolar sensitivity in detecting Zika virus but it included an additional RT step for isothermal amplification of Zika virus cDNA, which was ultimately back-transcribed into RNA for RNA-based detection, a method referred to as SHERLOCK (Specific High Sensitivity Enzymatic Reporter UnLOCKing) (Gootenberg et al., 2017). Although this method improved the sensitivity of Cas13a, it introduced two unwanted steps in the RT and *in vitro* transcription steps that minimizes its potential as a self-testing device. Further adjustments to the protocol enabled zeptomolar detection (Gootenberg et al., 2018).

Here we hypothesize that these RT and amplification steps are not necessary for attomolar detection if the Cas13a system is rigorously optimized. By systematically improving all components of the system (choice of Cas13a homolog, optimization of crRNA and fluorescent reporter RNA) and by coupling it to sensitive cell phone-based detection technology, we plan to engineer a rationally designed single-step assay amenable to home testing.

We first designed a pilot set of 8 crRNAs based on previously published primer sites (Laird et al., 2015; Pasternak et al., 2008; Procopio et al., 2015). The HIV-1 RNA genome has extensive secondary structure composed of many local and long-distance interactions (Sukosd et al., 2015). These interactions are important as Cas13a preferentially cleaves ssRNA, and not dsRNA found in i.e. hairpins, and is affected by target accessibility. Briefly, we form Cas13a ribonucleoprotein complexes (RNPs) by incubating purified Cas13a protein with HIV-specific crRNAs. Cas13a RNPs are combined with purified RNA from cell lines and a quenched reporter RNA (RNase Alert,

IDT). When the Cas13a RNP complex binds its activator, HIV RNA, the complex becomes activated as a general, non-specific RNase. Active Cas13a then cleaves the quenched reporter RNA molecule, releasing fluorescence that is detected via Spectramax i3x plate reader or Tecan Infinite Pro plate reader. Background fluorescence is calculated by running Cas13a RNPs with non-activating Jurkat RNA and subtracting background fluorescence values. We found that of the original 8 crRNAs, two crRNAs in particular, crRNA 3 and crRNA 5, gave the highest signal against the HIV-1 RNA target, while minimizing target-independent background fluorescence from RNP alone controls (not shown). The locations of crRNA 3 and crRNA 5 are shown relative to the HIV-1 RNA genome (Sukosd et al., 2015) (**Figure 2.2**). We used the *Leptotrichia buccalis* (Lbu) Cas13a protein, as previous studies demonstrated that LbuCas13a gave the fastest kinetics of Cas13a-catalyzed ssRNA cleavage relative to other variants (East-Seletsky et al., 2017).

We next tested crRNA 3 against RNA isolated from two replication-competent cell lines: ACH-2 and U-1 cell lines. Following activation, these cell lines contain both cell-associated HIV RNA and release HIV virions into the supernatant (Emiliani et al., 1998; Emiliani et al., 1996) to phenocopy detection of circulating viruses in the blood. We treated U-1 and ACH-2 cell lines with $\text{TNF}\alpha$, and collected cell pellets and concentrated the remaining supernatant. We extracted RNA from each sample, and then determined presence of HIV RNA via Cas13a detection. We isolated Cas13a RNPs are able to detect both supernatant and cell-associated HIV RNA robustly (**Figure 2.3A**), and were able to detect supernatant RNA at lower total RNA concentrations than cell-associated RNA. We hypothesize this is due to reduced, background cellular RNA transcripts in the supernatant compared to the cell extracts.

We hypothesized that one way to improve detection sensitivity would be to combine crRNAs. Combining crRNAs increased sensitivity over using a single crRNA alone. We treated J-Lat 11.1 cells with $\text{TNF}\alpha$ and collected cell pellets. latently infected J-Lat cell lines. These Jurkat cells contain a full-length HIV-1 provirus encoding GFP in place of the *Nef* gene for monitoring

transcriptional activity by flow cytometry (Jordan et al., 2003). After combining two crRNAs Cas13a detected half as much HIV RNA than when using a single crRNA incubated with twice as much RNA (**Figure 2.3B**). Together, these studies demonstrate that the sensitivity of the assay may be improved by detecting virion HIV RNA and by combining crRNAs.

We next wanted to systematically optimize various aspects of the reaction to improve detection. We first tested various crRNA stem lengths: a 29-mer, 30-mer, and 31-mer stem region. The spacer region (20 nucleotide) remained unchanged. We found that the 30-mer stem gave the most sensitive detection at 3 different target concentrations (50 pM, 10 pM, and 1 pM) (**Figure 2.4A**). We next tested the formation of the RNPs by altering the molar ratio of crRNA to Cas13a. Tested over two concentrations of target RNA (10 pM and 1 pM), we found that the 1:1 molar ratio gave the highest signal to background ratio (**Figure 2.4B**). Finally, we have designed and tested new FAM-based reporters based on cleavage preferences for LbuCas13a. Previous studies showed that LbuCas13a exhibits preferred cleavage of the homo-uridine substrate (East-Seletsky et al., 2017). We tested a 5-mer polyU reporter (UUUUU reporter) with a 5'-FAM fluorophore and 3'-Iowa Black quencher, and compared it to a reporter containing a single uridine (CCUCC reporter) and our original reporter, RNase Alert (IDT). We found significantly improved detection using 400 nM of the polyU reporter, compared to the single uridine or RNase Alert reporters, when detecting the same concentration of target (**Figure 2.4C**).

Together, these improvements can be combined into an optimized assay that allows for more robust detection of HIV RNA. In **Figure 2.4D**, our advancements (multiplexing guides and improving the reporter) have been combined with improvements in crRNA design and RNP formation into a “new,” optimized assay. When compared with the “old,” non-optimized assay, we observe improvement in detection of HIV RNA transcripts from TNF α -treated J-lat 11.1 cellular RNA samples (**Figure 2.4D**). We anticipate that these optimizations, when combined, will allow for sensitive detection of HIV RNA from patient samples.

We have additionally worked to design and synthesize a set of 100 crRNAs targeting conserved regions of Group M and Subtype B HIV strains in collaboration with Dr. Bette Korber and Dr. James Theiler at the Los Alamos National Laboratory. In addition to targeting conserved HIV sequences, these crRNAs were also designed to take into account *Leptotrichia buccalis* (Lbu) Cas13a preferences for mismatches along the 20-nucleotide spacer regions. We screened each crRNA individually against RNA extracted from VSV-G-pseudotyped HIV-1 NL4-3 Δ Env EGFP reporter virus (Zhang et al., 2004). The HIV-1 NL4-3 plasmid was sequenced to be able to accurately predict precise mismatches. In order to normalize the screen fluorescence results across multiple plates and identify top-performing, we also ran control reactions using the same concentration of RNA against our two best crRNAs, crRNA 3 and crRNA 5. In order to more precisely identify crRNAs that would provide the best kinetics for HIV detection, we calculated the slope of the simple linear regression of the two hour time course for each crRNA. The *slope ratio* for each guide was calculated as follows: $Slope\ ratio = \frac{Slope\ of\ RNP+NL4-3\ RNA}{Slope\ of\ RNP\ alone}$. Each individual guide slope ratio is shown in **Figure 2.5A**. We next compared each guide to crRNA 3. We calculated the “*crRNA 3 score*” as follows: $crRNA\ 3\ score = \frac{Slope\ ratio\ of\ crRNA\ x}{Slope\ ratio\ of\ crRNA\ 3}$ (**Figure 2.5B**), and the “*crRNA 5 score*” as follows: $crRNA\ 5\ score = \frac{Slope\ ratio\ of\ crRNA\ x}{Slope\ ratio\ of\ crRNA\ 5}$ (**Figure 2.5C**). Any score greater than or equal to 1.0 (white or green on the heat map) means that the candidate crRNA performed at least as well as crRNA 3 or crRNA 5 against the same concentration of target RNA. To visualize how the crRNA performed according to position along the sequenced genome, we plotted the *crRNA 5 score* against the genomic position of each crRNA, demonstrating that a handful of candidate crRNAs performed at least as well as crRNA 5 ($crRNA\ 5\ score \geq 1.0$) and that they were distributed along the genome (**Figure 2.5D**). Many crRNAs contained at least 1 mismatch, including mismatches in the central “seed” region of the spacer (crRNA spacer positions 5-8) (Tambe et al., 2018), that could impact the activation of Cas13a and subsequent reporter cleavage. We mapped the performance of the crRNAs by overall *slope ratio*, and

highlighted those with predicted spacer mismatches. As expected, many of the best performing crRNAs contained zero mismatches. However, some crRNAs continued to perform well despite mismatches along the spacer region, including in the mismatch-sensitive seed region (**Figure 2.5E**). Finally, to assess the impact of splitting the 100 crRNAs across three assay plates, we plotted the *crRNA 3 score* and *crRNA 5 score* for each crRNA. Although there were slight variations between plates, there did not appear to be major batch-related effects that would significantly impact our interpretation of the data together (**Figure 2.5F**).

In the future, we plan to take the top 15 performing crRNAs from this screen and systematically test them in combination to identify an ideal crRNA set for sensitive detection of HIV-1 RNA. We will then test the limit of detection of the optimized assay, first in lab-based samples, and then in clinical samples with greater sequence diversity. To enable eventual self-testing, we will determine which bodily fluids (whole blood, plasma, or serum) allow accurate testing without RNA purification and low background, how to best stabilize test reagents for use at room temperature, and how the Cas13a-based assay compares to conventional viral load assays in a large number of cryopreserved and fresh samples from HIV⁺ individuals.

In summary, CRISPR-Cas13a has emerged as a viable alternative to conventional methods of detecting and quantifying RNA with RT-PCR, and can be leveraged for CRISPR-based diagnostics. Cas13a, which targets RNA directly, can be programmed with crRNAs to provide a platform for specific RNA sensing. By coupling it to an RNA-based reporter, we can harness its collateral or non-specific RNase activity for HIV detection. In the future, to enable self-testing, we will combine this with innovative mobile phone-based detection. Mobile phone spread is high worldwide with an estimated 91% mobile phone penetration in the US alone. As mobile phone usage “democratizes” and “cultivates” next generation biomedical research, we expect a large surge in new diagnostic tools suitable for self-testing (McLeod et al., 2015; Ozcan, 2014). Cell phone cameras are the most ubiquitous optical sensors in the developed and developing worlds, and have been used both as microscopes and spectrometers (Berg et al., 2015; Lin et al.,

2015; Skandarajah et al., 2014; Smith et al., 2011). In addition, the cell phone with its core-processors, data connectivity, and bandwidth has unique computational power, which can be utilized for advanced diagnostics applications. Combining Cas13a and mobile phone-based technologies, we expect this discovery to open new research directions and applications, particularly in diagnostics of HIV and other RNA-based pathogens.

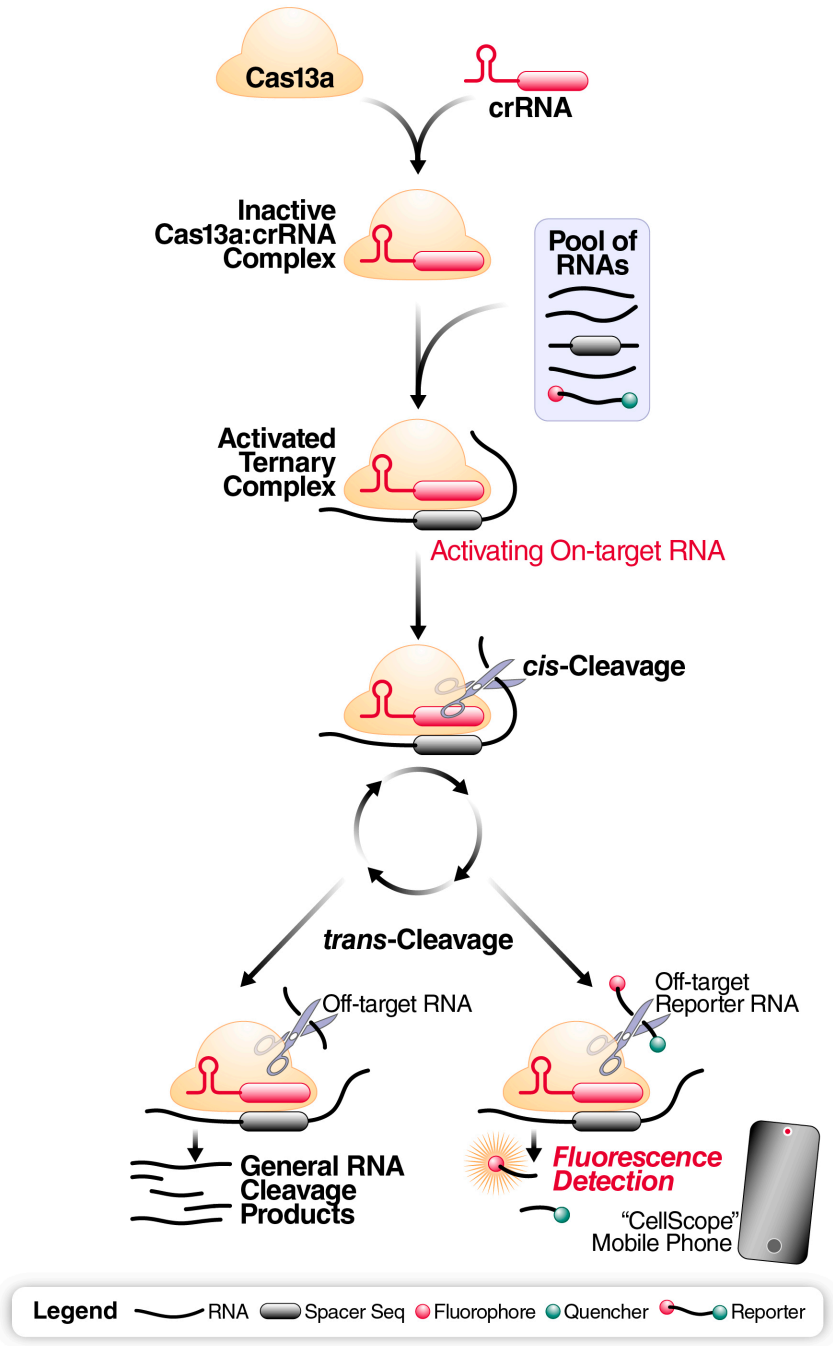
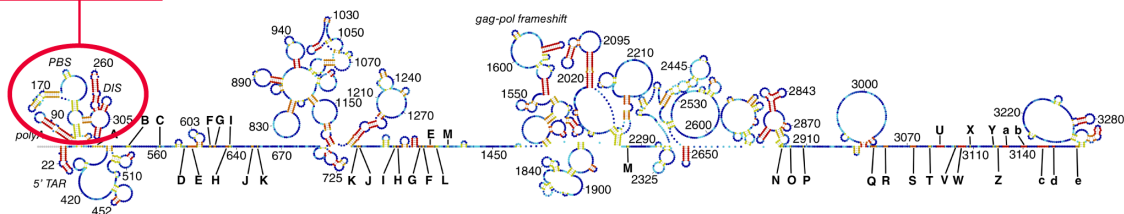
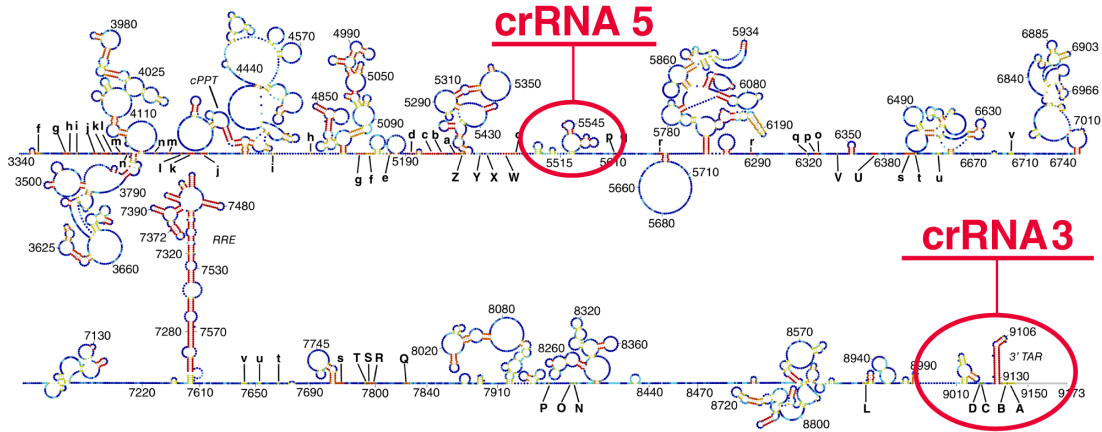


Figure 2.1: CRISPR-Cas13a can be paired with an RNA-based quenched-fluorescent reporter to provide specific detection of HIV RNA.

crRNA 3



crRNA 5



crRNA 3

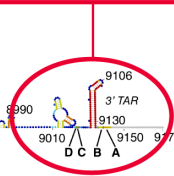


Figure 2.2: Schematic of crRNA 3 and crRNA 5 recognition sites overlaid on the HIV-1 RNA genome. The predicted HIV-1 RNA map is adapted from (Sukosd et al., 2015).

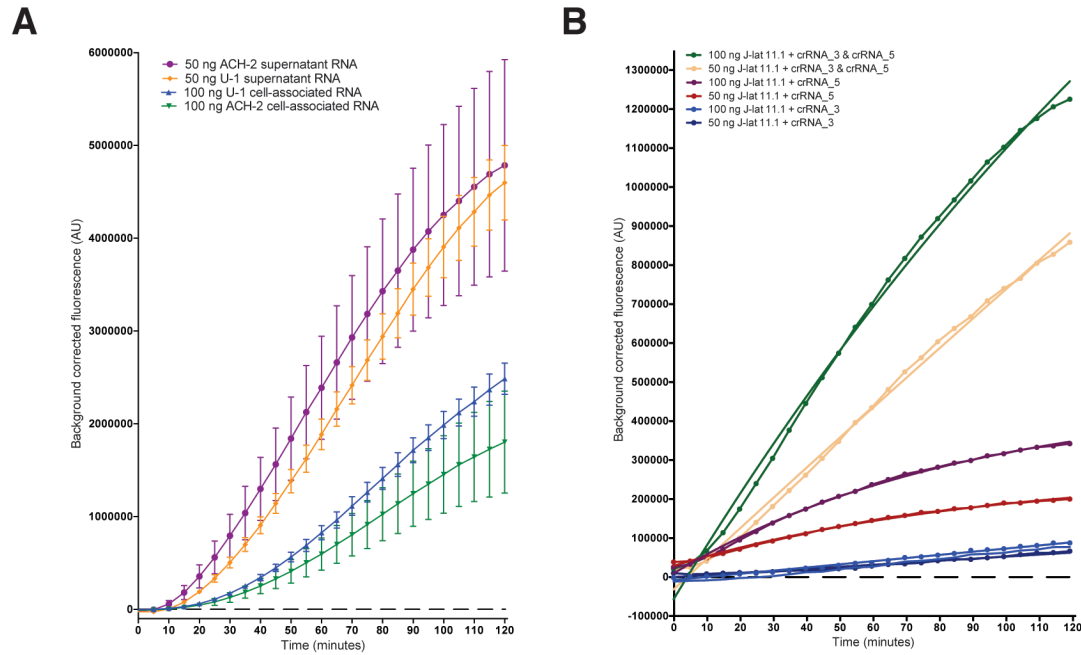


Figure 2.3: Cas13a RNPs detect HIV transcripts from diverse cell lines and combining crRNAs improves sensitivity. (A) Cas13a RNPs formed with crRNA 3 detect HIV transcripts in total RNA isolated from TNF α -treated U-1 and ACH-2 cell pellets and concentrated supernatant fractions, and require less RNA to achieve robust detection in the supernatant fraction. Mean \pm SD are shown. (B) Multiplexing of crRNAs allows for more robust detection of lower quantities of HIV RNA. Using Cas13a RNPs formed with both crRNA #3 and crRNA #5 simultaneously allowed for better detection of cell-associated HIV transcripts from TNF α -treated J-Lat 11.1 cells. Using both RNPs allowed for improved HIV detection from only 50 ng of total RNA compared to detection of 100 ng total RNA using a single crRNA. Shown are means of technical triplicates, with a corresponding line to indicate the linear regression of the curve. Background corrected fluorescence refers to computational subtraction of RNP only values at each time point from reactions with target RNA.

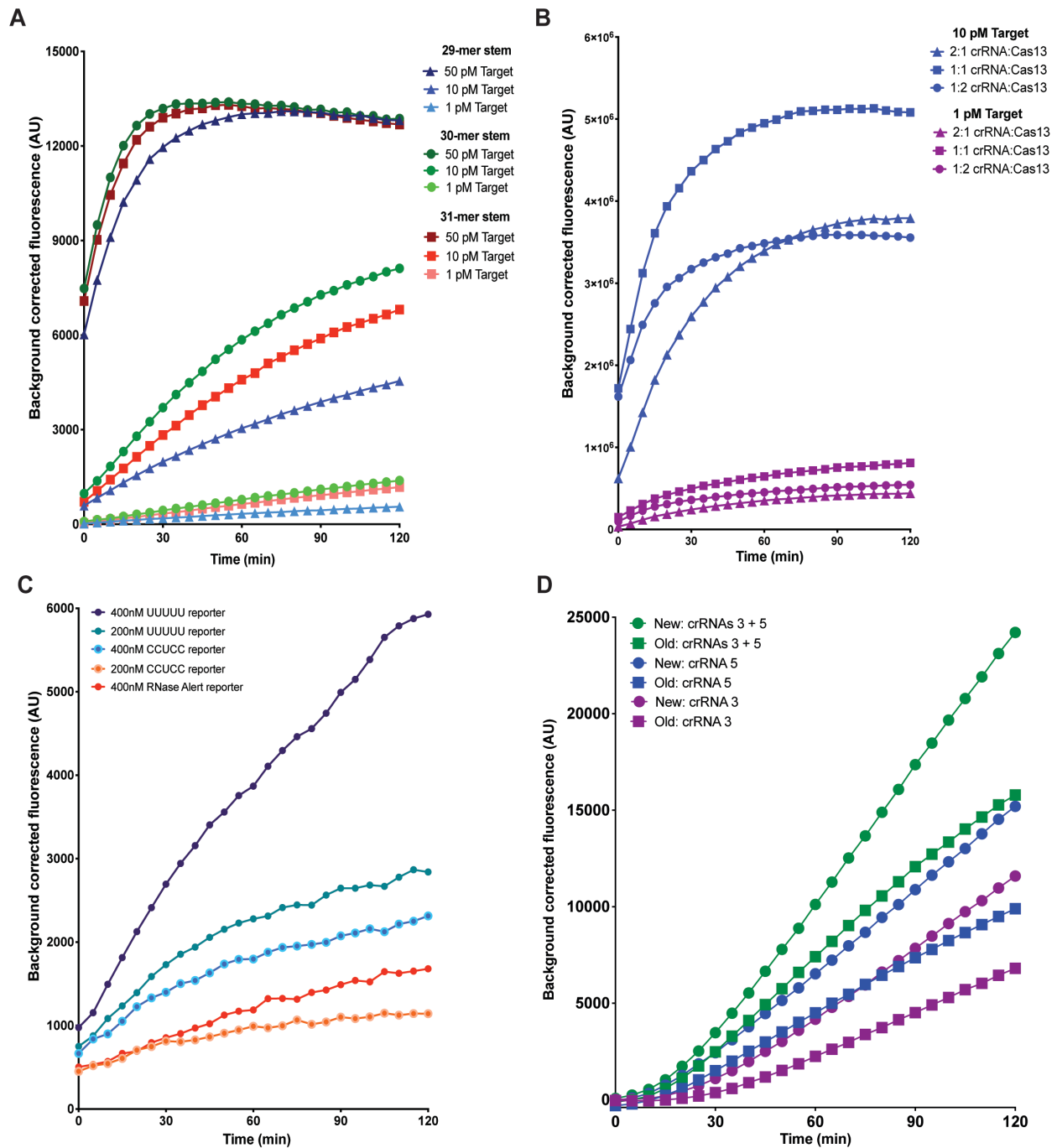


Figure 2.4: Optimization of the Cas13a assay leads to improved detection of target RNA. (A) Alterations to the crRNA stem sequence and length leads to improved detection of low levels of target RNA. The 30-mer crRNA stem sequence allowed for the most robust detection of target RNA across all concentrations (50 pM, 10 pM, or 1 pM). (B) Formation of the RNP complex at varying ratios of crRNA and Cas13a leads to differential detection of target RNA. Forming RNPs at a 1:1 ratio allowed for the most robust detection of target RNA at 10 pM and 1 pM concentrations. (C) Changing the reporter RNA sequence towards LbuCas13a cleavage preferences improves detection of target RNA. Adjusting the reporter sequence to UUUUU allowed for significant improvement in detection of 50 fM of target RNA. (D) The “new” assay

combines improvements in RNP formation (1:1 ratio) and reporter concentration (400 nM) compared to the “old” assay (1:2 ratio crRNA:Cas13 and 167 nM reporter). 100 ng of RNA isolated from TNF α -treated J-lat 11.1 cell pellets were used in each reaction. Shown for all are means of triplicates. Background corrected fluorescence refers to computational subtraction of RNP only values at each time point from reactions with target RNA.

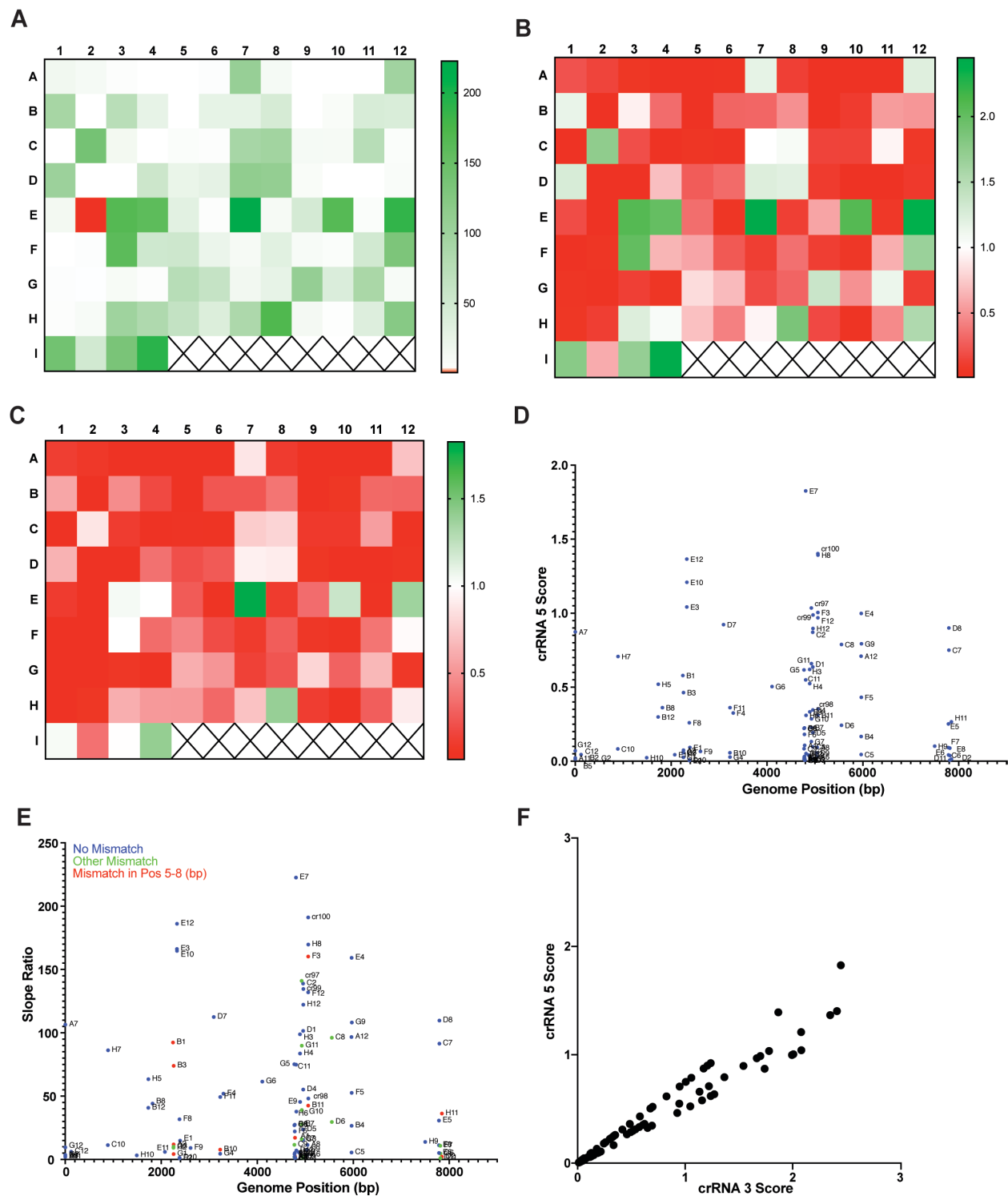


Figure 2.5: Screening of 100 candidate crRNAs reveals potential crRNAs for sensitive HIV-1 detection. (A) The *slope ratio* of each individual crRNA is shown. **(B)** The *crRNA 3 score* for each candidate crRNA is shown to provide cross-plate normalization and to highlight crRNAs with improved detection (indicated by a score ≥ 1.0). **(C)** The *crRNA 5 score* for each candidate crRNA is shown to provide cross-plate normalization and to highlight crRNAs with improved detection

(indicated by a score ≥ 1.0). **(D)** The *crRNA 5 score* for each individual crRNA is shown, plotted against its location on the HIV-1 genome. **(E)** The *slope ratio* for each candidate crRNA is shown, plotted against its location on the HIV-1 genome. Mismatches are identified by color, indicating 0 mismatches, or at least 1 mismatch either in position 5-8 of the crRNA spacer or on another location along the 20-nucleotide spacer sequence. **(F)** *crRNA 5 score* vs. *crRNA 3 score* for each candidate crRNA is shown.

REFERENCES

- Abudayyeh, O.O., Gootenberg, J.S., Konermann, S., Joung, J., Slaymaker, I.M., Cox, D.B., Shmakov, S., Makarova, K.S., Semenova, E., Minakhin, L., *et al.* (2016). C2c2 is a single-component programmable RNA-guided RNA-targeting CRISPR effector. *Science* 353, aaf5573.
- Berg, B., Cortazar, B., Tseng, D., Ozkan, H., Feng, S., Wei, Q., Chan, R.Y., Burbano, J., Farooqui, Q., Lewinski, M., *et al.* (2015). Cellphone-Based Hand-Held Microplate Reader for Point-of-Care Testing of Enzyme-Linked Immunosorbent Assays. *ACS Nano* 9, 7857-7866.
- Branson, B.M., Handsfield, H.H., Lampe, M.A., Janssen, R.S., Taylor, A.W., Lyss, S.B., Clark, J.E., Centers for Disease, C., and Prevention (2006). Revised recommendations for HIV testing of adults, adolescents, and pregnant women in health-care settings. *MMWR Recomm Rep* 55, 1-17; quiz CE11-14.
- Bustin, S., Dhillon, H.S., Kirvell, S., Greenwood, C., Parker, M., Shipley, G.L., and Nolan, T. (2015). Variability of the reverse transcription step: practical implications. *Clin Chem* 61, 202-212.
- Crooks, A.M., Bateson, R., Cope, A.B., Dahl, N.P., Griggs, M.K., Kuruc, J.D., Gay, C.L., Eron, J.J., Margolis, D.M., Bosch, R.J., *et al.* (2015). Precise Quantitation of the Latent HIV-1 Reservoir: Implications for Eradication Strategies. *J Infect Dis* 212, 1361-1365.
- East-Seletsky, A., O'Connell, M.R., Burstein, D., Knott, G.J., and Doudna, J.A. (2017). RNA Targeting by Functionally Orthogonal Type VI-A CRISPR-Cas Enzymes. *Mol Cell* 66, 373-383 e373.
- East-Seletsky, A., O'Connell, M.R., Knight, S.C., Burstein, D., Cate, J.H., Tjian, R., and Doudna, J.A. (2016). Two distinct RNase activities of CRISPR-C2c2 enable guide-RNA processing and RNA detection. *Nature* 538, 270-273.

- Emiliani, S., Fischle, W., Ott, M., Van Lint, C., Amella, C.A., and Verdin, E. (1998). Mutations in the tat gene are responsible for human immunodeficiency virus type 1 postintegration latency in the U1 cell line. *J Virol* 72, 1666-1670.
- Emiliani, S., Van Lint, C., Fischle, W., Paras, P., Jr., Ott, M., Brady, J., and Verdin, E. (1996). A point mutation in the HIV-1 Tat responsive element is associated with postintegration latency. *Proc Natl Acad Sci U S A* 93, 6377-6381.
- Gootenberg, J.S., Abudayyeh, O.O., Kellner, M.J., Joung, J., Collins, J.J., and Zhang, F. (2018). Multiplexed and portable nucleic acid detection platform with Cas13, Cas12a, and Csm6. *Science* 360, 439-444.
- Gootenberg, J.S., Abudayyeh, O.O., Lee, J.W., Essletzbichler, P., Dy, A.J., Joung, J., Verdine, V., Donghia, N., Daringer, N.M., Freije, C.A., *et al.* (2017). Nucleic acid detection with CRISPR-Cas13a/C2c2. *Science* 356, 438-442.
- Jordan, A., Bisgrove, D., and Verdin, E. (2003). HIV reproducibly establishes a latent infection after acute infection of T cells in vitro. *EMBO J* 22, 1868-1877.
- Laird, G.M., Bullen, C.K., Rosenbloom, D.I., Martin, A.R., Hill, A.L., Durand, C.M., Siliciano, J.D., and Siliciano, R.F. (2015). Ex vivo analysis identifies effective HIV-1 latency-reversing drug combinations. *J Clin Invest* 125, 1901-1912.
- Lin, R., Skandarajah, A., Gerver, R.E., Neira, H.D., Fletcher, D.A., and Herr, A.E. (2015). A lateral electrophoretic flow diagnostic assay. *Lab Chip* 15, 1488-1496.
- McLeod, E., Wei, Q., and Ozcan, A. (2015). Democratization of Nanoscale Imaging and Sensing Tools Using Photonics. *Anal Chem* 87, 6434-6445.
- Ozcan, A. (2014). Mobile phones democratize and cultivate next-generation imaging, diagnostics and measurement tools. *Lab Chip* 14, 3187-3194.
- Pasternak, A.O., Adema, K.W., Bakker, M., Jurriaans, S., Berkhout, B., Cornelissen, M., and Lukashov, V.V. (2008). Highly sensitive methods based on seminested real-time reverse

- transcription-PCR for quantitation of human immunodeficiency virus type 1 unspliced and multiply spliced RNA and proviral DNA. *J Clin Microbiol* 46, 2206-2211.
- Pilcher, C.D., Christopoulos, K.A., and Golden, M. (2010). Public health rationale for rapid nucleic acid or p24 antigen tests for HIV. *J Infect Dis* 201 Suppl 1, S7-15.
- Procopio, F.A., Fromentin, R., Kulpa, D.A., Brehm, J.H., Bebin, A.G., Strain, M.C., Richman, D.D., O'Doherty, U., Palmer, S., Hecht, F.M., *et al.* (2015). A Novel Assay to Measure the Magnitude of the Inducible Viral Reservoir in HIV-infected Individuals. *EBioMedicine* 2, 874-883.
- Shmakov, S., Abudayyeh, O.O., Makarova, K.S., Wolf, Y.I., Gootenberg, J.S., Semenova, E., Minakhin, L., Joung, J., Konermann, S., Severinov, K., *et al.* (2015). Discovery and Functional Characterization of Diverse Class 2 CRISPR-Cas Systems. *Mol Cell* 60, 385-397.
- Skandarajah, A., Reber, C.D., Switz, N.A., and Fletcher, D.A. (2014). Quantitative imaging with a mobile phone microscope. *PLoS One* 9, e96906.
- Smith, Z.J., Chu, K., Espenson, A.R., Rahimzadeh, M., Gryshuk, A., Molinaro, M., Dwyre, D.M., Lane, S., Matthews, D., and Wachsmann-Hogiu, S. (2011). Cell-phone-based platform for biomedical device development and education applications. *PLoS One* 6, e17150.
- Sukosd, Z., Andersen, E.S., Seemann, S.E., Jensen, M.K., Hansen, M., Gorodkin, J., and Kjems, J. (2015). Full-length RNA structure prediction of the HIV-1 genome reveals a conserved core domain. *Nucleic Acids Res* 43, 10168-10179.
- Tambe, A., East-Seletsky, A., Knott, G.J., Doudna, J.A., and O'Connell, M.R. (2018). RNA Binding and HEPN-Nuclease Activation Are Decoupled in CRISPR-Cas13a. *Cell Rep* 24, 1025-1036.
- Whitney, J.B., Hill, A.L., Sanisetty, S., Penaloza-MacMaster, P., Liu, J., Shetty, M., Parenteau, L., Cabral, C., Shields, J., Blackmore, S., *et al.* (2014). Rapid seeding of the viral reservoir prior to SIV viraemia in rhesus monkeys. *Nature* 512, 74-77.

Wood, B.R., Ballenger, C., and Stekler, J.D. (2014). Arguments for and against HIV self-testing. *HIV AIDS (Auckl)* 6, 117-126.

Zhang, H., Zhou, Y., Alcock, C., Kiefer, T., Monie, D., Siliciano, J., Li, Q., Pham, P., Cofrancesco, J., Persaud, D., *et al.* (2004). Novel single-cell-level phenotypic assay for residual drug susceptibility and reduced replication capacity of drug-resistant human immunodeficiency virus type 1. *J Virol* 78, 1718-1729.

Chapter 3: Amplification-free detection of SARS-CoV-2 with CRISPR-Cas13a and mobile phone microscopy

Parinaz Fozouni^{1,2,3,4,24}, Sungmin Son^{5,24}, María Díaz de León Derby^{5,6,24}, Gavin J. Knott^{7,8}, Carley N. Gray^{1,4}, Michael V. D'Ambrosio⁵, Chunyu Zhao⁹, Neil A. Switz¹⁰, G. Renuka Kumar^{1,4}, Stephanie I. Stephens^{1,4}, Daniela Boehm^{1,4}, Chia-Lin Tsou^{1,4}, Jeffrey Shu^{1,4}, Abdul Bhuiya^{5,6}, Maxim Armstrong¹¹, Andrew R. Harris⁵, Pei-Yi Chen^{1,4}, Jeannette M. Osterloh¹, Anke Meyer-Franke¹, Bastian Joehnk^{12,13}, Keith Walcott¹², Anita Sil^{2,3,12}, Charles Langelier^{9,14}, Katherine S. Pollard^{1,3,9,15,16}, Emily D. Crawford^{9,12}, Andreas S. Puschnik⁹, Maira Phelps⁹, Amy Kistler⁹, Joseph L. DeRisi^{2,3,9,17}, Jennifer A. Doudna^{1,7,11,18,19,20}, Daniel A. Fletcher^{1,5,6,9,21,22,23*}, Melanie Ott^{1,2,3,4,25*}

Affiliations

¹J. David Gladstone Institutes, San Francisco, CA 94158, USA

²Medical Scientist Training Program, University of California, San Francisco, CA 94143, USA

³Biomedical Sciences Graduate Program, University of California, San Francisco, CA 94143, USA

⁴Department of Medicine, University of California, San Francisco, CA 94143, USA

⁵Department of Bioengineering, University of California, Berkeley, CA 94720, USA

⁶UC Berkeley-UC San Francisco Graduate Program in Bioengineering, University of California, Berkeley, CA 94720 USA

⁷Department of Molecular and Cell Biology, University of California, Berkeley, CA 94720, USA

⁸Monash Biomedicine Discovery Institute, Department of Biochemistry & Molecular Biology, Monash University, Victoria 3800, Australia

⁹Chan Zuckerberg Biohub, San Francisco, CA 94158, USA

¹⁰Department of Physics and Astronomy, San José State University, San Jose, CA 95192, USA

¹¹Molecular Biophysics and Integrated Bioimaging Division, Lawrence Berkeley National Laboratory, Berkeley, CA 94720, USA

¹²Department of Microbiology and Immunology, University of California, San Francisco, CA 94143, USA

¹³Current address: LegenDairy Foods GmbH, Rheinbach 53359, Germany

¹⁴Division of Infectious Diseases, University of California, San Francisco, CA 94143, USA

¹⁵Institute for Human Genetics, University of California, San Francisco, CA 94143, USA

¹⁶Department of Epidemiology and Biostatistics and Institute of Computational Health Sciences, University of California, San Francisco, CA 94143, USA

¹⁷Division of Biochemistry and Biophysics, University of California, San Francisco, CA 94143, USA

¹⁸Department of Chemistry, University of California, Berkeley, CA 94720, USA

¹⁹Innovative Genomics Institute, University of California, Berkeley, CA 94720, USA

²⁰Howard Hughes Medical Institute, University of California, Berkeley, CA 94720, USA

²¹Biophysics Program, University of California, Berkeley, CA, 94720, USA

²²California Institute for Quantitative Biosciences (QB3), University of California, Berkeley, CA 94720, USA

²³Division of Biological Systems and Engineering, Lawrence Berkeley National Laboratory, Berkeley, CA 94720, USA

²⁴These authors contributed equally

²⁵Lead Contact

*Correspondence: Daniel A. Fletcher, fletch@berkeley.edu, and Melanie Ott, melanie.ott@gladstone.ucsf.edu.

SUMMARY

The December 2019 outbreak of a novel respiratory virus, SARS-CoV-2, has become an ongoing global pandemic due in part to the challenge of identifying symptomatic, asymptomatic and pre-symptomatic carriers of the virus. CRISPR diagnostics can augment gold-standard PCR-based testing if they can be made rapid, portable and accurate. Here we report the development of an amplification-free CRISPR-Cas13a assay for direct detection of SARS-CoV-2 from nasal swab RNA that can be read with a mobile phone microscope. The assay achieved ~100 copies/ μ L sensitivity in under 30 minutes of measurement time and accurately detected pre-extracted RNA from a set of positive clinical samples in under 5 minutes. We combined crRNAs targeting SARS-CoV-2 RNA to improve sensitivity and specificity, and directly quantified viral load using enzyme kinetics. Integrated with a reader device based on a mobile phone, this assay has the potential to enable rapid, low-cost, point-of-care screening for SARS-CoV-2.

Keywords

CRISPR-Cas13, CRISPR Dx, SARS-CoV-2, COVID-19, point-of-care diagnostics, mobile phone microscopy

INTRODUCTION

In late 2019, a novel infectious respiratory RNA virus, severe acute respiratory syndrome (SARS)-coronavirus (CoV)-2, emerged in the human population, likely from a zoonotic source (Wang et al., 2020a; Zhu et al., 2020). In most people, SARS-CoV-2 infection causes mild or no symptoms. Critically, however, asymptomatic or lowly symptomatic carriers spread the virus, leading to delayed isolation of carriers and worldwide spread (Bai et al., 2020; Lavezzo et al., 2020). In particular, this silent transmission has led to the infection of individuals who are at increased risk of severe illness due to age or pre-existing conditions such as obesity, diabetes, cancer, immunosuppression, or cardiac, pulmonary, and kidney disease (Williamson et al., 2020).

The current gold-standard diagnostic for SARS-CoV-2 infection, quantitative reverse transcription polymerase chain reaction (RT-qPCR), is well established and widely used for screening. Based on primers directed against the nucleocapsid (N), envelope (E), and open reading frame 1ab (ORF1ab) genes, RT-qPCR has an analytical limit of detection (LOD) of 1,000 viral RNA copies/mL (1 copy/ μ L) (Vogels et al., 2020). However, recent modeling of viral dynamics suggests that frequent testing with a fast turnaround time is required to break the current pandemic (Larremore et al., 2020). Notably, the model ranked sensitivity of the test as a lower priority, and estimated that an LOD of 100,000 copies/mL (100 copies/ μ L) would be sufficient for screening (Larremore et al., 2020). Although there is not yet broad consensus on the exact target LOD that is necessary, frequent testing and rapid turnaround times will allow less sensitive tests to help reduce viral transmission. In clinical studies, when viral load drops below a million copies/mL (1,000 copies/ μ L), few infectious particles are detected and consequently the risk of transmission is low (La Scola et al., 2020; Quicke et al., 2020; Wolfel et al., 2020).

The need for SARS-CoV-2 tests that are rapid, widespread, and able to identify infectious individuals has motivated efforts to explore new strategies for viral RNA detection based on CRISPR technology. Cas12 and Cas13 proteins are RNA-guided components of bacterial

adaptive immune systems that directly target single- and double-stranded DNA or single-stranded (ss)RNA substrates, respectively (Abudayyeh et al., 2016; Chen et al., 2018; East-Seletsky et al., 2016; Zetsche et al., 2015). Cas13 is complexed with a CRISPR RNA (crRNA) containing a programmable spacer sequence to form a nuclease-inactive ribonucleoprotein complex (RNP). When the RNP binds to complementary target RNA, it activates the HEPN (higher eukaryotes and prokaryotes nucleotide-binding domain) motifs of Cas13 that then indiscriminately cleave any surrounding ssRNAs. Target RNA binding and subsequent Cas13 cleavage activity can be detected with a fluorophore-quencher pair linked by an ssRNA, which fluoresces after cleavage by active Cas13 (East-Seletsky et al., 2016). To date, four type VI CRISPR-Cas13 subtypes have been identified: Cas13a (previously known as C2c2) (Abudayyeh et al., 2016; East-Seletsky et al., 2016; Shmakov et al., 2015), Cas13b (Smargon et al., 2017), Cas13c (Shmakov et al., 2017), and Cas13d (Konermann et al., 2018; Yan et al., 2018).

What initially evolved as a successful strategy in bacteria to induce cellular dormancy to reduce phage transmission (Meeske et al., 2019) is now being harnessed for viral diagnostics (Chen et al., 2018; East-Seletsky et al., 2016; Gootenberg et al., 2018; Gootenberg et al., 2017; Myhrvold et al., 2018). To achieve high sensitivity, current CRISPR diagnostics (CRISPR Dx) rely on pre-amplification of target RNA for subsequent detection by a Cas protein. In the case of RNA-sensing Cas13 proteins, this entails the conversion of RNA to DNA by reverse transcription, DNA-based amplification (i.e., isothermal amplification, loop-mediated isothermal amplification (LAMP)), and transcription back to RNA for detection by Cas13a or Cas13b, an approach named “SHERLOCK” (Gootenberg et al., 2018; Gootenberg et al., 2017). This was recently adapted for SARS-CoV-2 detection (Joung et al., 2020b), and further developed as “SHINE” for testing unextracted samples (Arizti-Sanz et al., 2020). The conversion of amplified DNA back into RNA can be avoided by using the DNA-sensing Cas12 for detection, a method called “DETECTR” (Chen et al., 2018), which has recently been adapted for SARS-CoV-2 detection (Broughton et al., 2020). Both SHERLOCK and DETECTR take approximately an hour to complete and can be

read with paper-based lateral flow strips appropriate for point-of-care use, although current FDA-approved protocols are still laboratory-based.

Here, we report the development and demonstration of a rapid CRISPR-Cas13a-based assay for direct detection of SARS-CoV-2 RNA. This assay, unlike previous CRISPR diagnostics, does not require pre-amplification of the viral genome for detection. By directly detecting the viral RNA without additional manipulations, the test yields quantitative RNA measurements rather than simply a positive or negative result. To demonstrate the simplicity and portability of this assay, we measure fluorescence with a mobile phone camera in a compact device that includes low-cost laser illumination and collection optics. The high sensitivity of mobile phone cameras, together with their connectivity, GPS and data-processing capabilities, have made them attractive tools for point-of-care disease diagnosis in low-resource regions (Breslauer et al., 2009; D'Ambrosio et al., 2015; Kamgno et al., 2017; Wood et al., 2019). By combining multiple crRNAs to increase Cas13a activation and analyzing the change in fluorescence over time rather than solely endpoint fluorescence, we are able to achieve detection of ~ 100 copies/ μL of pre-isolated SARS-CoV-2 RNA within 30 minutes of measurement time on the device. We also correctly identified all SARS-CoV-2 positive patient RNA samples tested (Ct values 14.37 to 22.13) within 5 minutes of measurement time on the device. This approach has the potential to enable a fast, accurate, portable, and low-cost option for point-of care SARS-CoV-2 screening.

RESULTS

Quantitative Direct Detection of Viral SARS-CoV-2 RNA with Cas13a

When the SARS-CoV-2 sequence became public in January 2020, we set out to develop a Cas13-based direct detection assay for viral RNA that would avoid the need for amplification and enable point-of-care testing. To do this, we needed to optimize Cas13 activation through careful crRNA selection and develop a sensitive and portable fluorescence detection system for our assay (Figure 3.1A). Initially, we designed 12 crRNAs (Table S3.1) along the N gene of SARS-CoV-2, corresponding to the three Centers for Disease Control and Prevention (CDC) N qPCR primer sets and a N qPCR primer set developed in Wuhan, China (Zhu et al., 2020). Every Cas13-crRNA RNP should detect a single 20-nucleotide region in the N gene (Figure 3.1B).

We first tested each crRNA individually in a direct detection assay on a plate reader. We selected the Cas13a homolog from *Leptotrichia buccalis* (Lbu) as it demonstrated the highest sensitivity and robust *trans*-cleavage activity relative to other characterized Cas13a homologs (East-Seletsky et al., 2017; East-Seletsky et al., 2016). The assay used purified LbuCas13a (East-Seletsky et al., 2017; East-Seletsky et al., 2016) and a quenched fluorescent RNA reporter (East-Seletsky et al., 2017; East-Seletsky et al., 2016), together with *in vitro* transcribed (IVT) target RNA corresponding to the viral N gene (nucleotide positions 28274–29531). At a target RNA concentration of 480 fM (2.89×10^5 copies/ μ l), we identified 10 crRNAs with reactivity above the RNP alone control containing the same RNP and probe but no target RNA (Figure 3.1C). The use of RNase-free buffers minimized background fluorescence, and the plate reader gain and filter bandwidth settings were optimized to capture low-level reporter cleavage. Similar trends in specific crRNA performance were observed when genomic SARS-CoV-2 RNA was used as target RNA, with lower overall activities corresponding to a lower concentration of RNA (Figure S3.1A). For initial studies, we selected two crRNAs (crRNAs 2 and 4) that generated the greatest Cas13a activation as determined by the fluorescent reporter while maintaining low levels of target-independent fluorescence (indicated by the RNP alone curve).

We next carried out serial dilutions of the target RNA to independently determine the limit of detection for each crRNA. LbuCas13a exhibits detectable reporter cleavage with as little as 10 fM (~6000 copies/ μ L) of target RNA (East-Seletsky et al., 2017). SHERLOCK had previously reported a limit of detection of ~50 fM without pre-amplification (Gootenberg et al., 2017). Consistent with this, we found that RNPs made with either crRNA 2 and crRNA 4 did not appear to generate signals above the RNP controls for an IVT target RNA concentration of 1,000 copies/ μ L (Figure 3.1D). The signal generated by direct detection with Cas13a appeared proportional to the concentration of target RNA in the assay. Given that the signal generated depends solely on the RNase activity of Cas13a, the linear rate of the reaction should approximate Michaelis-Menten enzyme kinetics. To determine if our assay was indeed quantitative, we compared the slopes determined by linear regression for different target RNA concentrations, using 1 to 3 μ M K_M and 600/s K_{cat} for the modeling (Slaymaker et al., 2019). The results confirmed that crRNA 2 and 4 each facilitated detection of at least 10,000 copies/ μ L of IVT N gene RNA (Figure 3.1E). Since the measured slopes are proportional to the concentration of activated Cas13a, we could confirm that the rate of Cas13a activity scaled with concentration of target RNA (Figure S3.1B-D). This ability to estimate target RNA concentration from the measured slope allows for direct quantification of viral load in unknown samples.

Combining crRNAs Improves Sensitivity of Cas13a

We next evaluated whether combining crRNAs to form two different populations of RNPs in the same reaction could enhance overall Cas13a activation and, therefore, the sensitivity of the assay. In theory, a single target RNA could activate multiple Cas13a RNPs if each RNP is directed to different regions of the same viral target RNA, effectively doubling the active enzyme concentration (Figure 3.2A). Targeting multiple sites is especially beneficial in cases where target RNA is the limiting reagent, i.e. in the absence of target pre-amplification. To test this, we combined crRNAs 2 and 4 in the same reaction, keeping the total concentration of Cas13a RNPs

constant but divided equally between RNPs made with each crRNA. We found that combining crRNA 2 and 4 markedly increased the slope of the detection reaction and the sensitivity of the reaction when measured with a fixed IVT target RNA concentration (480 fM) (Figure 3.2B). The slope increased from 213 AU/min (SE \pm 1.6) (crRNA 2) and 159 AU/min (SE \pm 1.7) (crRNA 4), individually, to 383 AU/min (SE \pm 3.0) in combination, without increasing the slope of the RNP control reactions. This nearly doubling of the average slope compared to the individual crRNA reactions demonstrates the advantage of crRNA combinations.

To determine how crRNA combinations affect the limit of detection, we tested crRNA 2+4 with a dilution series of IVT N gene RNA. The RNP combination improved the limit of detection, compared to the no-target RNP control (RNP 2+4), to at least 100 copies/ μ L of IVT target RNA (Figure 3.2C). We performed the same assay with genomic SARS-CoV-2 RNA isolated from the supernatant of SARS-CoV-2-infected Vero CCL-81 cells and found that the assay could detect at least 270 viral copies/ μ L (Slope 12.4 \pm SE 0.3) (Figure 3.2D). Viral copy numbers were determined by standard RT-qPCR. The difference between the N gene IVT and full viral genome limits of detection could be explained by different quantification techniques of the target RNA or by considerable secondary structure in the viral RNA (Manfredonia et al., 2020; Sanders et al., 2020) that could reduce the accessibility of the target RNA for the RNP (Abudayyeh et al., 2017; Abudayyeh et al., 2016).

A major advantage of CRISPR diagnostics is that they can be highly specific. To confirm the specificity of our crRNAs, we tested them against a set of other respiratory viruses, including alphacoronavirus HCoV-NL63 and betacoronaviruses HCoV-OC43 and Middle East respiratory syndrome coronavirus (MERS-CoV), which are among seven coronaviruses that infect human hosts and cause respiratory diseases (Fung and Liu, 2019). We extracted RNA from the supernatant of Huh 7.5.1-ACE2 or Vero E6 cells infected with HCoV-NL63 or HCoV-OC43, respectively, and produced IVT N gene RNA from MERS-CoV. In our Cas13a direct detection

assay with crRNA 2 and 4, individually and in combination, we detected no signal above RNP background for any of viral RNAs tested (Figure 3.3A). Similarly, no signal was detected with H1N1 Influenza A or Influenza B viral RNA, or with RNA extracted from primary human airway organoids (Figure 3.3B).

Cas13a Directly Detects SARS-CoV-2 RNA in Patient Samples

We then examined if our assay could be used with patient samples, where the swab and patient matrix (e.g., mucous from a nasal swab) could contribute additional background signal and reduce sensitivity. To increase assay performance prior to testing patient samples, we examined an additional set of crRNAs (crRNAs 19-22) (Table S3.1) targeting the viral E gene, based on published qPCR primer and Cas12 guide sets (Broughton et al., 2020; Corman et al., 2020) (Figure S3.2A). When tested against genomic SARS-CoV-2 RNA, the crRNA that performed best, both individually (Figure S3.2B) and in combination (Figure S3.2C) with crRNA 2 and 4, was crRNA 21. Adding crRNA 21 to the combination also allowed us to have at least one crRNA in the assay at all times with perfect complementarity to 4115 out of 4118 sequenced genomes of SARS-CoV-2 (Figure S3.2D). When tested on RNA from five nasal swab samples confirmed negative for SARS-CoV-2, the triple combination (RNP 2+4+21) did not exhibit signal above the RNP control reaction (Figure 3.3C, Figure S3.2E).

To determine if adding crRNA 21 would improve the limit of detection of our assay, we tested a combination reaction with crRNAs 2+4+21 on precisely titrated SARS-CoV-2 genomic RNA obtained from the Biodefense and Emerging Infections Research Resources Repository (BEI Resources). In serial dilution experiments using 20 replicate reactions, the triple combination detected as few as 31 copies/ μ L (Figure 3.3D, left), based on the viral copy number independently determined by BEI with digital droplet (dd) PCR. By comparing the slope of an individual reaction with that of the RNP control, we determined that, for all dilutions, 20/20 individual tests (100%) would be correctly identified as “positive” with the 95% confidence level (Figure 3.3D, right).

Finally, we obtained five de-identified RNA samples extracted from nasal swabs taken from SARS-CoV-2⁺ individuals. Clinical RT-qPCR measurements resulted in Ct values of 14.37–22.13 for the patient samples, correlating to copy numbers 2.08×10^7 – 1.27×10^5 copies/ μ L. Using the direct detection assay on a plate reader, we correctly identified all five positive samples (ranging from 3.2×10^5 – 1.65×10^3 copies/ μ L in the Cas13a reaction), which showed slopes significantly above that of the negative swab control (Figure 3.3E). The positive sample slopes correlated significantly with their input copy number (Pearson r coefficient = 0.9966, two-tailed p-value = 0.0002), reinforcing the quantitative nature of the assay. Including the negative swab allows for us to account for potential matrix effects in clinical samples (McNerney et al., 2019). We also tested all samples with a non-targeting control crRNA and did not detect any significant signal (Figure S3.2F).

Harnessing the Mobile Phone Camera as a Portable Plate Reader

To demonstrate that SARS-CoV-2 screening with Cas13a would be possible outside of laboratory settings, we designed a mobile phone-based fluorescence microscope and reaction chamber to quantify the fluorescent signal generated by the Cas13a direct detection assay (Figure 3.4A, Figure S3.3A-C). The goal was to show that mass-produced consumer electronics, rather than specialized laboratory equipment, are sufficient to capture the small fluorescent signals generated by Cas13a direct detection. Interestingly, we found that our device was approximately an order of magnitude more sensitive than the plate reader used in the development of this assay due to reduced measurement noise and the ability to collect more time points, which decreased the uncertainty in slope estimations and therefore enabled us to distinguish smaller slopes relative to the control (Figure S3.3D).

We tested the performance of the mobile phone-based device for detecting SARS-CoV-2 RNA using the triple crRNA Cas13a assay and a dilution series with genomic viral RNA isolated from supernatants of infected Vero CCL-81 cells (Figures 3.4B-D). Fluorescence generated in

each reaction chamber was collected simultaneously and quantified over time, with measurements every 30 seconds. As with the plate reader, the data showed a steady increase in fluorescence for genomic SARS-CoV-2 virus concentrations of 200–500 copies/ μL , compared to RNP controls (Figure 3.4B, Figure S3.3E). As before, the slopes of each curve can be calculated, along with the 95% confidence interval indicated by the error bars (Figure 3.4C). To determine the limit of detection of the direct detection assay on the device, several replicates of dilutions of virus corresponding to 500, 200, 100, and 50 copies/ μL were measured, as determined by RT-qPCR. Slopes were calculated based on data for the first 10, 20, and 30 minutes of the assay, and each slope was then compared to the RNP control slope calculated over the same time (see Methods). For each dilution and assay time, the ability of the assay to detect the target RNA relative to the RNP control was quantified as percent accuracy, with eight positive tests out of eight replicates for 500 copies/ μL for all assay times corresponding to 100% accuracy (Figure 3.4D). The results over all dilutions indicate 100% accuracy for 200 copies/ μL over 30 minutes of measurement, with accuracy dropping to 50% at 50 copies/ μL .

Next, we analyzed the same RNA from patient samples as in Figure 3.3E to compare detection on the plate reader to that on the mobile phone-based device. We imaged each reaction for 60 minutes, along with the RNP control (Figure 3.4E), and the slope for a patient with Ct = 17.65 (Positive Swab 3, 3.71×10^4 copies/ μL) is significantly greater than the slope for a patient with Ct = 20.37 (Positive Swab 4, 6.21×10^3 copies/ μL) (Figure 3.4F, Figure S3.3F), as expected. To assess the detection accuracy, we performed a simple linear regression using data from the first 5, 10, 15 and 20 minutes of the assay and compared the slope of each sample to the RNP control. We determined all five samples to be positive within the first 5 minutes of measurement, indicating that the device can provide a very fast turnaround time of results for patients with clinically relevant viral loads (Figure 3.4G). This result highlights the inherent tradeoff between sensitivity and time in the Cas13a direct detection assay. High viral loads can be detected very

rapidly because their high signals can be quickly determined to be above the control, and low viral loads can be detected at longer times once their signal can be distinguished above the control (Figure S3.4).

DISCUSSION

Here we show that direct detection of SARS-CoV-2 RNA with CRISPR-Cas13a and a mobile phone offers a promising option for rapid, point-of-care testing. A key advance in this work is demonstrating that combinations of crRNAs can increase sensitivity by activating more Cas13a per target RNA. We show that combinations of two or three crRNAs can be used to detect viral target RNA in the attomolar range, detecting as few as ~ 30 copies/ μL . The use of multiple crRNAs that target different parts of the genome can also safeguard against a potential loss of detection due to naturally occurring viral mutations.

A second key advance is the ability to directly translate the fluorescent signal into viral loads. Other CRISPR Dx assays, such as CRISPR-COVID, achieve high sensitivity via isothermal amplification but provide only qualitative information rather than viral copy numbers. Fluorescent signal from 7500 copies/ μL to 7.5 copies/ μL are remarkably similar, despite three orders of magnitude difference in copy number (Hou et al., 2020). By avoiding amplification and employing direct detection, we show that the reaction rate directly correlates with viral copy number and may be used for quantification. When coupled with frequent testing, quantitative data are potentially beneficial: the course of a patient's infection can be monitored and can determine if the infection is increasing or waning. In symptomatic cases, viral loads follow the course of the infection (Wolfel et al., 2020). Notably, samples with viral loads below 10^6 copies/mL or 1000 copies/ μL did not yield infectious viral isolates in one study in Germany (Wolfel et al., 2020). SARS-CoV-2 transmission from asymptomatic carriers has also been documented (Bai et al., 2020), and they have viral RNA loads similar to those of symptomatic patients (Chamie et al., 2020; Lee et al., 2020). Monitoring viral loads quantitatively would allow estimation of infection stage and help predict infectivity, recovery and return from quarantine in real time.

A third key advance in our work is the demonstration that a compact microscope based on a mobile phone and low-cost optics can accurately read the Cas13a direct detection assay,

enabling ~100 copies/ μ L sensitivity in 30 minutes of measurement and accurate diagnosis of a set of pre-extracted RNA from patient samples in 5 minutes of measurement time on the device. This suggests that a portable diagnostic device based on consumer electronics, rather than specialized laboratory technology, can be built to work with the Cas13a assay. Mobile phones were an attractive choice for evaluating the requirements of reading the Cas13a assay because of their high-quality sensors, intuitive user interface, and powerful computational capabilities, as well as communication capabilities. For similar reasons, previous diagnostic efforts have utilized mobile phones to detect fluorescent signals from LAMP (Chen et al., 2017; Ganguli et al., 2017; Kong et al., 2017; Priye et al., 2017; Sun et al., 2020), PCR (Angus et al., 2015; Gou et al., 2018; Jiang et al., 2014), next-generation DNA sequencing (Kuhnemund et al., 2017), and recombinase polymerase amplification (Chan et al., 2018). Combined with efficient contact tracing and HIPAA-compliant upload into cloud-based systems, a mobile SARS-CoV-2 diagnostic could play an important role in the current and future pandemics.

The Cas13a direct detection assay reported here could fulfill the need for a test that provides rapid results and can be administered frequently (Larremore et al., 2020). Other tests in this category include Abbott Lab's ID NOW and Roche's cobas Liat System, both portable PCR-based tests, and several antigen tests, such as Quidel's Sofia 2 SARS Antigen FIA and Abbot Lab's BinaxNOW Antigen Test. In the case of influenza, antigen tests span a wide range of sensitivities (e.g., 51–67.5%) (Babin et al., 2011; Chartrand et al., 2012; Chu et al., 2012). Due to the low-to-moderate sensitivity of these tests, the CDC still recommends re-testing samples that are negative with a more sensitive test, such as RT-qPCR (Green and StGeorge, 2018). Notably, none of the current rapid testing options provide precise quantitative results, which could help assess viral dynamics and evaluate an individual's level of infection and disease progression.

While we demonstrate rapid detection with reasonable sensitivity using crRNAs based on existing PCR primers, we anticipate further improvement by systematically searching for the best crRNA combinations across the entire viral RNA genome. As more information becomes available

about viral variants (Osorio and Correia-Neves, 2020; Vanaerschot et al., 2020), crRNA design can be adapted to avoid false negatives. However, while combining crRNAs improves sensitivity, it also offers more opportunities for unintentional off-target detection, and lower viral loads could be registered when one crRNA in the combination does not precisely match the viral sequence in the sample. Further improvements are also anticipated in the reporter, the choice of Cas13 proteins, and in device and camera sensitivity. These advancements can improve the rate of the reaction, allowing for improvements in detection accuracy and limit of detection in shorter periods of time.

A recent national survey of over 19,000 respondents showed that the average wait time for nasal swab-based qPCR test results was 4.1 days, with 31% of tests taking more than 4 days and 10% of tests taking 10 days or more (Lazer et al., 2020). The national backlog in processing these laboratory-based tests clearly illustrates the need for rapid, point-of-care tests that can reliably detect SARS-CoV-2 RNA. As the long-term immunity induced by natural infection or vaccination may decay in as little as 2–4 months (Ibarrondo et al., 2020; Long et al., 2020), the need for rapid and frequent testing for SARS-CoV-2 will likely remain. In the future, direct detection by Cas13a as outlined here could be quickly modified to target the next respiratory pathogen that emerges, hopefully in time to help curb global spread.

Limitations of Study

This study demonstrates a proof-of-concept for sensitive and rapid SARS-CoV-2 RNA detection by a mobile phone-based device. Additional work will be necessary to fully translate this work to a widely available point-of-care device. First, while the current study used a lab-based RNA extraction step, an extraction-free protocol for sample preparation (Arizti-Sanz et al., 2020; Joung et al., 2020a; Myhrvold et al., 2018) will be necessary to minimize the number of steps in the assay and the overall sample-to-answer turnaround time. Second, while we chose to integrate a mobile phone into our detection device as a way of rapidly demonstrating what mass-produced

electronics could achieve, other configurations of an image-based diagnostic, including use of an embedded sensor that wirelessly connects to a mobile phone, could be built at scale with at least comparable performance. Finally, while we demonstrate a limit of detection of ~ 100 copies/ μL in 30 minutes of measurement on the device, we expect improvements to the sensitivity and turnaround time with optimization of crRNA combinations, Cas13 protein engineering, and additional device advancements. Furthermore, the sensitivity of the assay can be adjusted by changing the measurement time. This ability to tune sensitivity could make Cas13a direct detection useful for screening applications as well as more sensitive diagnostic applications.

ACKNOWLEDGEMENTS

We thank all members of the Ott, Fletcher, and Doudna laboratories for sharing reagents, expertise and feedback in the preparation of this manuscript. We thank Dr. Nadia Roan and Dr. Stephen Floor for helpful discussions. We also thank Michael Frumkin, Michael Brenner, Ellen Klein, Alex Schiffhauer, Daniel Harbuck, Francois Bleibel, Paul Rohde, Jon Barron, and Sam Hasinoff for helpful discussions. We thank Lauren Weiser and Veronica Fonseca for administrative support, Gary Howard for editorial support, and John Carroll for graphical support. We are grateful to Kevin Mullane, Stephen B. Freedman, and Robert Wicks at the Gladstone Institutes, and JF Van Kerckhove, Savi Baveja, and Daniel LeClerc at Bain & Company for their guidance and advice. We thank Dr. Paula Ladd, Dr. Cristina Tato, Dr. Larry Brilliant, and Dr. Harvey Fineberg for helpful discussions and support. We thank the Gladstone Assay Development and Drug Discovery Core, particularly Michael Jobling, for assistance with high-throughput assays.

We gratefully acknowledge support from the NIH: NIH/NIAID Grant 5R61AI140465-03 to J.A.D., D.A.F., and M.O., and NIH/NIDA Grant 1R61DA048444-01 to M.O. This project is supported by the NIH Rapid Acceleration of Diagnostics (RADx) program and has been funded in whole or in part with Federal funds from National Heart, Lung and Blood Institute, National Institute of Biomedical Imaging and Bioengineering, National Institutes of Health, Department of Health and Human Services, under Grant No. 3U54HL143541-02S1. P.F. was supported by the UCSF Medical Scientist Training Program (T32GM007618) and the NIH/NIAID (F30AI143401). M.D.L.D was supported by the UC MEXUS-CONACYT Doctoral Fellowship. G.J.K. is supported by an NHMRC Investigator Grant (EL1, APP1175568) and previously an American Australian Association Fellowship. J.A.D. is an HHMI Investigator. We are grateful for philanthropic support from Fast Grants, the James B. Pendleton Charitable Trust, the Roddenberry Foundation, and multiple individual donors. This work was made possible by a generous gift from an anonymous private donor in support of the ANCeR diagnostics consortium.

Purified LbuCas13a was a kind gift from Shanghai ChemPartner. We thank Synthego for support with synthetic crRNAs. The following reagents were deposited by the Centers for Disease Control and Prevention and obtained through BEI Resources, NIAID, NIH: Genomic RNA from SARS-Related Coronavirus 2, Isolate USA-WA1/2020, NR-52285; SARS-Related Coronavirus 2, Isolate USA-WA1/2020, NR-52281; and Human Coronavirus, NL63, NR-470.

AUTHOR CONTRIBUTIONS

P.F., S.S., M.D.L.D., D.A.F., and M.O. conceived and designed the study. P.F., S.S., M.D.L.D., C.N.G., S.I.S., D.B., C.T., P.Y.C., and J.S. performed experiments and data analysis. C.Z. and K.S.P. performed bioinformatics analysis. S.S., M.D.L.D., M.V.D., N.A.S., A.B, M.A., and A.R.H. developed the mobile phone-based device and reaction chambers. G.R.K. and J.M.O supervised and provided feedback. A.M.F. provided assistance with high-throughput assays. B.J., K.W., and A.S. assisted with BSL-3 work. A.S.P provided HCoV-NL63 and HCoV-OC43 viral supernatants. C.L., E.D.C., M.P., A.K., and J.D.L provided patient samples and reagents. G.J.K. and J.A.D provided reagents, and critical expertise and feedback. D.A.F. and M.O. supervised the study design and data collection. J.A.D., D.A.F., and M.O. secured funding. P.F., S.S., M.D.L.D, D.A.F., and M.O. wrote the manuscript, with input from G.J.K. and J.A.D.

DECLARATION OF INTERESTS

P.F., S.S., G.J.K, J.A.D., D.A.F., and M.O. have filed patent applications related to this work. The Regents of the University of California have patents issued and pending for CRISPR technologies on which J.A.D. is an inventor.

J.A.D. is a cofounder of Caribou Biosciences, Editas Medicine, Scribe Therapeutics, Intellia Therapeutics and Mammoth Biosciences. J.A.D. is a scientific advisory board member of Caribou Biosciences, Intellia Therapeutics, eFFECTOR Therapeutics, Scribe Therapeutics, Mammoth Biosciences, Synthego, Algen Biotechnologies, Felix Biosciences and Inari. J.A.D. is a Director at Johnson & Johnson and has research projects sponsored by Biogen, Pfizer, AppleTree Partners and Roche.

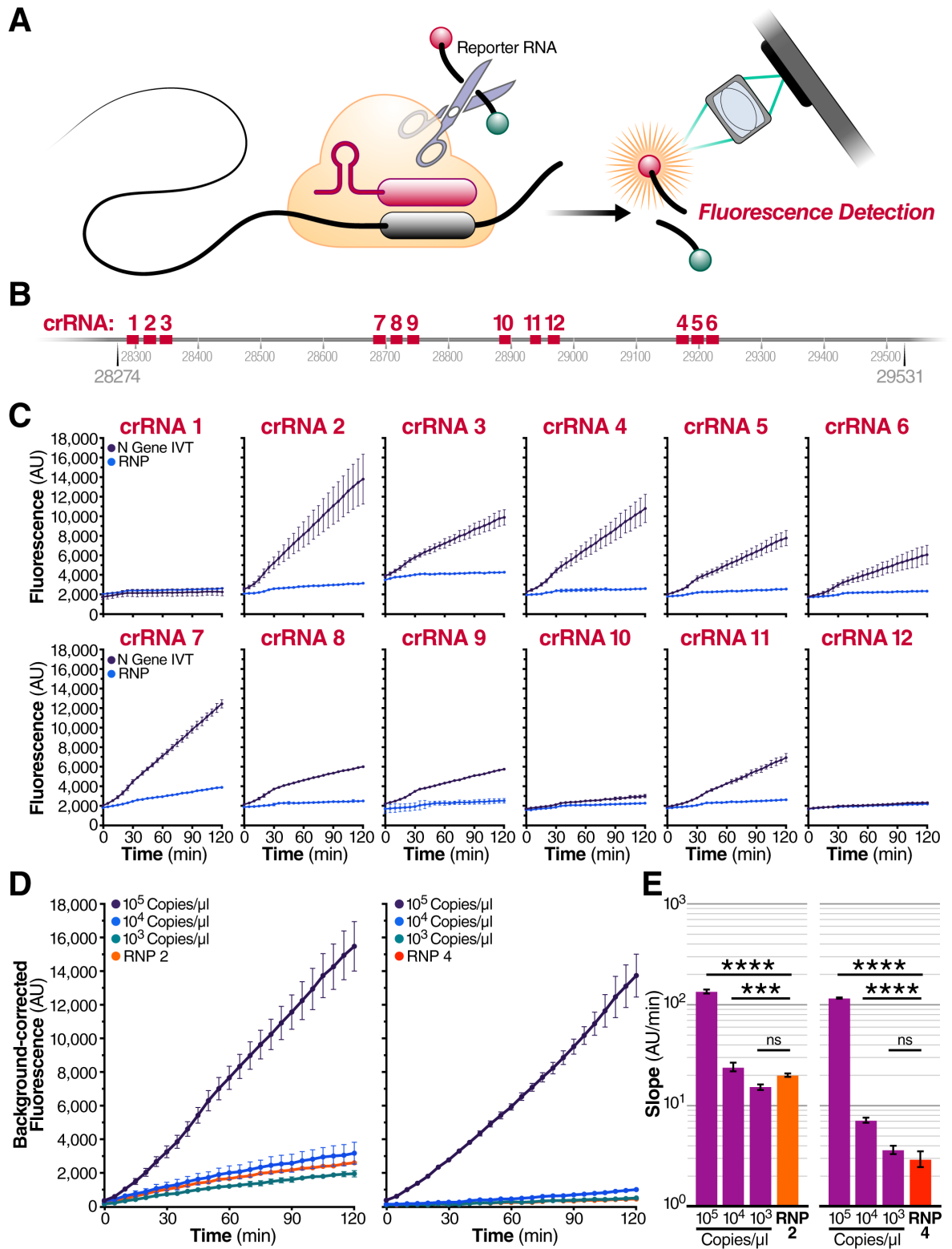


Figure 3.1: Quantitative Direct Detection of Viral SARS-CoV-2 RNA with Cas13a
 (A) Schematic of a Cas13a (beige)-crRNA (red) RNP complex binding target RNA (black), resulting in activation of the HEPN nuclease (denoted by scissors) domain. Upon target

recognition and RNP activation, Cas13a indiscriminately cleaves a quenched-fluorophore RNA reporter, allowing for fluorescence detection as a proxy for Cas13a activation and target RNA.

(B) Schematic of the SARS-CoV-2 N gene, and the corresponding location of each crRNA spacer region.

(C) Cas13a RNPs made individually with each crRNA were tested against 2.89×10^5 copies/ μL (480 fM) of SARS-CoV-2 IVT N gene RNA in a total 20 μL reaction volume. Background fluorescence by the individual RNP in the absence of target RNA is shown as "RNP." Raw fluorescence values over two hours is shown. Data are represented as mean \pm standard deviation (SD) of three technical replicates. See also Figure S3.1A.

(D) Limit of detection of crRNA 2 and crRNA 4 was determined by testing 100 nM of each RNP individually against 10^5 , 10^4 , and 10^3 copies/ μL of N gene IVT RNA. "RNP 2" and "RNP 4" represent no target RNA RNP alone controls. Background correction of fluorescence was performed by subtraction of reporter alone fluorescence values. Data are represented as mean \pm standard error of the difference between means of three technical replicates. See also Figure S3.1B-D.

(E) Slope of the curve over two hours from Figure 3.1D was calculated by performing simple linear regression to data merged from replicates and is shown as slope \pm 95% confidence interval. Slopes were compared to the RNP alone control through an Analysis of Covariance (ANCOVA): **** $p < 0.0001$, *** $p < 0.001$, ns=not significantly higher than RNP control.

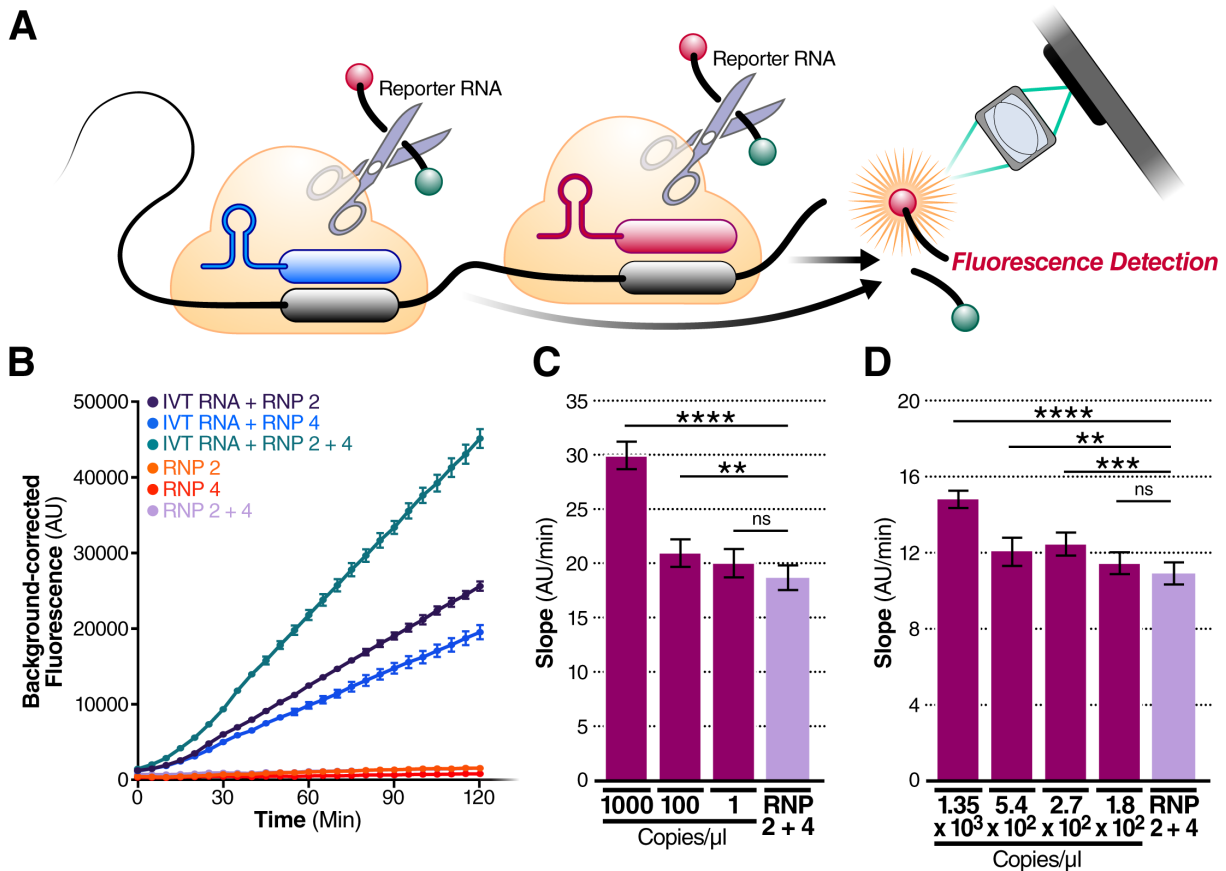


Figure 3.2: Combining crRNAs Improves Sensitivity of Cas13a

(A) Schematic of two different RNPs binding to different locations of the same SARS-CoV-2 RNA, leading to cleavage of the RNA reporter and increased fluorescence.

(B) RNPs made with crRNA 2 and crRNA 4 individually and in combination (50 nM total RNP concentration per reaction) were tested against 2.9×10^5 copies/ μ L (480 fM) of SARS-CoV-2 IVT N gene RNA, and compared to fluorescence from no target RNA RNP alone controls (“RNP 2,” “RNP 4,” and “RNP 2+4”). Background correction of fluorescence was performed by subtraction of reporter-alone fluorescence values. Data are represented as mean \pm standard error of the difference between means of three technical replicates.

(C) Limit of detection of crRNA 2 and crRNA 4 in combination was determined by combining 50 nM of RNP 2 and 50 nM of RNP 4 (100 nM total) against 1000, 100, and 1 copy/ μ L of SARS-CoV-2 IVT RNA (n=3, technical replicates). Slope of the curve over two hours was calculated by performing simple linear regression of data merged from replicates and is shown as slope \pm 95% confidence interval. Slopes were compared to the no target RNA RNP alone control using ANCOVA: ****p<0.0001, **p=0.0076, ns=not significant.

(D) Limit of detection of crRNA 2 and crRNA 4 in combination was determined by combining 50 nM of RNP 2 and 50 nM of RNP 4 (100 nM total) against 1.35×10^3 , 5.4×10^2 , 2.7×10^2 , and 1.8×10^2 copies/ μ L of genomic SARS-CoV-2 viral RNA as quantified by qPCR (n=3, technical replicates). Slope of the curve over two hours was calculated by performing simple linear regression of data merged from replicates and is shown as slope \pm 95% confidence interval. Slopes were compared to the no target RNA RNP alone control using ANCOVA: ****p<0.0001, ***p=0.0002, **p=0.0023, ns=not significant.

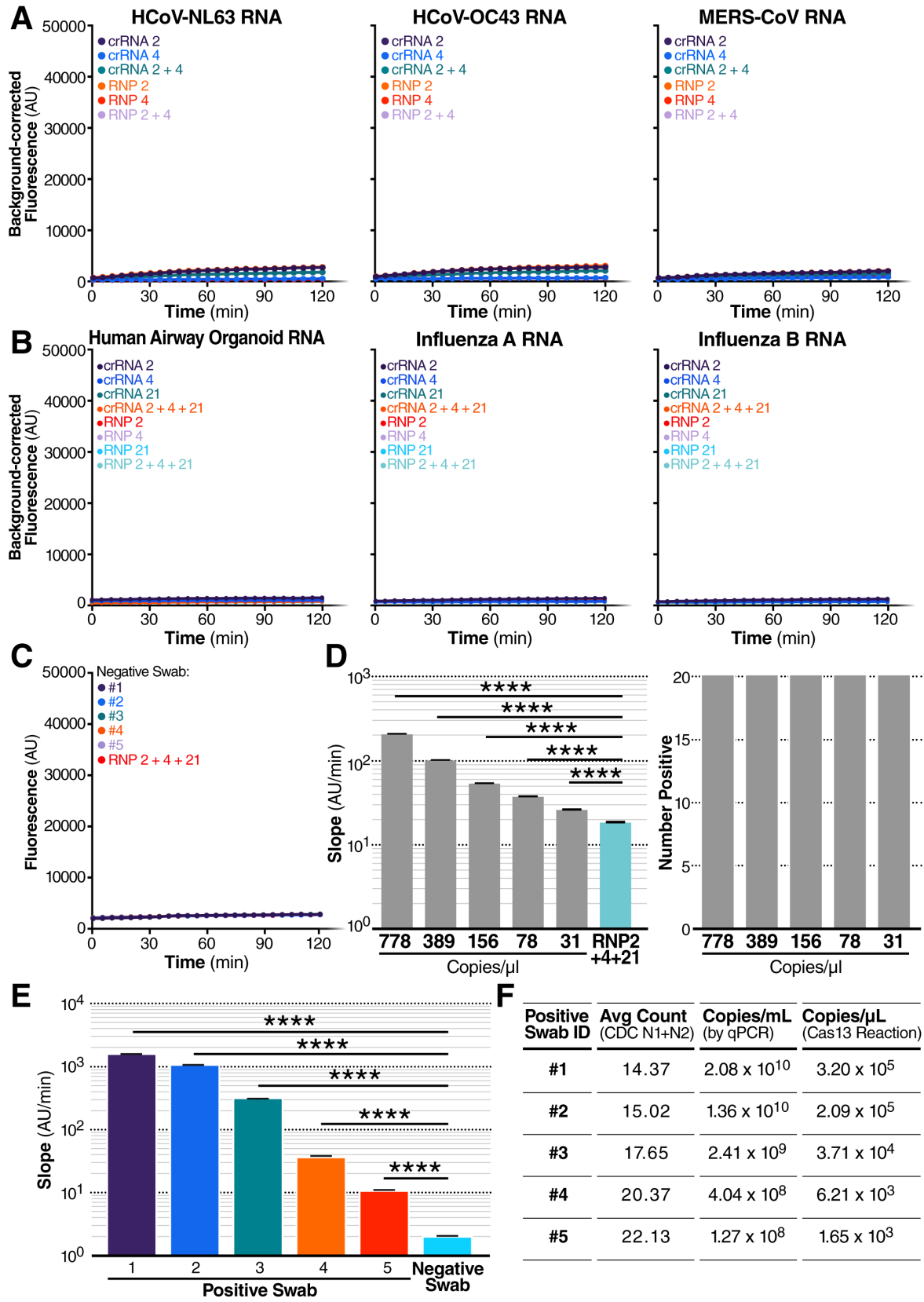


Figure 3.3: Cas13a Directly Detects SARS-CoV-2 RNA in Patient Samples

(A) crRNA 2 and crRNA 4 were tested individually (100 nM total RNP concentration) and in combination (100 nM total RNP concentration: 50 nM each of RNP 2 and RNP 4) against RNA isolated from HCoV-NL63 viral supernatant (left) and HCoV-OC43 viral supernatant (center) or the IVT N gene RNA from MERS-CoV (right). No target RNA RNP alone controls are denoted as “RNP 2,” “RNP 4,” and “RNP 2+4.” Background correction of fluorescence was performed by subtraction of reporter alone fluorescence values. Data are represented as mean \pm standard error of the difference between means of three technical replicates.

(B) crRNA 2 and crRNA 4 and crRNA 21 were tested individually (100 nM total RNP concentration) and in combination (100 nM total RNP concentration: 33 nM each of RNP 2, RNP 4, and RNP 21) against RNA isolated from human airway organoids (left), H1N1 Influenza A (center), and Influenza B (right). No target RNA RNP alone controls are denoted as “RNP 2,” “RNP 4,” “RNP 21,” “RNP 2+4+21.” Background correction of fluorescence was performed by subtraction of reporter alone fluorescence values. Data are represented as mean \pm standard error of the difference between means of three technical replicates. See also Figure S3.2A-D.

(C) RNA from 5 nasopharyngeal swabs confirmed negative for SARS-CoV-2 by RT-qPCR was tested against RNP 2+4+21 (100 nM total RNP concentration). The no target RNA RNP control is denoted as “RNP 2+4+21.” Raw fluorescence values over two hours is shown. Data are represented as mean \pm SD of three technical replicates. See also Figure S3.2E.

(D) Dilutions of genomic SARS-CoV-2 RNA independently quantified by BEI using ddPCR was tested against RNP 2+4+21 to determine the limit of detection (n=20, technical replicates). Slope of the raw fluorescence curve over two hours was calculated by performing simple linear regression of data merged from replicates and is shown as slope \pm 95% confidence interval (left). Slopes were compared to the no target RNA RNP alone control using ANCOVA: ****p<0.0001. An individual reaction containing the diluted SARS-Cov-2 RNA was compared with the reaction without the target RNA and the number of true positives was counted at the 95% confidence level (right).

(E) Pre-extracted RNA from 5 nasopharyngeal swabs confirmed positive for SARS-CoV-2 by RT-qPCR was tested against RNP 2+4+21 (100 nM total RNP concentration) (n=3, technical replicates). A confirmed negative swab was tested against RNP 2+4+21 for comparison. We added 0.3 μ L of RNA from Patient Swabs 1-4, 0.26 μ L of RNA from Patient Swab 5, and 0.3 μ L of RNA from a confirmed negative swab to each 20 μ L Cas13a reaction (in triplicate). Slope of the raw fluorescence curve over two hours was calculated by performing simple linear regression of data merged from replicates and is shown as slope \pm 95% confidence interval. Slopes were compared to the negative swab RNP background control using ANCOVA: ****p<0.0001. See also Figure S3.2F.

(F) The Ct value (average Ct count using CDC N1/N2 primers in RT-qPCR), the copies/mL of the original sample determined by qPCR, and the copies/ μ L in the Cas13a reaction are described for the RNA samples from each positive swab used in Figure 3.3E.

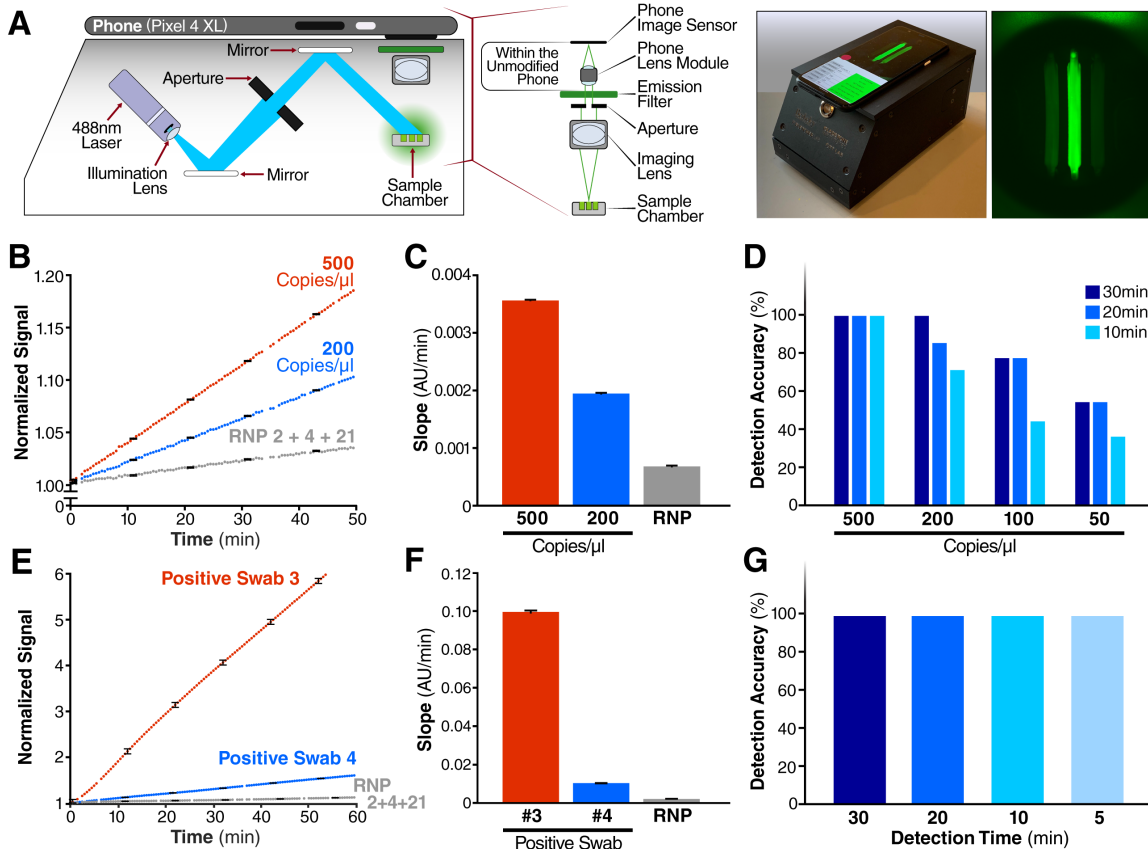


Figure 3.4: Harnessing the Mobile Phone Camera as a Portable Plate Reader

(A) Schematic of mobile phone-based microscope for fluorescence detection showing illumination and image collection components (left). Picture of assembled device used for data collection and sample image taken by the mobile phone camera after running a Cas13a assay (right). See also Figure S3.3A-C.

(B) Results from the Cas13a assay run on the mobile device with two different dilutions of genomic SARS-CoV-2 viral RNA isolated from infected Vero CCL-81 cells (500 and 200 copies/ μ L) and RNP alone, using three combined crRNAs (crRNA 2, crRNA 4 and crRNA 21). Y-axis is the fluorescent signal of each sample normalized by the first time point. The error bars indicate the root-mean-square error (RMSE) of simple linear regression to individual curves. See also Figure S3.3D-E.

(C) Slope of the curve over 30 minutes of measurement on the device from Figure 3.4B was calculated by simple linear regression and is shown as slope \pm 95% confidence interval.

(D) Detection accuracy of the Cas13a assay is characterized in the mobile device using genomic SARS-CoV-2 viral RNA. For each target dilutions, the slope at three different times - 10, 20 and 30 minutes of measurement time on the device - were compared to the slope of the no target RNA RNP alone controls, and the detection accuracy was determined at the 95% confidence level. The number of replicates for each concentration is 8 (500 copies/ μ L), 7 (200 copies/ μ L), 9 (100 copies/ μ L), and 11 (50 copies/ μ L). See also Figure S3.4A-C.

(E) Results from a Cas13a assay run on mobile device with two different nasal swab samples, confirmed positive for SARS-CoV-2 using RT-qPCR, and the RNP alone control, all using the crRNA combination of crRNA 2, crRNA 4 and crRNA 21. The error bars indicate the RMSE of simple linear regression to individual curves. See also Figure S3.3F.

(F) Slope of the curve over 30 minutes from Figure 3.4E was calculated by simple linear regression and is shown as slope \pm 95% confidence interval.

(G) Detection accuracy of Cas13a assay for 5 nasal swab samples, confirmed positive by RT-qPCR. Detection accuracy was evaluated at four different time points: 5, 10, 20 and 30 minutes of measurement time on the device.

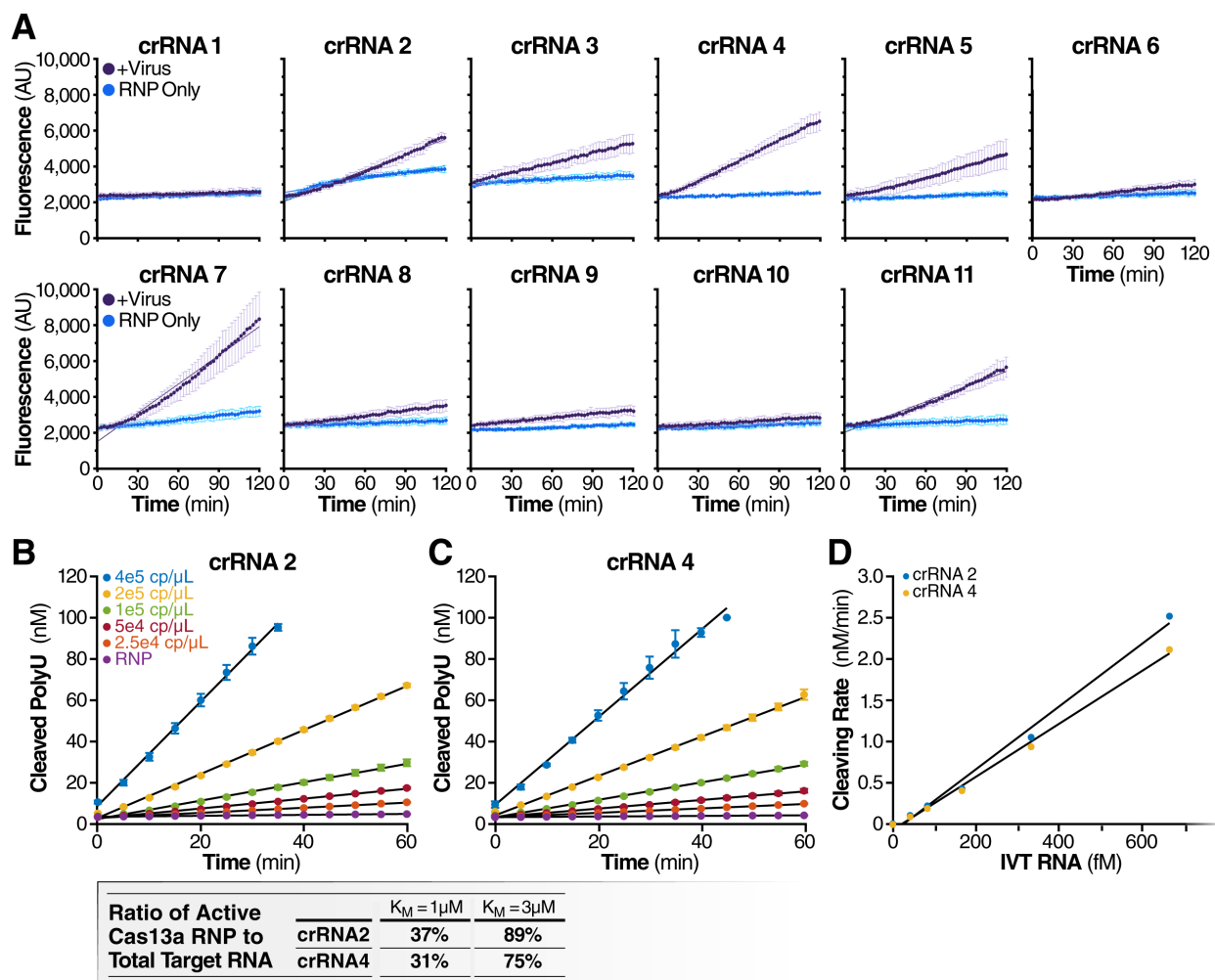


Figure S3.1: Related to Figure 3.1. Individual crRNAs Quantitatively Detect SARS-CoV-2 RNA

(A) Cas13a RNPs made individually with each N gene crRNA (final RNP complex concentration of 100 nM) were tested against extracted SARS-CoV-2 viral RNA. Background fluorescence by the individual RNP in the absence of target RNA is shown as “RNP Only.” Raw fluorescence values over 2 hours is shown. Data are represented as mean \pm SD of three technical replicates.

(B-C) Cas13a reaction rate is linearly proportional to the target RNA concentration.

(B) The reaction rate of Cas13a was measured by adding a range of concentrations of IVT N gene RNA to reactions that contain 100nM of Cas13a RNP with crRNA2 and 400 nM of polyU reporter (error bars indicate the standard deviation of triplicate measurements). The reaction rate is determined by fitting a linear curve to the data (black curves).

(C) The reaction rate of Cas13a for a range of IVT N gene RNA concentrations as measured in Figure S3.1B but with crRNA 4 used in place of crRNA2.

(D) Cas13a reaction rate – either with crRNA 2 or crRNA 4 – scales linearly with the target IVT RNA concentration ($R^2 = 0.990$ for crRNA 2 and 0.996 for crRNA 4). Assuming that Cas13a enzymatic activity can be described by the Michaelis-Menten kinetics model, and that the amount of IVT RNA sets the upper limit of active Cas13a RNP, we predict the ratio of active Cas13a to IVT RNA in for $K_{cat} = 600/s$ and $K_M = 1\mu\text{M}$ or $3\mu\text{M}$, which is the range of K_M previously found for Cas13b (Slaymaker et al., 2019).

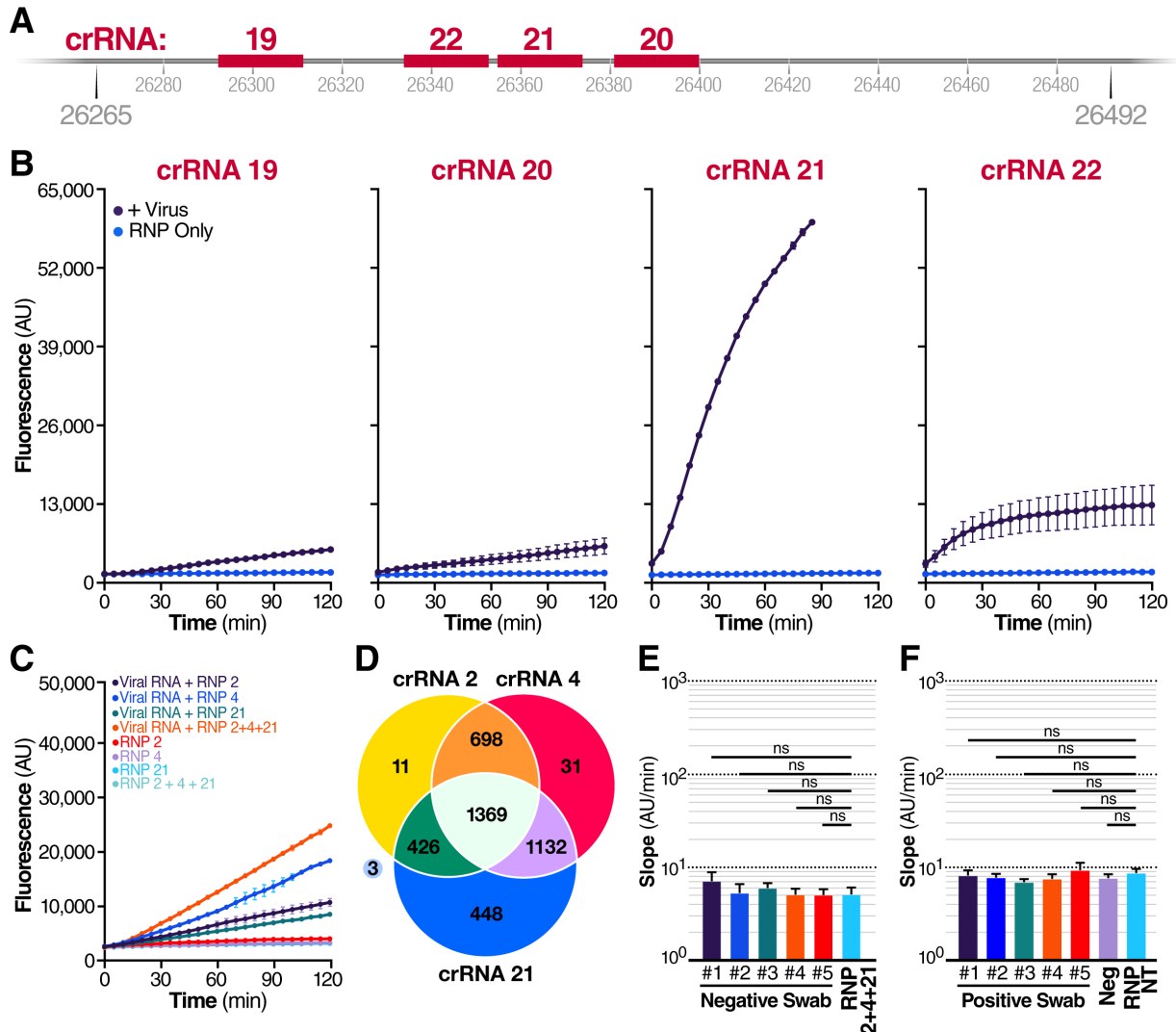


Figure S3.2: Related to Figure 3.3. Combining crRNAs Improves SARS-CoV-2 Detection

(A) Schematic of the SARS-CoV-2 envelope (E) gene, and the corresponding location of each crRNA spacer region.

(B) Cas13a RNPs made individually with each E gene crRNA (final RNP complex concentration of 100 nM) were tested against genomic SARS-CoV-2 RNA. Background fluorescence by the RNP alone in the absence of target RNA is shown as “RNP Only.” Raw fluorescence values over 2 hours are shown. Data are represented as mean \pm SD of three technical replicates.

(C) RNPs made with crRNA 2, crRNA 4, and crRNA 21 individually and in combination (100 nM total RNP concentration for each reaction) were tested against 1.5×10^4 copies/ μ L of extracted SARS-CoV-2 RNA, and compared to fluorescence from no target RNA RNP alone controls (“RNP 2,” “RNP 4,” “RNP 21,” and “RNP 2+4+21”). Raw fluorescence values over 2 hours is shown. Data are represented as mean \pm SD of three technical replicates.

(D) 4118 complete SARS-CoV-2 genome sequences deposited in NCBI RefSeq under taxonomy ID (2697049) were downloaded on 06/05/2020. Each crRNA was compared against the downloaded genomes for genomes with zero mismatches to each individual crRNA. The Venn diagram shows how many complete genomes have 100% homology to crRNAs 2, 4, and 21, as well as the overlap between crRNAs.

(E) Slope of the curves in Figure 3.3C over two hours was calculated by performing simple linear regression of data from each replicate (n=3) individually. The mean of the replicate slopes is shown as slope \pm 95% confidence interval. Slopes were compared to the no target RNA RNP alone control using repeated-measures one-way analysis of variance (ANOVA) and Dunnett's multiple comparisons test: ns=not significant.

(F) The same swabs as in Figure 3.3E were tested against a non-targeting crRNA (RNP NT) (final RNP complex concentration of 100 nM). Slope of the raw fluorescence curve over 2 hours was calculated by performing simple linear regression of data merged from replicates (n=3) and is shown as slope \pm 95% confidence interval. Slopes were compared to the no target RNA RNP alone control using ANCOVA: ns=not significant.

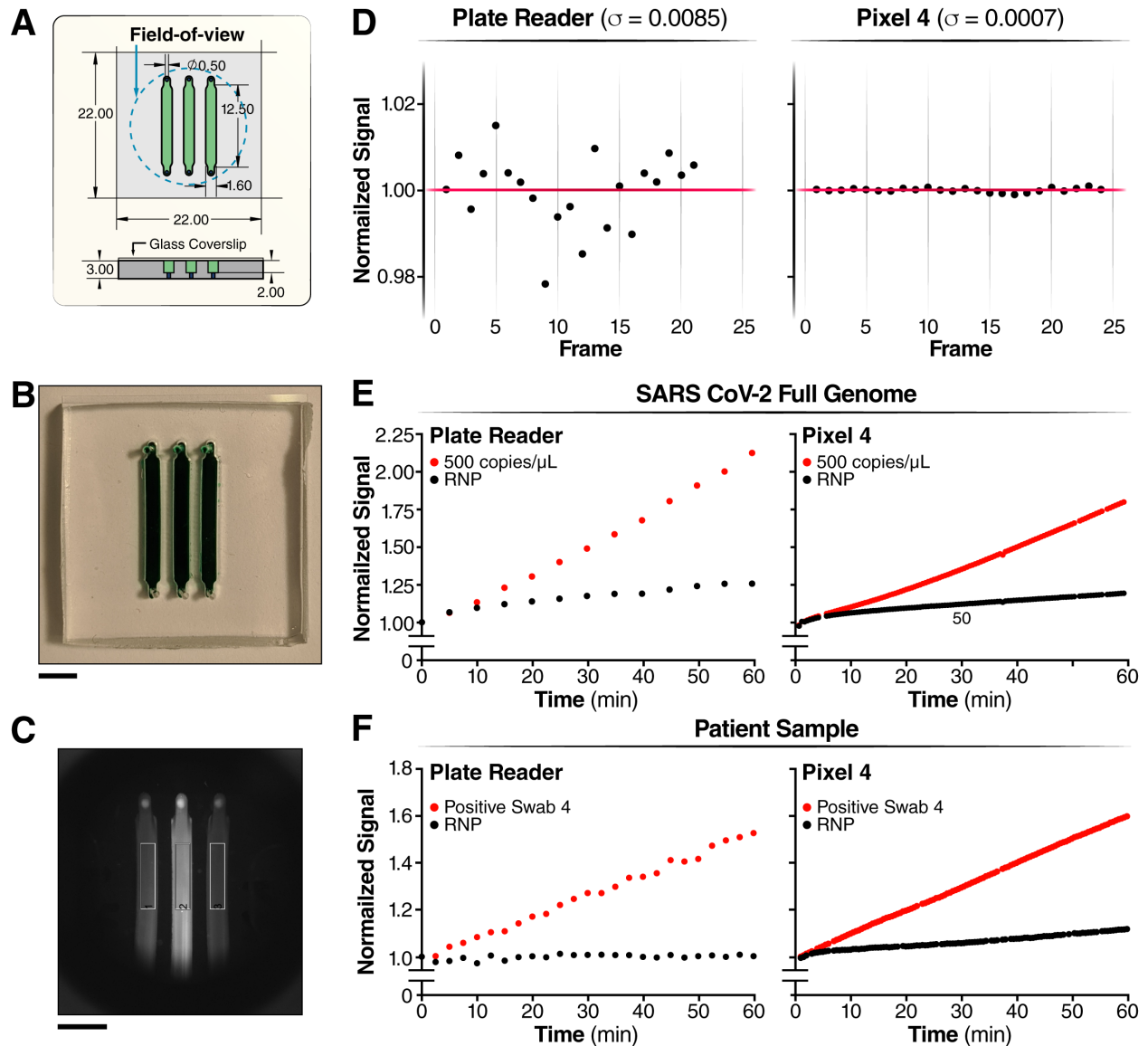


Figure S3.3: Related to Figure 3.4. Comparison of the Cas13a Reaction Measured in the Plate Reader and the Mobile Phone Device

(A-C) Schematic of the reaction chamber and the sample region-of-interest (ROI)

(A) Reaction chamber dimensions are described here.

(B) Photo of a reaction chamber loaded with an artificial green dye (Scale bar = 5mm).

(C) Raw image of patient sample and the sample ROIs (black rectangle) (Scale bar = 5mm).

(D) The measurement error of the plate reader (left) versus the mobile device (right) for typical conditions used for Cas13a reaction (37°C, measurement interval: 30 seconds).

(E) The triple crRNA combination with 500 copies/μL of genomic SARS CoV-2 viral RNA was measured in the plate reader (left) and in the mobile phone device (right).

(F) The triple crRNA combination with Positive Swab 4 was measured in the plate reader (left) and in the mobile phone device (right).

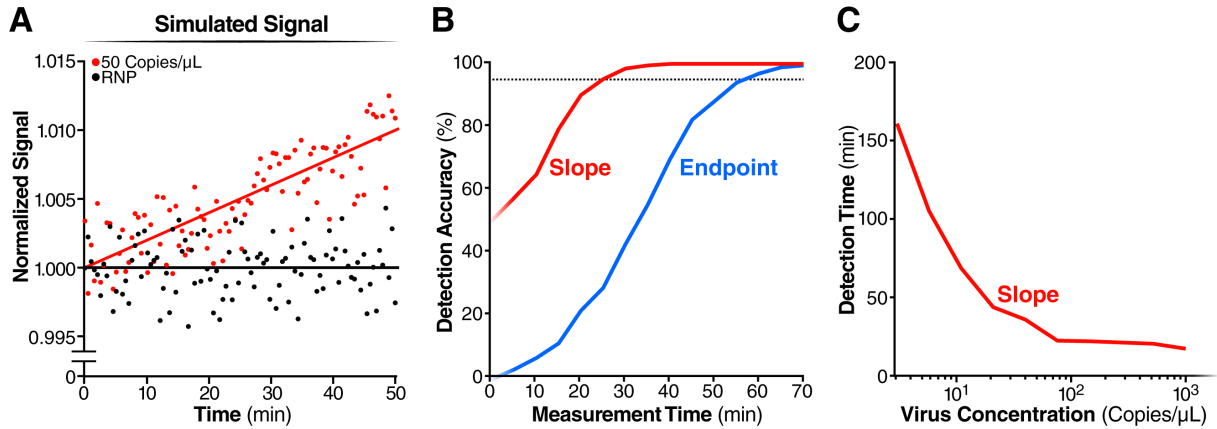


Figure S3.4: Related to Figure 3.4. Limit of Detection of the Mobile Phone Device

(A) We simulated the signal of mobile phone device for triple crRNA combination with the target viral RNA at 50 copies/μL (red dots) or without the target (RNP alone) (black dots) (see Methods). The red and black lines indicate the linear fit of the simulated signal.

(B) For each simulated measurement, we estimated the slope and the 95% confidence interval of the slope and tested whether the slope of the positive sample was significantly larger than the slope of the RNP alone (red line). Similarly, we tested whether the endpoint signal of the positive sample was significantly larger than the endpoint signal of the RNP alone (blue line). By repeating this procedure 1,000 times for different assay times, we estimated the difference in detection accuracy of the two methods.

(C) The simulation using the slope analysis in panel (B) was repeated for varying amounts of target viral RNA, and the time where detection accuracy reached 95% was determined.

METHODS

Resource Availability

Lead Contact

Further information and requests for resources and reagents should be directed to and will be fulfilled by the Lead Contact, Melanie Ott (melanie.ott@gladstone.ucsf.edu).

Materials Availability

This study did not generate new unique reagents.

Data and Code Availability

The custom MATLAB code for image processing and data analysis is available from Mendeley

Data at <http://dx.doi.org/10.17632/r3vwyr2w5x.1>.

Experimental Models and Subject Details

Mammalian cell lines and culture conditions

Human hepatocellular carcinoma cells (Huh7.5.1, gift from Frank Chisari) and monkey kidney epithelial cells (Vero, ATCC CCL-81, and Vero E6, ATCC CRL-1586) were cultured in DMEM (Corning) supplemented with 10% fetal bovine serum (FBS, Sigma), penicillin/streptomycin (Corning), and L-glutamine (Corning) at 37°C and 5% CO₂. Cell lines were tested negative for mycoplasma contamination.

Generation of Huh7.5.1-ACE2 cell line

Huh7.5.1-ACE2 cells were generated as described previously in (Wang et al., 2020b). Briefly, hACE2 (Addgene, #1786, gift from Hyeryun Choe) was amplified and cloned into EcoRV-cut plenti-CMV-Hygro-DEST (Addgene, #17454, gift from Eric Campeau & Paul Kaufman) using NEBuilder HiFi DNA Assembly Master Mix (NEB). Lentivirus was produced in HEK293FT by co-transfection of plenti-hACE2-Hygro together with pCMV-dR8.2 dvpr (Addgene, #8455, gift from Bob Weinberg), pCMV-VSV-G (Addgene, #8454, gift from Bob Weinberg) and pAdVantage

(Promega) using FugeneHD (Promega). Supernatant was collected 48 hours post-transfection, filtered and added to Huh7.5.1 cells. Transduced cells were subsequently selected using Hygromycin for 7 days.

Viral strains

SARS-CoV-2 virus culture

Isolate USA-WA1/2020 of SARS-CoV-2 was used for genomic SARS-CoV-2 RNA. All live virus experiments were performed in a Biosafety Level 3 laboratory. SARS-CoV-2 stocks were propagated in Vero CCL-81 cells. Viral supernatant was collected by centrifugation and stored at -80°C.

HCoV-NL63 virus culture

Isolate Amsterdam I of HCoV-NL63 (NR-470, BEI Resources) was propagated in Huh7.5.1-ACE2 cells. Supernatant was harvested 5 days post infection, filtered and stored at -80°C.

HCoV-OC43 virus culture

HCoV-OC43 (VR-1558, ATCC) was propagated in Vero E6 cells. Supernatant was harvested 6 days post infection, filtered and stored at -80°C.

Influenza virus

H1N1 Influenza virus A (California/04/2009) and Influenza virus B (Brisbane/60/2008) in chicken allantoic fluid was purchased from Virapur and used directly for RNA extraction (see below).

Human airway organoid culture

Human airway organoids are generated using upper bronchia/trachea cells from lung resection tissue. They are cultured using the protocol previously described in (Sachs et al., 2019). Airway organoids are seeded in drops of diluted basement membrane matrix (Cultrex, diluted 3:4 with basal media) in flat-bottom, low-attachment plates. Airway Organoid (AO) media is added after the drops have solidified. Organoids are cultured at 37°C, 5% CO₂, and passaged every two weeks. During passaging, the airway organoids drops are collected with cold basal media, washed and dissociated manually and chemically with TryPLE 10X (Gibco) and Trypsin-EDTA (Corning), then re-seeded into new plates. Basal media and AO media compositions are taken from (Zhou et al., 2018).

Patient samples

De-identified RNA samples from nasopharyngeal swabs from patients testing positive and negative for SARS-CoV-2 were obtained from the Chan Zuckerberg Biohub. The institutional review board at University of California, San Francisco, approved this study under IRB #17-24056. Positive samples were quantified previously using CDC N1 and N2 SARS-CoV-2 primers.

Method Details

Cas13a protein expression and purification

Expression vectors deposited with Addgene (Plasmid #83482) were used for expression of LbuCas13a. The codon-optimized Cas13a genomic sequences are *N*-terminally tagged with a His₆-MBP-TEV cleavage site sequence, with expression driven by a T7 promoter. Purification of was based off of a previously published protocol with some modifications (East-Seletsky et al., 2017; East-Seletsky et al., 2016). Briefly, expression vectors were transformed into Rosetta2 DE3 or BL21 *E. coli* cells grown in Terrific broth at 37°C, induced at mid-log phase (OD₆₀₀ ~0.6) with

0.5 mM IPTG, and then transferred to 16°C for overnight expression. Cell pellets were resuspended in lysis buffer (50 mM Tris-Cl pH 7.0, 500 mM NaCl, 5% glycerol, 1 mM TCEP, 0.5 mM PMSF, and EDTA-free protease inhibitor (Roche)), lysed by sonication, and clarified by centrifugation at 35,000xg. Soluble His6-MBP-TEV-Cas13a was isolated over metal ion affinity chromatography, and in order to cleave off the His6- MBP tag, the protein-containing eluate was incubated with TEV protease at 4°C overnight while dialyzing into ion exchange buffer (50 mM Tris-Cl pH 7.0, 250 mM KCl, 5% glycerol, 1 mM TCEP). Cleaved protein was loaded onto a HiTrap SP column (GE Healthcare) and eluted over a linear KCl (0.25-1.0M) gradient. Cas13a-containing fractions were pooled, concentrated, and further purified via size-exclusion chromatography on a S200 column (GE Healthcare) in gel filtration buffer (20 mM HEPES-K pH 7.0, 200 mM KCl, 10% glycerol, 1 mM TCEP) and were subsequently flash frozen for storage at -80°C.

In vitro RNA transcription

SARS-CoV-2 N gene was transcribed off a single-stranded DNA oligonucleotide template (IDT). HCoV-MERS N gene was transcribed off of a MERS-CoV Control plasmid (IDT, Cat# 10006624) by first adding a T7 promoter via PCR using Q5 High-Fidelity DNA Polymerase (NEB) (see Table S1 for primers). A single PCR product was confirmed via gel electrophoresis. *In vitro* transcription was performed using HiScribe T7 Quick High Yield RNA Synthesis Kit (NEB) following manufacturer's recommendations. Template DNA was removed by addition of DNase I (NEB), and IVT RNA was subsequently purified using RNA STAT-60 (AMSBIO) and the Direct-Zol RNA MiniPrep Kit (Zymo Research). RNA concentration was quantified by Nanodrop and copy number was calculated using full transcript length and concentration.

RNA extraction

RNA was extracted from SARS-CoV-2, HCoV-NL63, HCoV-OC43, Influenza A, and Influenza B viral supernatant via RNA STAT-60 (AMSBIO) and the Direct-Zol RNA MiniPrep Kit (Zymo Research). RNA was extracted from human airway organoid cells using the RNeasy Mini Kit (Qiagen).

Quantitative polymerase chain reaction

RNA from SARS-CoV-2 viral supernatant was quantified via qPCR. Briefly, RNA was reverse transcribed to cDNA via AMV Reverse Transcriptase (Promega) using oligo(dt)₁₈ and random hexamers (Thermo Scientific). cDNA was added to the qPCR reaction using PrimeTime Gene Expression Master Mix (IDT). N and E gene standards were used to generate a standard curve for copy number quantification. N gene standard was generated by PCR from the 2019-nCoV_N_Positive Control Plasmid (IDT, Cat# 10006625). E gene standard was generated by PCR using extracted genomic SARS-CoV-2 RNA as template. A single product was confirmed by gel electrophoresis and DNA was quantified by Nanodrop. cDNA was analyzed using the 7500 Fast Real-Time PCR system (Applied Biosystems). See Table S1 for primers.

crRNA design parameters

20 nucleotide crRNA spacer sequences targeting the N gene were chosen using previously published qPCR sequences from the Centers for Disease Control and Prevention (CDC) and based on (Zhu et al., 2020). For spacer sequences targeting the E gene, we based our spacers on a previously published qPCR primer set as well as a published Cas12 guide (Broughton et al., 2020; Corman et al., 2020). We confirmed the specificity of each crRNA to SARS-CoV-2 using NCBI BLAST, setting a threshold of 16/20 sequence identity to human transcripts to reduce the odds of off-target detection from human tissue. We used the following 30 nucleotide crRNA stem

sequence: 5'-GACCACCCCAAAAUGAAGGGGACUAAAAC-3'. See Table S1 for full sequences.

4118 complete SARS-CoV-2 genome sequences deposited in NCBI RefSeq under the taxonomy ID (2697049) were downloaded on 06/05/2020. We searched each guide against the downloaded SC2 genomes with no mismatches (using grep command) and the Venn diagram (Figure S3.2D) was generated using R package VennDiagram (version 1.6.20).

Fluorescent Cas13a nuclease assays

LbuCas13a-crRNA RNP complexes were individually preassembled by incubating 1.33 μ M of LbuCas13a with 1.33 μ M of crRNA for 15 minutes at room temperature. In Figures 3.1C and 3.2B, 677 nM of crRNA was used. These complexes were then diluted to 100 nM LbuCas13a and 100 nM (or 50 nM for Figures 3.1C and 3.2B) crRNA in cleavage buffer (20 mM HEPES-Na pH 6.8, 50 mM KCl, 5 mM MgCl₂, and 5% glycerol) in the presence of 400 nM of reporter RNA (5'-FAM-rUrUrUrUrU-lowaBlack FQ-3'), 1 U/ μ L Murine RNase Inhibitor (NEB, Cat# M0314), and varying amounts of target RNA. In Figures 3.1C and 3.2B, the final RNP complex concentration was 50 nM. In all other figures, the final RNP complex concentration was 100 nM. In Figures 3.1C and 3.2B, 167 nM of RNase Alert substrate (IDT) was used as the reporter RNA, and in Figure 3.2D, 400 nM of RNase Alert substrate was used. In Figure 3.3D and 3.3E, the complexes were also diluted in 0.1% Tween-20 (Sigma) and the cleavage buffer was pH 7.1. These reactions were loaded into a 384-well (Corning, Cat# 3820) incubated in a fluorescence plate reader (TECAN, Infinite 200 Pro M Plex) for up to 120 minutes at 37°C with fluorescence measurements taken every 5 minutes (or every 2.5 minutes in Figure 3.3E) (λ_{ex} :485 nM; λ_{em} :535 nM; Gain: 130). Background-corrected fluorescence values were obtained by subtracting fluorescence values obtained from reactions carried out containing only reporter and buffer. For assays containing

more than one crRNA simultaneously, the LbuCas13a-crRNA RNP complexes were separately assembled by incubating for 15 minutes at room temperature, then combined in the reaction at half (in 2 RNP combinations) or one-third (in 3 RNP combinations) the volume to keep the total or combined concentration of RNP constant. Representative graphs of experiments are shown. Most experiments were replicated at least twice, with the exception of Figure 3.3E (only Patient Swabs 1-3 and 5 were repeated twice) due to limited sample material. For Patient Swab 5, a slightly smaller quantity of swab material was used compared to other swabs (0.26 μL rather than 0.3 μL) to achieve a lower viral concentration in the Cas13a reaction. This allowed us to demonstrate a lower copy number that the Cas13a reaction could detect in patient samples.

Mobile phone fluorescent microscope

We built a mobile phone fluorescent microscope using a 488 nm diode laser (GH04850B2G, Sharp Microelectronics), a green fluorescence interference filter (Chroma Technology AT 535/40), and a Pixel 4 XL phone camera (12.2 mega-pixel, pixel size 1.4 μm , aperture f/1.7, Google). The laser beam was expanded using a glass collimation lens (10° divergence half-angle), directed towards the sample plane using two ND4 filters used as mirrors (ND40B, Thorlabs), and reduced by an elliptical aperture to fill the circular image field-of-view with a uniform field intensity. The sample was illuminated with an oblique epi configuration and the illumination power was 18 mW at the sample plane; illuminated area at the sample plane was 15 x 15 mm². The imaging optics consist of an f=20mm compact triplet lens (TRH127-020-A, Thorlabs) followed by the interference filter for selection of the fluorescence reporter emission wavelength and the Pixel 4 XL camera lens. Total magnification from object to image plane is $\sim 1/4.5$ and the numerical aperture is 0.06. All optical and illumination components were enclosed in a custom-made dark box, into which a sample chip is loaded for imaging. Automated time-lapse imaging was implemented by a custom Android application and a Bluetooth receiver (Bluefruit Feather M0,

Adafruit), which triggered the laser at the time of image acquisition. The Cas13a reaction was performed by placing the device in a 37°C incubator for temperature control and the reaction curve was obtained by analyzing the image time series offline using a custom MATLAB (Mathworks) code. When measuring the Cas13 reporter background, the signal-to-noise ratio of our system that is limited by the noise of diode laser is ~1000 (Figure S3.3D).

Sample chip fabrication

Sample chips containing three fluid channels were made by casting polydimethylsiloxane (PDMS, Ellsworth adhesives) on an acrylic mold. The acrylic mold was assembled by adhering three laser cut acrylic lanes on a flat acrylic base. The width, height, and length of each acrylic lane were 1.6 mm, 2 mm, and 12.5 mm, respectively, resulting in a fluid channel volume of 40 μ L (Figure S3.3A-C). Inlet and outlet ports were created on both ends of the channels after curing and demolding the PDMS using a biopsy punch. The PDMS chips were subsequently adhered to a siliconized cover glass (Hampton research) to close the fluid channels. To avoid generation of bubbles in the chip during the measurement, both the Cas13a reaction mix and the sample chip were degassed in a house vacuum for 15 minutes before loading the samples and starting the measurement.

Mobile phone image acquisition and analysis

During typical device operation, a ~1 second exposure RGB image was acquired every 30 seconds for a period of 1 hour and the images were analyzed offline using custom MATLAB code. First, the RGB image of 2016 x 2512 pixels was demosaiced to a greyscale image. Second, the saturated pixels or pixels exhibiting two very different green submosaic values were excluded. Third, a rectangular image region-of-interest (ROI) of 400 x 90 pixels was manually drawn within an area of each fluid channel and the reporter signal in each ROI was determined by averaging the pixel values (Figure S3.3C). The ROI values are accumulated in time and analyzed for slope determination (see Quantification and Statistical Analysis).

Comparison of data with enzyme kinetics

We analyzed the Cas13a reaction with a single crRNA (Figure S3.1B-D) using the Michaelis-Menten enzyme kinetics model with the quasi-steady-state approximation to estimate R , the ratio of active Cas13 RNP to target RNA, from the measured reaction rate per target RNA, A (below). We first converted the plate reader signal to the molar concentration of cleaved reporter and determined the Cas13a reaction rate v for varying concentrations of target RNA $[E_0]$. We then determined the reaction rate per target RNA, A , by fitting a linear curve to the data. We used the total reporter concentration $[S] = 400$ nM, $K_{cat} = 600/s$, K_M from $1 \mu\text{M}$ to $3 \mu\text{M}$ (Slaymaker et al., 2019) to calculate R from A .

$$v = A \cdot [E_0]$$

$$A = R \cdot K_{cat} \frac{[S]}{K_M + [S]}$$

We estimated that, for both crRNA 2 and crRNA 4, the amount of active Cas13a RNP can be as small as 31 – 37 % of total target RNA (for $K_M = 1\mu\text{M}$), or as large as 75 – 89 % (for $K_M = 3\mu\text{M}$).

Simulation of mobile device data

We used MATLAB to simulate the mobile device data. We simulated the data by including the random noise with standard deviation of 0.002 to conservatively emulate the measured noise ~ 0.0007 in our system (Figure S3.3D). We assumed that for 50 copies/ μL of target viral RNA the signal increases at a rate of 0.0002 fold/min at 37°C , based on Figure 3.4C showing the difference of ~ 0.002 fold/min between reaction rates at 500 copies/ μL and RNP alone, and that reaction rate is constant in time as we validated with experimental data (Figure S3.1B-D). Although we observe slightly positive slopes in RNP alone control reactions, we simulated the control reaction as a flat line with a standard deviation of 0.002 after subtracting its slope from the positive reaction. In

each simulation, we tested whether the positive sample curve was significantly different from the RNP alone curve based on the comparison of either the endpoint signal or the signal slope. In both cases, we considered the signal positive if it did not overlap with the control within the 95% confidence interval. For each measurement time, we repeated the simulation 1,000 times and determined the detection accuracy by counting the positive tests.

Quantification and Statistical Analysis

The number of experiments and replicates are indicated in the individual Figure Legends. The slope of Cas13a reaction is calculated by simple linear regression of raw data from time 0 for the set duration. For all the plate reader samples and the patient samples measured in a mobile device, the measurement began immediately after sample loading. For the genomic SARS-COV-2 RNA samples measured in a mobile device, the sample was equilibrated for 10 minutes in the device before measurement began. The slope error bar indicates the 95% confidence intervals (CI) of linear regression performed either to individual data or data merged from the group of replicates. To assess significance between groups of positive Cas13a reaction vs the RNP only control, we employed a two-way ANCOVA to the slope during linear regression. When the slope of positive reaction is smaller than that of the RNP only control, it is considered non-significant. To evaluate the accuracy of our detection of positive samples, we tested whether the slope of an individual positive sample exceeded that of an RNP only control by greater than the 95% CI. The detection accuracy is quantified as the ratio of samples tested positive out of the total number of tests. The CI can be adjusted to enhance either the sensitivity or specificity of the test. For example, tightening to 99% CI will incur more potential false negatives, or loosening to 90% will risk more false positives. Data in Figures 3.1-3 were processed and visualized using GraphPad Prism 8. Data in Figure 3.4 were processed using MATLAB.

SUPPLEMENTAL TABLE

Table S3.1: Related to Figures 3.1-3.4 and S3.1-S3.4. List of custom oligonucleotides used in this study.

Oligo ID	Type	Source	Description	Sequence
PF039_crLbu_nCoV_1	crRNA	Synthego	SARS-CoV-2 crRNA 1	GACCACCCCAAAAAUGAAGGGGA CUAAAACUUUCGUGAUUUUUGG GGUCC
PF040_crLbu_nCoV_2	crRNA	Synthego	SARS-CoV-2 crRNA 2	GACCACCCCAAAAAUGAAGGGGA CUAAAACGGUCCACCAAACGUAA UGCG
PF041_crLbu_nCoV_3	crRNA	Synthego	SARS-CoV-2 crRNA 3	GACCACCCCAAAAAUGAAGGGGA CUAAAACUCUGGUUACUGCCAG UUGAA
PF042_crLbu_nCoV_4	crRNA	Synthego	SARS-CoV-2 crRNA 4	GACCACCCCAAAAAUGAAGGGGA CUAAAACUUUGCGGCCAAUGUU UGUAA
PF043_crLbu_nCoV_5	crRNA	Synthego	SARS-CoV-2 crRNA 5	GACCACCCCAAAAAUGAAGGGGA CUAAAACGAAGCGCUGGGGGCA AAUUG
PF044_crLbu_nCoV_6	crRNA	Synthego	SARS-CoV-2 crRNA 6	GACCACCCCAAAAAUGAAGGGGA CUAAAACAUGCGCGACAUUCCGA AGAA
PF045_crLbu_nCoV_7	crRNA	Synthego	SARS-CoV-2 crRNA 7	GACCACCCCAAAAAUGAAGGGGA CUAAAACUUGGUGUAUUCAAGG CUCC
PF046_crLbu_nCoV_8	crRNA	Synthego	SARS-CoV-2 crRNA 8	GACCACCCCAAAAAUGAAGGGGA CUAAAACGGAUUGCGGGUGCCA AUGUG
PF047_crLbu_nCoV_9	crRNA	Synthego	SARS-CoV-2 crRNA 9	GACCACCCCAAAAAUGAAGGGGA CUAAAACUGUAGCACGAUUGCAG CAUU
PF051_crLbu_nCoV_13	crRNA	Synthego	SARS-CoV-2 crRNA 10	GACCACCCCAAAAAUGAAGGGGA CUAAAACUCUAGCAGGAGAAGUU CCCC
PF052_crLbu_nCoV_14	crRNA	Synthego	SARS-CoV-2 crRNA 11	GACCACCCCAAAAAUGAAGGGGA CUAAAACUCUGUCAAGCAGCAGC AAAG
PF084_crLbu_nCov15 v2	crRNA	Synthego	SARS-CoV-2 crRNA 12	GACCACCCCAAAAAUGAAGGGGA CUAAAACGACAUUUUUGCUCUCA GCUG
PF088_crLbu_nCoV_19	crRNA	Synthego	SARS-CoV-2 crRNA 19	GACCACCCCAAAAAUGAAGGGGA CUAAAACCUAUUAACUAUUAACG UACC
PF089_crLbu_nCoV_20	crRNA	Synthego	SARS-CoV-2 crRNA 20	GACCACCCCAAAAAUGAAGGGGA CUAAAACUAUUGCAGCAGUACGC ACAC
PF090_crLbu_nCoV_21	crRNA	Synthego	SARS-CoV-2 crRNA 21	GACCACCCCAAAAAUGAAGGGGA CUAAAACAGCGCAGUAAGGAUG GCUAG
PF091_crLbu_nCoV_22	crRNA	Synthego	SARS-CoV-2 crRNA 22	GACCACCCCAAAAAUGAAGGGGA CUAAAACGUAACUAGCAAGAAUA CCAC

Oligo ID	Type	Source	Description	Sequence
PF030_crLbu_NT1_L	crRNA	Synthego	Nontargeting crRNA	GACCACCCCAAAAAUGAAGGGGA CUAAAACAGGUUCUUGACUACCG UAAUU
PolyU reporter	Reporter	IDT	PolyU Reporter	/56-FAM/rUrUrUrUrU/3IABkFQ/
PF_019_T7NgeneL_F	PCR	Elim Bio	Forward primer for N gene block	CTTCCATGCCAATGCGCGAC
PF_020_T7NgeneL_R	PCR	Elim Bio	Reverse primer for N gene block	TAATACGACTCACTATAG
PF_051_M13T7_F	PCR	Elim Bio	Forward primer for IDT SARS-CoV-2 and MERS-CoV N gene PCR	TAATACGACTCACTATAGTAAAAC GACGGCCAGT
PF_052_M13_R	PCR	Elim Bio	Reverse primer for IDT SARS-CoV-2 and MERS-CoV N gene PCR	CAGGAAACAGCTATGAC
PF_039_nCoV_N5_F	qPCR	Elim Bio	Forward N gene primer for SARS-CoV-2 qPCR	AAATTTTGGGGACCAGGAAC
PF_040_nCoV_N5_R	qPCR	Elim Bio	Reverse N gene primer for SARS-CoV-2 qPCR	TGGCACCTGTGTAGGTCAAC
PF_041_nCoV_N5_P	qPCR	Elim Bio	N gene probe for SARS-CoV-2 qPCR	FAM- ATGTCGCGCATTGGCATGGA- BHQ1
PF_042_nCoV_E_F	qPCR/PCR	Elim Bio	Forward E gene primer for SARS-CoV-2 qPCR/PCR	ACAGGTACGTTAATAGTTAATAGC GT
PF_043_nCoV_E_R	qPCR/PCR	Elim Bio	Reverse E gene primer for SARS-CoV-2 qPCR/PCR	ATATTGCAGCAGTACGCACACA
PF_044_nCoV_E_P	qPCR	Elim Bio	E gene probe for SARS-CoV-2 qPCR	FAM- ACACTAGCCATCCTTACTGCGCTT CG-BHQ1

Oligo ID	Type	Source	Description	Sequence
N gene block	gBlock	IDT	N gene IVT Template	CTTCCATGCCAATGCGCGACATT CCGAAGAACGCTGAAGCGCTGG GGGCAAATTGTGCAATTTGCGGC CAATGTTTGTAAATCAGTTCCTTGT CTGATTAGTTCCTGGTCCCCAAAA TTTCTTGGGTTTGTCTGGACCA CGTCTGCCGAAAGCTTGTGTTAC ATTGTATGCTTTAGTGGCAGTACG TTTTTGCCGAGGCTTCTTAGAAGC CTCAGCAGCAGATTTCTTAGTGA CAGTTTGGCCTTGTTGTTGTTGG CCTTTACCAGACATTTTGCTCTCA AGCTGGTTCAATCTGTCAAGCAG CAGCAAAGCAAGAGCAGCATCAC CGCCATTGCCAGCCATTCTAGCA GGAGAAGTTCCCCTACTGCTGCC TGGAGTTGAATTTCTTGAAGTGT GCGACTACGTGATGAGGAACGAG AAGAGGCTTGACTGCCGCCTCTG CTCCTTCTGCGTAGAAGCCTTTT GGCAATGTTGTTCTTGAGGAAG TTGTAGCACGATTGCAGCATTGTT AGCAGGATTGCGGGTGCCAATGT GATCTTTTGGTGTATTCAAGGCTC CCTCAGTTGCAACCCATATGATG CCGTCTTTGTTAGCACCATAGGG AAGTCCAGCTTCTGGCCCAGTTC CTAGGTAGTAGAAATACCATCTTG GACTGAGATCTTTCATTTTACCGT CACCACCACGAATTCGTCTGGTA GCTCTTCGGTAGTAGCCAATTTG GTCATCTGGACTGCTATTGGTGT AATTGGAACGCCTTGCCTCGAG GGAATTTAAGGTCTTCTTGCCAT GTTGAGTGAGAGCGGTGAACCAA GACGCAGTATTATTGGGTAAACC TTGGGGCCGACGTTGTTTTGATC GCGCCCCACTGCGTTCTCCATT TGGTTACTGCCAGTTGAATCTGA GGGTCCACCAAACGTAATGCGGG GTGCATTTGCTGATTTTGGGGT CCATTATCAGACCTATAGTGAGTC GTATTA

REFERENCES

- Abudayyeh, O.O., Gootenberg, J.S., Essletzbichler, P., Han, S., Joung, J., Belanto, J.J., Verdine, V., Cox, D.B.T., Kellner, M.J., Regev, A., *et al.* (2017). RNA targeting with CRISPR-Cas13. *Nature* 550, 280-284.
- Abudayyeh, O.O., Gootenberg, J.S., Konermann, S., Joung, J., Slaymaker, I.M., Cox, D.B., Shmakov, S., Makarova, K.S., Semenova, E., Minakhin, L., *et al.* (2016). C2c2 is a single-component programmable RNA-guided RNA-targeting CRISPR effector. *Science* 353, aaf5573.
- Angus, S.V., Cho, S., Harshman, D.K., Song, J.Y., and Yoon, J.Y. (2015). A portable, shock-proof, surface-heated droplet PCR system for *Escherichia coli* detection. *Biosens Bioelectron* 74, 360-368.
- Arizti-Sanz, J., Freije, C.A., Stanton, A.C., Boehm, C.K., Petros, B.A., Siddiqui, S., Shaw, B.M., Adams, G., Kosoko-Thoroddsen, T.F., Kembell, M.E., *et al.* (2020). Integrated sample inactivation, amplification, and Cas13-based detection of SARS-CoV-2. *bioRxiv*.
- Babin, S.M., Hsieh, Y.H., Rothman, R.E., and Gaydos, C.A. (2011). A meta-analysis of point-of-care laboratory tests in the diagnosis of novel 2009 swine-lineage pandemic influenza A (H1N1). *Diagn Microbiol Infect Dis* 69, 410-418.
- Bai, Y., Yao, L., Wei, T., Tian, F., Jin, D.Y., Chen, L., and Wang, M. (2020). Presumed Asymptomatic Carrier Transmission of COVID-19. *JAMA*.
- Breslauer, D.N., Maamari, R.N., Switz, N.A., Lam, W.A., and Fletcher, D.A. (2009). Mobile phone based clinical microscopy for global health applications. *PLoS One* 4, e6320.
- Broughton, J.P., Deng, X., Yu, G., Fasching, C.L., Servellita, V., Singh, J., Miao, X., Streithorst, J.A., Granados, A., Sotomayor-Gonzalez, A., *et al.* (2020). CRISPR-Cas12-based detection of SARS-CoV-2. *Nature Biotechnology* 38, 870-874.
- Chamie, G., Marquez, C., Crawford, E., Peng, J., Petersen, M., Schwab, D., Schwab, J., Martinez, J., Es, D.J., Black, D., *et al.* (2020). SARS-CoV-2 Community Transmission

- disproportionately affects Latinx population during Shelter-in-Place in San Francisco. *Clin Infect Dis*.
- Chan, K., Wong, P.Y., Parikh, C., and Wong, S. (2018). Moving toward rapid and low-cost point-of-care molecular diagnostics with a repurposed 3D printer and RPA. *Anal Biochem* 545, 4-12.
- Chartrand, C., Leeflang, M.M., Minion, J., Brewer, T., and Pai, M. (2012). Accuracy of rapid influenza diagnostic tests: a meta-analysis. *Ann Intern Med* 156, 500-511.
- Chen, J.S., Ma, E., Harrington, L.B., Da Costa, M., Tian, X., Palefsky, J.M., and Doudna, J.A. (2018). CRISPR-Cas12a target binding unleashes indiscriminate single-stranded DNase activity. *Science* 360, 436-439.
- Chen, W., Yu, H., Sun, F., Ornob, A., Brisbin, R., Ganguli, A., Vemuri, V., Strzebonski, P., Cui, G., Allen, K.J., *et al.* (2017). Mobile Platform for Multiplexed Detection and Differentiation of Disease-Specific Nucleic Acid Sequences, Using Microfluidic Loop-Mediated Isothermal Amplification and Smartphone Detection. *Anal Chem* 89, 11219-11226.
- Chu, H., Lofgren, E.T., Halloran, M.E., Kuan, P.F., Hudgens, M., and Cole, S.R. (2012). Performance of rapid influenza H1N1 diagnostic tests: a meta-analysis. *Influenza Other Respir Viruses* 6, 80-86.
- Corman, V.M., Landt, O., Kaiser, M., Molenkamp, R., Meijer, A., Chu, D.K., Bleicker, T., Brunink, S., Schneider, J., Schmidt, M.L., *et al.* (2020). Detection of 2019 novel coronavirus (2019-nCoV) by real-time RT-PCR. *Euro Surveill* 25.
- D'Ambrosio, M.V., Bakalar, M., Bennuru, S., Reber, C., Skandarajah, A., Nilsson, L., Switz, N., Kamgno, J., Pion, S., Boussinesq, M., *et al.* (2015). Point-of-care quantification of blood-borne filarial parasites with a mobile phone microscope. *Sci Transl Med* 7, 286re284.
- East-Seletsky, A., O'Connell, M.R., Burstein, D., Knott, G.J., and Doudna, J.A. (2017). RNA Targeting by Functionally Orthogonal Type VI-A CRISPR-Cas Enzymes. *Mol Cell* 66, 373-383 e373.

- East-Seletsky, A., O'Connell, M.R., Knight, S.C., Burstein, D., Cate, J.H., Tjian, R., and Doudna, J.A. (2016). Two distinct RNase activities of CRISPR-C2c2 enable guide-RNA processing and RNA detection. *Nature* 538, 270-273.
- Fung, T.S., and Liu, D.X. (2019). Human Coronavirus: Host-Pathogen Interaction. <https://doi.org/10.1146/annurev-micro-020518-115759>.
- Ganguli, A., Ornob, A., Yu, H., Damhorst, G.L., Chen, W., Sun, F., Bhuiya, A., Cunningham, B.T., and Bashir, R. (2017). Hands-free smartphone-based diagnostics for simultaneous detection of Zika, Chikungunya, and Dengue at point-of-care. *Biomed Microdevices* 19, 73.
- Gootenberg, J.S., Abudayyeh, O.O., Kellner, M.J., Joung, J., Collins, J.J., and Zhang, F. (2018). Multiplexed and portable nucleic acid detection platform with Cas13, Cas12a, and Csm6. *Science* 360, 439-444.
- Gootenberg, J.S., Abudayyeh, O.O., Lee, J.W., Essletzbichler, P., Dy, A.J., Joung, J., Verdine, V., Donghia, N., Daringer, N.M., Freije, C.A., *et al.* (2017). Nucleic acid detection with CRISPR-Cas13a/C2c2. *Science* 356, 438-442.
- Gou, T., Hu, J., Wu, W., Ding, X., Zhou, S., Fang, W., and Mu, Y. (2018). Smartphone-based mobile digital PCR device for DNA quantitative analysis with high accuracy. *Biosens Bioelectron* 120, 144-152.
- Green, D.A., and StGeorge, K. (2018). Rapid Antigen Tests for Influenza: Rationale and Significance of the FDA Reclassification. *J Clin Microbiol* 56.
- Hou, T., Zeng, W., Yang, M., Chen, W., Ren, L., Ai, J., Wu, J., Liao, Y., Gou, X., Li, Y., *et al.* (2020). Development and evaluation of a rapid CRISPR-based diagnostic for COVID-19. *PLoS Pathog* 16, e1008705.
- Ibarrondo, F.J., Fulcher, J.A., Goodman-Meza, D., Elliott, J., Hofmann, C., Hausner, M.A., Ferbas, K.G., Tobin, N.H., Aldrovandi, G.M., and Yang, O.O. (2020). Rapid Decay of Anti-SARS-CoV-2 Antibodies in Persons with Mild Covid-19. *N Engl J Med* 383, 1085-1087.

- Jiang, L., Mancuso, M., Lu, Z., Akar, G., Cesarman, E., and Erickson, D. (2014). Solar thermal polymerase chain reaction for smartphone-assisted molecular diagnostics. *Sci Rep* 4, 4137.
- Joung, J., Ladha, A., Saito, M., Kim, N.G., Woolley, A.E., Segel, M., Barretto, R.P.J., Ranu, A., Macrae, R.K., Faure, G., *et al.* (2020a). Detection of SARS-CoV-2 with SHERLOCK One-Pot Testing. *N Engl J Med* 383, 1492-1494.
- Joung, J., Ladha, A., Saito, M., Segel, M., Bruneau, R., Huang, M.W., Kim, N.G., Yu, X., Li, J., Walker, B.D., *et al.* (2020b). Point-of-care testing for COVID-19 using SHERLOCK diagnostics. medRxiv.
- Kamgno, J., Pion, S.D., Chesnais, C.B., Bakalar, M.H., D'Ambrosio, M.V., Mackenzie, C.D., Nana-Djeunga, H.C., Gounoue-Kamkumo, R., Njitchouang, G.R., Nwane, P., *et al.* (2017). A Test-and-Not-Treat Strategy for Onchocerciasis in Loa loa-Endemic Areas. *N Engl J Med* 377, 2044-2052.
- Konermann, S., Lotfy, P., Brideau, N.J., Oki, J., Shokhirev, M.N., and Hsu, P.D. (2018). Transcriptome Engineering with RNA-Targeting Type VI-D CRISPR Effectors. *Cell* 173, 665-676 e614.
- Kong, J.E., Wei, Q., Tseng, D., Zhang, J., Pan, E., Lewinski, M., Garner, O.B., Ozcan, A., and Di Carlo, D. (2017). Highly Stable and Sensitive Nucleic Acid Amplification and Cell-Phone-Based Readout. *ACS Nano* 11, 2934-2943.
- Kuhnemund, M., Wei, Q., Darai, E., Wang, Y., Hernandez-Neuta, I., Yang, Z., Tseng, D., Ahlford, A., Mathot, L., Sjoblom, T., *et al.* (2017). Targeted DNA sequencing and in situ mutation analysis using mobile phone microscopy. *Nat Commun* 8, 13913.
- La Scola, B., Le Bideau, M., Andreani, J., Hoang, V.T., Grimaldier, C., Colson, P., Gautret, P., and Raoult, D. (2020). Viral RNA load as determined by cell culture as a management tool for discharge of SARS-CoV-2 patients from infectious disease wards. *Eur J Clin Microbiol Infect Dis* 39, 1059-1061.

- Larremore, D.B., Wilder, B., Lester, E., Shehata, S., Burke, J.M., Hay, J.A., Tambe, M., Mina, M.J., and Parker, R. (2020). Test sensitivity is secondary to frequency and turnaround time for COVID-19 surveillance. medRxiv.
- Lavezzo, E., Franchin, E., Ciavarella, C., Cuomo-Dannenburg, G., Barzon, L., Vecchio, C.D., Rossi, L., Manganelli, R., Loregian, A., Navarin, N., *et al.* (2020). Suppression of a SARS-CoV-2 outbreak in the Italian municipality of Vo'. *Nature*, 1-5.
- Lazer, D., Santillana, M., Perlis, R.H., Ognyanova, K., Baum, M.A., Quintana, A., Druckman, J., Della Volpe, J., Chwe, H., and Simonson, M. (2020). THE STATE OF THE NATION: A 50-STATE COVID-19 SURVEY REPORT #8: FAILING THE TEST. OSF Preprints.
- Lee, S., Kim, T., Lee, E., Lee, C., Kim, H., Rhee, H., Park, S.Y., Son, H.J., Yu, S., Park, J.W., *et al.* (2020). Clinical Course and Molecular Viral Shedding Among Asymptomatic and Symptomatic Patients With SARS-CoV-2 Infection in a Community Treatment Center in the Republic of Korea. *JAMA Intern Med*.
- Long, Q.X., Tang, X.J., Shi, Q.L., Li, Q., Deng, H.J., Yuan, J., Hu, J.L., Xu, W., Zhang, Y., Lv, F.J., *et al.* (2020). Clinical and immunological assessment of asymptomatic SARS-CoV-2 infections. *Nat Med* 26, 1200-1204.
- Manfredonia, I., Nithin, C., Ponce-Salvatierra, A., Ghosh, P., Wirecki, T.K., Marinus, T., Ogando, N.S., Snider, E.J., Hemert, M.J.v., Bujnicki, J.M., *et al.* (2020). Genome-wide mapping of therapeutically-relevant SARS-CoV-2 RNA structures.
- McNerney, M.P., Zhang, Y., Steppe, P., Silverman, A.D., Jewett, M.C., and Styczynski, M.P. (2019). Point-of-care biomarker quantification enabled by sample-specific calibration. *Sci Adv* 5, eaax4473.
- Meeske, A.J., Nakandakari-Higa, S., and Marraffini, L.A. (2019). Cas13-induced cellular dormancy prevents the rise of CRISPR-resistant bacteriophage. *Nature* 570, 241-245.

- Myhrvold, C., Freije, C.A., Gootenberg, J.S., Abudayyeh, O.O., Metsky, H.C., Durbin, A.F., Kellner, M.J., Tan, A.L., Paul, L.M., Parham, L.A., *et al.* (2018). Field-deployable viral diagnostics using CRISPR-Cas13. *Science* 360, 444-448.
- Osorio, N.S., and Correia-Neves, M. (2020). Implication of SARS-CoV-2 evolution in the sensitivity of RT-qPCR diagnostic assays. *Lancet Infect Dis.*
- Priye, A., Bird, S.W., Light, Y.K., Ball, C.S., Negrete, O.A., and Meagher, R.J. (2017). A smartphone-based diagnostic platform for rapid detection of Zika, chikungunya, and dengue viruses. *Sci Rep* 7, 44778.
- Quicke, K., Gallichote, E., Sexton, N., Young, M., Janich, A., Gahm, G., Carlton, E.J., Ehrhart, N., and Ebel, G.D. (2020). Longitudinal Surveillance for SARS-CoV-2 RNA Among Asymptomatic Staff in Five Colorado Skilled Nursing Facilities: Epidemiologic, Virologic and Sequence Analysis. *medRxiv.*
- Sachs, N., Papaspyropoulos, A., Zomer-van Ommen, D.D., Heo, I., Böttinger, L., Klay, D., Weeber, F., Huelsz-Prince, G., Iakobachvili, N., Amatngalim, G.D., *et al.* (2019). Long-term expanding human airway organoids for disease modeling. *EMBO J* 38.
- Sanders, W., Fritch, E.J., Madden, E.A., Graham, R.L., Vincent, H.A., Heise, M.T., Baric, R.S., and Moorman, N.J. (2020). Comparative analysis of coronavirus genomic RNA structure reveals conservation in SARS-like coronaviruses. *bioRxiv.*
- Shmakov, S., Abudayyeh, O.O., Makarova, K.S., Wolf, Y.I., Gootenberg, J.S., Semenova, E., Minakhin, L., Joung, J., Konermann, S., Severinov, K., *et al.* (2015). Discovery and Functional Characterization of Diverse Class 2 CRISPR-Cas Systems. *Mol Cell* 60, 385-397.
- Shmakov, S., Smargon, A., Scott, D., Cox, D., Pyzocha, N., Yan, W., Abudayyeh, O.O., Gootenberg, J.S., Makarova, K.S., Wolf, Y.I., *et al.* (2017). Diversity and evolution of class 2 CRISPR-Cas systems. *Nat Rev Microbiol* 15, 169-182.

- Slaymaker, I.M., Mesa, P., Kellner, M.J., Kannan, S., Brignole, E., Koob, J., Feliciano, P.R., Stella, S., Abudayyeh, O.O., Gootenberg, J.S., *et al.* (2019). High-Resolution Structure of Cas13b and Biochemical Characterization of RNA Targeting and Cleavage. *Cell Rep* 26, 3741-3751 e3745.
- Smargon, A.A., Cox, D.B.T., Pyzocha, N.K., Zheng, K., Slaymaker, I.M., Gootenberg, J.S., Abudayyeh, O.A., Essletzbichler, P., Shmakov, S., Makarova, K.S., *et al.* (2017). Cas13b Is a Type VI-B CRISPR-Associated RNA-Guided RNase Differentially Regulated by Accessory Proteins Csx27 and Csx28. *Mol Cell* 65, 618-630 e617.
- Sun, F., Ganguli, A., Nguyen, J., Brisbin, R., Shanmugam, K., Hirschberg, D.L., Wheeler, M.B., Bashir, R., Nash, D.M., and Cunningham, B.T. (2020). Smartphone-based multiplex 30-minute nucleic acid test of live virus from nasal swab extract. *Lab Chip* 20, 1621-1627.
- Vanaerschot, M., Mann, S.A., Webber, J.T., Kamm, J., Bell, S.M., Bell, J., Hong, S.N., Nguyen, M.P., Chan, L.Y., Bhatt, K.D., *et al.* (2020). Identification of a polymorphism in the N gene of SARS-CoV-2 that adversely impacts detection by a widely-used RT-PCR assay. *bioRxiv*.
- Vogels, C.B.F., Brito, A.F., Wyllie, A.L., Fauver, J.R., Ott, I.M., Kalinich, C.C., Petrone, M.E., Casanovas-Massana, A., Muenker, M.C., Moore, A.J., *et al.* (2020). Analytical sensitivity and efficiency comparisons of SARS-CoV-2 RT-qPCR primer-probe sets. *Nature Microbiology*, 1-7.
- Wang, C., Horby, P.W., Hayden, F.G., and Gao, G.F. (2020a). A novel coronavirus outbreak of global health concern. *Lancet* 395, 470-473.
- Wang, R., Simoneau, C.R., Kulsuptrakul, J., Bouhaddou, M., Travisano, K., Hayashi, J.M., Carlson-Stevermer, J., Oki, J., Holden, K., Krogan, N.J., *et al.* (2020b). Functional genomic screens identify human host factors for SARS-CoV-2 and common cold coronaviruses. *bioRxiv*.

- Williamson, E.J., Walker, A.J., Bhaskaran, K., Bacon, S., Bates, C., Morton, C.E., Curtis, H.J., Mehrkar, A., Evans, D., Inglesby, P., *et al.* (2020). Factors associated with COVID-19-related death using OpenSAFELY. *Nature* 584, 430-436.
- Wolfel, R., Corman, V.M., Guggemos, W., Seilmaier, M., Zange, S., Muller, M.A., Niemeyer, D., Jones, T.C., Vollmar, P., Rothe, C., *et al.* (2020). Virological assessment of hospitalized patients with COVID-2019. *Nature* 581, 465-469.
- Wood, C.S., Thomas, M.R., Budd, J., Mashamba-Thompson, T.P., Herbst, K., Pillay, D., Peeling, R.W., Johnson, A.M., McKendry, R.A., and Stevens, M.M. (2019). Taking connected mobile-health diagnostics of infectious diseases to the field. *Nature* 566, 467-474.
- Yan, W.X., Chong, S., Zhang, H., Makarova, K.S., Koonin, E.V., Cheng, D.R., and Scott, D.A. (2018). Cas13d Is a Compact RNA-Targeting Type VI CRISPR Effector Positively Modulated by a WYL-Domain-Containing Accessory Protein. *Mol Cell* 70, 327-339 e325.
- Zetsche, B., Gootenberg, J.S., Abudayyeh, O.O., Slaymaker, I.M., Makarova, K.S., Essletzbichler, P., Volz, S.E., Joung, J., van der Oost, J., Regev, A., *et al.* (2015). Cpf1 is a single RNA-guided endonuclease of a class 2 CRISPR-Cas system. *Cell* 163, 759-771.
- Zhou, J., Li, C., Sachs, N., Chiu, M.C., Wong, B.H., Chu, H., Poon, V.K., Wang, D., Zhao, X., Wen, L., *et al.* (2018). Differentiated human airway organoids to assess infectivity of emerging influenza virus. *Proc Natl Acad Sci U S A* 115, 6822-6827.
- Zhu, N., Zhang, D., Wang, W., Li, X., Yang, B., Song, J., Zhao, X., Huang, B., Shi, W., Lu, R., *et al.* (2020). A Novel Coronavirus from Patients with Pneumonia in China, 2019. *N Engl J Med* 382, 727-733.

Chapter 4: Conclusions & Outlook

As I complete this dissertation and my PhD work, the FDA has just granted approval to the first two COVID-19 vaccines, which each show ~95% effectiveness at preventing COVID-19 (Polack et al., 2020). The first vaccinations in the US will be given on the day of my dissertation seminar, and I feel hope entering 2021 that the social, economic, and personal devastation SARS-CoV-2 has wreaked in the last year is close to the end. However, the need for rapid, portable diagnostics remains. It will likely take nearly a year from the start of vaccinations to reach herd immunity, and the US is currently in the midst of a deadly third wave. On the same day that the first vaccinations were given, the US crossed the grim threshold for 300,000 deaths from COVID-19. By implementing rapid, frequent testing of the population, the COVID-19 pandemic can be mitigated, and the reopening of society can be hastened prior to population-wide vaccination.

On another note, the COVID-19 pandemic is unlikely to be the last coronavirus or viral pandemic humanity encounters. Globalization, human expansion into the territory of wildlife, and human mobility ensure that zoonotic diseases will continue to enter the human population and have the opportunity to spread worldwide. Without a significant investment in both broad surveillance and rapid, adaptable diagnostics, future uncontrolled pandemics are likely. Moreover, many established viruses, including HIV-1, require improved access to diagnostics to enable diagnosis and cure strategies. CRISPR-Cas13a diagnostics, paired with a mobile phone-based read-out, offer the opportunity for easily re-programmable diagnostics that can be used at the point-of-care or at home and provide accurate and sensitive results. Collectively, this dissertation demonstrates a blueprint for the development and adaptation of these tools.

REFERENCES

Polack, F.P., Thomas, S.J., Kitchin, N., Absalon, J., Gurtman, A., Lockhart, S., Perez, J.L., Perez Marc, G., Moreira, E.D., Zerbini, C., *et al.* (2020). Safety and Efficacy of the BNT162b2 mRNA Covid-19 Vaccine. *N Engl J Med.*

Publishing Agreement

It is the policy of the University to encourage open access and broad distribution of all theses, dissertations, and manuscripts. The Graduate Division will facilitate the distribution of UCSF theses, dissertations, and manuscripts to the UCSF Library for open access and distribution. UCSF will make such theses, dissertations, and manuscripts accessible to the public and will take reasonable steps to preserve these works in perpetuity.

I hereby grant the non-exclusive, perpetual right to The Regents of the University of California to reproduce, publicly display, distribute, preserve, and publish copies of my thesis, dissertation, or manuscript in any form or media, now existing or later derived, including access online for teaching, research, and public service purposes.

DocuSigned by:

Palmas Fozam

6ED8677A498D495...

Author Signature

12/16/2020

Date